Investigation on Integrated AlGaN/GaN Ion-Sensitive Field-Effect Transistors

集積化AlGaN／GaNイオン感応性電界効果トランジスタに関する研究

Jiyu Zhou

周　継禹

DOCTORAL DEGREE THESIS

ELECTRICAL AND ELECTRONIC ENGINEERING

TOKUSHIMA UNIVERSITY

September 2021

Abstract

AlGaN/GaN heterostructure ion-sensitive field-effect transistors (ISFETs) can provide high sensitivity and fast response due to the high electron mobility and high electron density providing by the two-dimensional electron gas (2DEG) generated at the AlGaN/GaN heterostructure interface. My research mainly focuses on the investigation of the integrated AlGaN/GaN ISFETs for pH sensing.

To achieve high performance on AlGaN/GaN ISFET pH sensor, we fabricated sensors with different Al composition (25%, and 35%). We compared the characteristics of the sensors with 25% and 35% Al composition. The pH sensor with Al composition (35%) in the barrier layer with a 16 nm transition layer of 25% Al composition shows better surface sensitivity (S_V) of 56.01 mV/pH, which is higher than that of the sensor with 25% Al composition (53.94 mV/pH), but worse current sensitivity S_A (-0.095 mA/pH Vs -0.102 mA/pH). In addition, threshold voltage increases from approximately -1.6 V to approximately -0.8 V when measured in alkaline solution for 5 times, along with a decreasing output current. High-resolution SEM photos show that there are high density hexagonal pits with the size of approximately 100 nm on the device surface, presenting the etching effect along the dislocations during alkaline sensing. The X-ray photoelectron spectroscopy (XPS) demonstrates that the intensity of the Ga3d and Al2p spectra decreases after pH sensing measurement, implying the variation of chemical component occurs in the upper AlGaN thin layer. Many voids with a size of approximately 100 nm were observed from the transmission electron microscope (TEM) pictures, which are comparable with that of the scanning electron microscope (SEM). Combining with the energy dispersive X-ray spectroscopy (EDX), the degradation in electrical performance can be attributed to the transformation of AlGaN into oxide as well as the followed alkaline solution dissolve.

To avoid the reaction of surface Al with solution, a 3 nm GaN cap layer was added. To reduce the barrier layer thickness, a recessed gate with a length of 2 μm and a depth of about 14 nm was formed. The current sensitivity of the AlGaN/GaN ISFET pH sensors has been improved by 61%, from 52.25 to 84.39 μA/pH, by the recessed-gate structure and ammoniate water treatment.

Abstract

A pH meter system based on the GaN pH sensor was constructed and evaluated. GaN-based ISFET can measure the pH value of the solutions with similar circuit, whether in the linear region or the saturation region. The measurement is stable and repeatable. The small current in the linear region can make the measurement stable and fast, but the resolution is a bit low. High resolution can be obtained in the saturation region, but the measurement is unstable due to excessive current.

The Schottky barrier diode (SBD) based on GaN can be used for temperature sensing, and the temperature sensitivity can be improved by different structure design. A recessed anode AlGaN/GaN SBD is suitable to integrate with GaN-based power device for temperature sensor application. The temperature dependent forward voltage at a fixed current shows good linearity, resulting in a sensitivity of approximately 1.0 mV/K. The p-NiO guard ring can suppress the electric field at the anode/GaN interface and field crowding at the anode edge effectively, which enhances the breakdown voltage to approximately -250 V. Using the same material, we can design an integrated device sensor based on GaN to measure temperature and pH simultaneously, which will solve the measurement deviation of pH sensor at different temperatures.

Keywords: GaN, integrated sensor, SBD, recessed-anode, guard ring, pH meter system.

Outline

Chapter 1：Introduction

§1.1. pH sensor based on ion-sensitive field-effect transistors

Ion sensor transforms the sensing ion quantity into output signal with the ion selective electrode. Ion sensor measures the specific ion concentration (activity) in the solution. Now it plays an extremely important role in all scientific fields. In recent years, due to the development of semiconductor integrated technology, ion sensors are also heading for diversification and intelligent telemetry. Ion sensors have been widely used in drainage automatic measurement in factories, river monitoring for environmental sanitation, automatic monitoring of solutions production and daily analysis in laboratory. In the future, there is great expectation for clinical examination and application of embedded sensors in vivo. In order to meet these needs, although preliminary studies have been done, sensitivity, selectivity and durability improvement are indispensable.

With the continuous development of semiconductor technology, more and more attention has been paid to the research of ion-sensitive field-effect transistors (ISFETs). The introduction of silicon as a substrate for microelectrodes, specifically meant for electrophysiological measurements (action potentials), started in the late 1960s at the Stanford University by Wise et al. [1]

There was considerable controversy about the theory of operation of the ISFET. The physical origin of the ISFET response to electrolyte pH had been ascribed to virtually all regions of the ISFET structure. Basically, there were three schools of thought, which are briefly summarized as follows.

(1) The ISFET gate insulator was considered to behave as a glass electrode and the potential developed across the E-I interface can be treated by conventional glass electrode theory [3]. This assumption implies there is H^+ ion transport through the gate insulator to some distance within the insulator and that thermodynamic equilibrium is reached between the potential determining ions in the electrolyte and those within the insulator. The result of such a consideration is a Nernstian sensitivity (In (10)x(kT/q) per pH unit). Bergveld [2], Moss et. al [4], Lauks & Zemel [5] and Matsu o & Esashi [6] have considered this approach.

(2) The H^+ ion or H-bearing species in the electrolyte was considered to diffuse into the insulator, causing changes in the interface states at the insulator/Si interface. These

changes of the interface states in turn modulate the threshold voltage of the field effect transistor. De Rooij & Bergveld [7], Barabash & Cobbold [8], Revesz [9] have elaborated on this mechanism for the case of SiO_2.

(3) The insulator is essentially blocking the ion species in the electrolyte. The termination of the insulator at the E-I interface gives rise to ionize surface groups or surface sites. H_+ ions interact with these amphoteric surface sites, establishing a dynamic equilibrium characterized by equilibrium constants. The result of H^+ ions bonded to these surface sites /traps is a net charge residing at the E-I interface. This surface charge at the E-I interface modulates the electric field in the insulator of the field effect transistor and changes its threshold voltage. This model, known as the site-binding model, is adopted from the work of Levine & Smith [10], and Yates, Levine &Healy [11] on colloidal chemistry, and has been used successfully by m any groups of researchers, notably Harame et. al. [12], Fung et. al. [13], Bousse et. al. [14], Chan &. White [15], Siu & Cobbold [16), and Barabash & Cobbold [17].

Summarizing on the theoretical explanation of the pH sensitivity of ISFETs, it should be concluded that an ISFET is an electronic component, similar with the MOSFET, but with a modulation possibility of the threshold voltage by means of the oxide/solution interface potential. The relation between this interface potential and the pH is determined by the buffer capacity of the oxide surface.

Unfortunately, such devices typically require a reference electrode in order to bias the gate of the transistor beyond the threshold voltage, to allow majority carriers to travel through the conductive channel [18]. On-chip miniaturized Ag/AgCl reference electrodes have been designed and tested, but their fabrication is typically complex and electrode solution leakage remains a serious issue compromising sensor accuracy and device lifetime [19]. A simpler solution for biasing the transistor is to add an on-chip noble metal (e.g. gold) contact/electrode, but this addition alone is not adequate as the metal/electrolyte interface potential is not stable. A reference field-effect transistor (REFET), which has a chemically passivated gate surface and is insensitive to changes in solution composition, can be used in conjunction with the ISFET device to compensate for these changes in interfacial potential [20]. However, despite many attempts, this method also suffers from chemical instability and drift [21]. Si-based transistors can be heavily doped resulting in a “normally-on” state possibly precluding the necessity for a reference electrode, but heavy doping results in

decreased device performance (e.g. poor electron mobility) and increased manufacturing costs.

§1.2. Advantage of GaN ISFET in pH sensor application

Gallium nitride (GaN) is a wide bandgap (WBG) semiconductor material which is desirable and promising in developing high frequency and high power devices because of its superior material properties such as thermal stability, high critical electric field, high electron-saturation velocity and high mobility in heterojunction 2-D electron gas (2DEG) channel. The superior properties of the WBG GaN are also desirable for sensing applications. It is well acknowledged that the polarized Ⅲ-nitride surface is susceptible to the surface charge, which can induce 2DEG conductivity change (drain to source current change). In power electronic devices, the surface charge effect can cause adverse dynamic R_{ON} degradation problem, however, such unique property can be exploited and used as a highly sensitive sensor.

The Si-based ISFET is limited at the high-temperature operation owning to the narrow bandgap (1.12 eV) and it is easy to be corroded in some specific solution during its working. So silicon is not a suitable material for developing ISFET in harsh environments. III-nitride materials, such as gallium nitride, have been widely studied, since they are potential semiconductors for developing high-frequency and high-power devices owing to their superior thermal stability, excellent conductivity and chemical stability. Hence, GaN-based semiconductors show more advantages than the Si-based semiconductors for ISFETs developing. So, if the AlGaN/GaN heterostructure is used to develop a pH sensor, high output of current or voltage can be expected, which is beneficial for achieving high sensitivity and high response pH sensor. Recently, ISFETs based on AlGaN/GaN-heterostructure have attracted wide attentions. The AlGaN/GaN-heterostructure ISFETs can provide high sensitivity and fast response due to the high electron mobility and high electron density providing by the 2DEG generated at the AlGaN/GaN interface [22, 23].

With proper functionalization of the gate sensitive membrane, the AlGaN/GaN-based sensor can detect targets such as ions, DNA, protein, antigen, glucose, cellular response and gases. Even without any functionalization, the bare AlGaN surface is sensitive to the pH change in the solution.

As a type of WBG material, GaN-based sensor has many superior characteristics.

The transparency of GaN-on-Sapphire (or GaN-on-SiC, GaN-on-GaN) devices makes them very convenient to be integrated with the traditional optical sensing equipment. Because of the WBG characteristic, GaN material is chemically inert and high temperature endurable, these features make the AlGaN/GaN-based sensor suitable to work under harsh environment. In recent years, GaN can be grown on low-cost and large-diameter Si substrate which makes it possible to use GaN device on high-end sensor applications. Moreover, GaN sensor can be monolithically integrated with signal processing and amplification circuits or RF signal transmitting circuits which are very convenient for the data readout and the remote signal reception.

§1.3. Progress in GaN ISFET pH sensor

pH sensor fabricated using AlGaN/GaN ISFETs are promising for high-temperature application owing to its wide bandgap and chemical inertness. Besides, the 2DEG channel generated by the built-in polarization electric field at AlGaN/GaN interface presents high electron mobility and saturation velocity, which can effectively enhance the sensitivity of pH sensor. According to the site dissociation model, the sensing membrane formed on surface plays a key role in varying surface potential (2DEG concentration) of the sensing area when the ISFETs are dipped into different pH electrolytes. To date, surface modification has been extensively carried out through many techniques such as photo-assisted electrochemical (PEC) oxidation, atomic layer deposition, diamond coating, ZnO coating and so on.

AlGaN/GaN devices with various capping layers (such as native or deposited oxides) have been shown to be effective pH sensors [24, 25]. It has recently been shown that with an ultrathin GaN/AlGaN/GaN device that a reference electrode is not necessary to achieve very sensitive measurements of solution pH [26]. In other reports it has been shown that for uncapped reference electrode free AlGaN/GaN device measurements the device sensitivity is towards negative ions (i.e. chloride) and not exclusively changes in pH [27].

There has been significant interest in group III-nitrides based chemical sensors during the last years, especially since the first evidence of pH-sensitivity of GaN surfaces [28] and its application in pH-sensitive AlGaN/GaN field effect transistors [29]. According to the site-binding model [30], the pH-sensitivity is due to amphoteric hydroxyl groups, in this case from the thin Ga_xO_y surface layer formed after wet

chemical oxidation or even after a simple exposure to atmosphere. In addition, the oxidic surface of group III-nitride devices allows the covalent immobilization of biomolecules after silanization [31, 32], and makes the surface naturally biocompatible [33-35]. For sensor applications in electrolyte solutions, high electron mobility transistors (HEMTs) based on AlGaN/GaN heterostructure have frequently been used. In such structures, the conductivity of a two-dimensional electron gas (2DEG), located typically 20-30nm beneath the surface, is affected by chemically induced changes of the surface potential.

Transistor structures based on GaN or AlGaN/GaN heterostructure grown on sapphire substrates can easily provide metal oxide gate layers and can benefit from the high chemical stability of the III-nitrides. Due to the optical transparency of both the thin semiconducting film and the sapphire substrate, GaN-based ISFETs allow simultaneous electronic and microscopic detection of processes on the device surface in biophysical and biochemical applications.

Georg Steinhoff et. al demonstrated the applicability of the group III nitride material system for the fabrication of novel biosensors based on transparent AlGaN/GaN field-effect transistor structures. [33] These devices exhibit an almost Nernstain pH sensitivity and a low drift in aqueous electrolytes. Non-toxic, chemically stable metal oxide surfaces of all AlGaN compounds allow direct attachment of living cells on the FET gate area. Furthmore, the deposition of continuous lipid bilayer membranes on hidrophilized AlGaN surfaces has been achieved for differently charged lipids. Interestingly, the lateral diffusing constants of lipids do not depend on the chemical surface composition and the electrochemical surface charge, but rather on the molecular net charges. Thus, the AlGaN material system combines chemical inertness of the metal-oxide-like surface, optical transparency, and electronic sensitivity in a unique way, which may open a new area for multifunctional biosensors devices.

M. Bayer presented a model to explain the sensitivity of GaN heterostructure to surface charges that may be controlled by the pH value of an electrolyte. [36] The model for the electrolyte at an amphoteric surface is based on the solution of the Poisson–Boltzmann equation for the potential and the site-binding model for the explanation of the surface charge density on the amphoteric oxide. The 2DEG formation in the GaN heterostructure has been attributed to the large polarization fields. We have used experimental results to determine values for the dissociation

constants and the concentration of sites on the oxide. The introduction of a pH dependent sheet charge at the GaN/Oxide interface explains the high sensitivity of the system on the pH value. It has been further shown that N-face polarity of the GaN heterostructure will improve the sensing features significantly. Additionally, the efficiency of the sensor can be enhanced by increasing the oxide thickness as well as decreasing the Al mole fraction in the AlGaN layer. Also, the area exposed to the electrolyte should be as large as possible relative to the total surface of the device.

I. Cimalla et.al. investigated the impact of typical device processing steps (KOH, HCl, HF wet chemical etching, SF_6 and Cl plasma etching) on the surface properties (roughness, chemical composition, contact angle to water) of group III-nitride based chemical sensors with emphasis on the electrical performance of the sensor and the biocompatibility. [35] They summarize the following conclusion: Both investigated cell lines are growing well on AlGaN/GaN and are only little affected by the different processing steps. Good proliferation was also observed on polyimide, which consequently is suitable for passivation on sensor devices. The contact to cells and cell media contaminates the surface with metal ions, and a non-destructive procedure for their complete removal is not available at present. However, its influence on the sensing behavior is not known. The sterilization by autoclaving, which is very commonly used in working with cell cultures, contaminates the surface with carbon-containing species. Consequently, a modified sterilization method has to be developed for the AlGaN/GaN sensor surface, e.g., additional purification with surfactants or alcoholic derivatives. The established cleaning procedure with HCl and HF indeed decreases the surface concentration of oxygen and carbon. The remaining traces of chlorine and fluorine have no measurable effect on the sensor properties. The electrical performance of an AlGaN/GaN sensor degrades after the first use, however, stabilizes thereafter. This phenomenon has to be taken into account for the calibration procedure of the sensors (and for repetitive use of the “expensive” sensor material in future biomedical applications).

In order to find a suitable passivation for the application of the pH sensor in the food industry, several layer combinations have been investigated by St. Linkohr et.al. in a CIP test and analyzed focus on the morphological stability. [37] With insufficient chemical and mechanical stability, the parallel plate plasma CVD generated layer stacks are inappropriate for passivation purposes under these conditions. Beyond that, all stacks containing a SiO_2 or AlN layer were etched by the NaOH solution in the CIP

process. Better results were obtained by the ICP CVD grown SiNx and the ICP and sputtered SiNx double layer, where only the insufficient step coverage was responsible for failing the CIP test. A layer stack capable of surviving the CIP test has ultimately been found with the diamond reinforced passivation. The sensitivity of the sensor was found to be stable after several CIP cycles. The interaction of the alkaline solution with the sensor, however, induces a positive shift in the measured pH value of around 0.2 pH per cycle. This shift is dependent on the operation point of the ISFET. At optimum reference voltage, this shift is nearly constant for all CIP cycles and, thus, might be implemented in the calibration routine in order to ensure the needed accuracy in pH determination.

Niketa Sharma et. al. investigated the characteristics of pH and salinity sensor derived from the gated AlGaN/GaN HEMT structures in phosphate buffer saline (PBS) and aqueous salt solutions (NaCl + DI) [38]. In DI water, the GaN HEMT demonstrated competent drain I–V characteristics close to the I–V characteristics of typical HEMTs when exposed to the air. These devices illustrate the dramatic variation in output drain–source current upon exposure to PBS in the gate region. This is due to the equivalent potential difference at the AlGaN surface, resulting in the enhancement in channel carrier density. A high level of sensitivity 4.32 μA/mm-pH at Vds =1 V and Vgs = 0 V was obtained. Next, we also reported on the modification in the current with the various molar concentrations of NaCl present in the DI water. This additionally demonstrated a systematic potential change at the AlGaN surface as a result of change in molar concentration of saline liquid. A femto-level molar concentration NaCl in DI was also detected by the fabricated GaN HEMT sensor. A possible mechanism for the change in drain current with variation in molar concentration of the AlGaN surface was discussed with regard to equilibrium reactions of hydroxyls ions at the AlGaN surface concerning H^+ in a solution. A minimal concentration of NaCl in DI and in PBS (femto-level molar concentration) was fairly distinguished by the fabricated GaN HEMT sensor. A high device sensitivity of 6.48 mA/mm-molar for NaCl in DI was recorded at Vds = +1 V and V gs = 0 V and 2.02 mA/mm-molar for NaCl in PBS at Vds = +5 V and Vgs =0 V. They also performed transient response of the devices toward change in molar concentration. A quite good response time was retrieved 250–350 ms. It would be concluded from the mentioned above results that the AlGaN/GaN HEMT devices are very promising with high-level sensitivity pH and saline sensors for chemical sensing

in biomedical and space applications.

Dongyang Xue et. al found that the threshold voltage (V_T) of the AlGaN/GaN HEMT based pH sensor was adjusted by the method of the photoelectrochemical (PEC) oxidation on the GaN cap layer surface [39]. After the PEC oxidation treatments, the V_T of the device shifted from -3.46V to -1.15 V and the gate voltage (V_G) corresponding to the maximum transconductance G_{MMAX}) position (V_G |G_{MMAX}) of the device shifted from -2.6 V to -0.1V. The drain current (I_D) variation per pH of the AlGaN/GaN HEMT based pH sensor without reference electrode increased from 0.7μA to14 μA when the drain voltage (V_D) was 0.5V. The sensitivity of the reference electrode free AlGaN/GaN HEMT based pH sensor can be significantly increased by regulating the V T to make V_G |G_{MMAX} approached the equivalent V_G when liquid droplet on the sensing window surface ($V_{G\text{-}EQU}$), which is beneficial to the miniaturization and integration of the AlGaN/GaN HEMT based sensors in the future.

Anna Podolska et. al reported on a methodology for quick and simple prediction and optimization of AlGaN/GaN device sensitivity operated in reference electrode free configuration desirable for miniaturized sensors [40]. They demonstrated that by optimization of the AlGaN layer (composition and thickness), the sensitivity of reference-electrode-free AlGaN/GaN heterostructure-based ion sensors can be dramatically improved. A model was applied to estimate the sensitivity of different structures and showed sensitivity can be maximized by designing a structure to have near-zero threshold voltage. One example of an ISFET device with maximal sensitivity is demonstrated. However, there are many other heterostructure designs that would produce similar sensitivity. In particular, due to practical limitations high-x Al or x Al = 1 (AlN/GaN) structures were not experimentally investigated in this work but are certainly indicated to be highly sensitive for very thin Al(Ga)N layers. Future improvements in this technology could include investigation of thin AlN layer devices with low threshold voltage. The model allows selection of appropriate design taking into account other factors such as complementary devices, material quality, or processing issues that may influence selection of specific AlGaN composition or thickness. Experimental results confirmed the predictions of the model, with high signal to noise ratio and gain in conductivity with KOH exposure for the devices grown on the structures with near zero thresholds. These results can be used to improve performance for future chemical and biochemical sensors.

Y. Maeda et. al developed and evaluated pH sensors composed of an

AlGaN/GaN heterostructure with different surface conditions [41]. They found that the sensors showed good pinch-off characteristics for all the samples with different surface conditions and the drain current decreased and the threshold voltage had a positive shift with increasing pH value. The result of their experiments showed that the sensitivity of the pH sensor on AlGaN/GaN heterostructure increases if AlGaN surface was adopted and increases with increasing aluminum content.

Kazutaka Niigata.et.al evaluated the temperature dependence of the GaN-based pH sensor on an AlGaN/GaN heterostructure at temperature ranging from room temperature to 80℃ [42]. They found that pH sensors fabricated on an AlGaN/GaN heterostructure showed good pinch-off and transfer characteristics at temperatures ranging from room temperature to 80℃ and that the drain current decreased while the threshold voltage showed a positive shift with increasing pH value. They proved that the drain current of pH sensor decrease and positive threshold voltage shift were also noted with increasing temperature.

Lei Wang et.al demonstrated AlGaN/GaN ISFETs with O_2 plasma treatment on the AlGaN surface [43]. It demonstrated that the ISFET with short-time O_2 plasma treatment exhibited excellent pH sensing properties, including a higher sensitivity of 55.7mV/pH, a much hydrophilic surface with the water contact angle of approximately 5–7°, and a much smooth and clean surface. While, after a long-time O_2 plasma treatment, the pH sensing properties changed to a much poor level. According to the XPS results, the AlGaN/GaN surface with a rich aluminum oxide is the main reason to improve the sensitivity of the AlGaN/GaN ISFETs. With the O_2 plasma treatment time increasing, the aluminum oxide dominated AlGaN/GaN surface changes to a gallium oxide dominated surface, leading to the decreasing on the ISFET sensitivity. Thus, the short-time O_2 plasma treatment method is a quick and simple technique to increase the property of the AlGaN/GaN ISFETs. Later they passivated the AlGaN surface to improve the performance of the ISFETs using thermal oxidation treatment at different temperatures [44]. The effect of oxidizing temperature on the ISFET sensor properties was evaluated and a possible mechanism has also been proposed to explain the results. A mass of existing hydroxide in the native oxide film is responsible for the high surface state density, which leading to the weak performance of the AlGaN ISFETs. Through the thermal oxidation treatment on the AlGaN ISFETs surface, the performances of the ISFETs were improved, such as the

stability and high sensitivity. This mainly contributed to the $Al(OH)_3$ transferred to the Al_2O_3 owing the good chemical stability. Moreover, the pure α-Al_2O_3 crystal phase generated on the AlGaN ISFETs surface at 700℃, not only provided a high sensitivity to 57.7 mV/pH which is very close to the Nernstian limit, but also provide a relatively smooth surface. These results mean that the thermal oxidation treatment for AlGaN ISFETs is an effective method to improve the performances of the AlGaN ISFETs.

Liuan Li et. al fabricated an AlGaN/GaN ion-sensitive field-effect transistor through the photoelectrochemical method for pH sensor application [45]. It demonstrated that the partial oxidation of the AlGaN barrier can facilitate the depletion of 2DEG and achieve the normally-off operation. Moreover, the PEC process can transfer the needle-like native oxide (a mixture of Al_2O_3 and Ga_2O_3) on the ISFET surface into a flat Al_2O_3 dominating layer. The improved surface status and transconductance of the normally-off device is regarded as the possible reason to enhance the sensitivity from 48.5 mV/pH of ISFETS to 56.3 mV/pH of MOS-ISFETs.

§1.4. The motivation of this work

My research mainly focuses on investigation on the integration of AlGaN/GaN Ion-Sensitive Field-Effect Transistors pH sensor. Firstly, we adopted AlGaN barrier with different Al-content and thickness to find whether the high Al content could enhance the sensitivity of the pH sensor or not. Secondly, we made a practical pH meter based on GaN to observe the problems in practical application. Then we developed GaN based temperature sensors, which can be integrated with the pH sensor to monitor the temperature of the device to eliminate the instability and reflection speed caused by junction temperature. The main works are list below:

(1) The dependence of Al-content on AlGaN/GaN ISFET with AlGaN barrier layer was studied. It is found that the sensitivity of the sensor can be improved by increasing the aluminum content in the appropriate structure, and it is also found that the completely exposed AlGaN layer may be destroyed by the solution to be tested, especially the alkaline solution.

(2) The effects of adding GaN protective layer to avoid damage and adding recess to increase threshold voltage are studied. It is found that these two methods have obvious effects.

(3)A pH meter system was made to explore the effect of GaN ISFET sensor in

practical application. The results can lead to the following conclusions: 1. GaN based ISFET can measure the pH value of solution with similar circuit, whether working in the linear region or saturated region; 2. The measurement is stable and repeatable; 3.The small current in the linear region can make the measurement stable and fast, but the resolution is very low. High resolution can be obtained in the saturated region, but the measurement is unstable due to excessive current.

(4) In order to integrate the temperature sensor to eliminate the influence of temperature on pH measurement, we studied the GaN based temperature sensor. It is found that the recessed anode and the guard ring can improve the performance of the integrated sensor.

This thesis consists of the following parts: the first chapter is the introduction of research background. The second chapter is dependence of Al-content on AlGaN/GaN ISFET with AlGaN barrier layer. The third chapter is the results and discussion of AlGaN/GaN ISFETs with recessed structure. The fourth chapter is application of AlGaN/GaN ISFETs pH sensor. The fifth chapter is the research on GaN-based temperature sensors for integration. The sixth chapter is conclusions and the future works.

§1.5. References

[1] K. D. Wise, J. B. Angell, A. Starr, An integrated-circuit approach to extracellular microelectrodes, IEEE Trans. Biomed. Eng. BME-17 (3) (1970) 238.

[2] Piet Bergveld, Development of an ion-sensitive solid-state device for neurophysiological measurements, IEEE Trans. Biomed. Eng., Vol. BM E-17, Jan 1970, pp. 70.

[3] G. Eisenman, Glass electrodes for hydrogen and other ions, Mercel Dekker, 1967.

[4] S. D. Moss, C. C. Johnson, J. Janata, Hydrogen, calcium, and potassium ion-sensitive FET transducers: A preliminary report, IEEE Trans. Biomed. Eng., Vol. BM E-25, No. 1, Jan 1978, pp. 49.

[5] I. Lauks, J. N. Zemel, The Si3N4/Si ion sensitive semiconductor electrode, IEEE Trans. Electron Devices, Vol. ED -26, No. 12, Dec 1979, pp. 1959.

[6] T. Matsuo, E. Esashi, Methods of ISFET Fabrication, Sensors &Actuators, Vol. 1, 1981, pp. 77-96.

[7] N. F. de Rooij, P. Bergveld, The influence of the pH on the surface state density at

the Si02-Si interface, Proc. Intl. Topical Conf. on the Physics of SiO2 and its interfaces, Pergamon, New York, 1978, pp. 433.

[8] P. R. Barabash, R. S. C. Cobbold, Dependence of interface state properties of electrolyte -Si02/Si structures on pH, IEEE Trans, Electron Devices, Vol. ED -29, No. 1, Jan 1982, pp. 102.

[9] A. G. Revesz, On the mechanism of the ion sensitive field effect transistor, Sensors & Actuators, Vol. 6, 1984, pp. 65-78.

[10] S. Levine, A. L. Smith, Theory of the differential capacity of the oxide/aqueous electrolyte interface, Discuss. Faraday Soc., Vol. 52, 1971, pp. 290.

[11] D. E.Yates, S. Levine, T. W. Healy, Site-binding model of the electrical double layer at the oxide/water interface, J. Chem. Soc. Faraday Trans. I, Vol. 70, 1974, pp. 1807.

[12] D. Harame, J. Shott, J. Plummer, J. Meind, An Implantable Ion Sensor Transducer, IEEE International Electron Device Meeting Technical Digest, 1981, pp. 467-470.

[13] C. D. Fung, P. W. Cheung, W. H. Ko, Electrolyte-lnsulator-Semiconductor Field Effect Transistor, IEEE International Electron Device Meeting Technical Digest, 1980, pp. 689-692.

[14] L. Bousse, N. F. de Rooij, P. Bergveld, Operation of Chemically Sensitive Field Effect Sensors as a Function of the Insulator-Electrolyte Interface, IEEE Trans. Electron Devices, Vol. ED-30, 1983, pp. 1263.

[15] C. F. Chan, M. ll. White, Characterization of Surface and Buried Channel Ion Sensitive Field Effect Transistors (ISFETs), IEEE International Electron Device Meeting Technical Digest, 1983, pp. 651.

[16] W. M. Siu, R. S. C. Cobbold, Basic properties of the electroly te-Si02-Si system: Physical and theoretical aspects, IEEE Trans. Electron Devices, Vol. ED -26, No. 11, Nov 1979, pp. 1805.

[17] R. R. Barabash, R. S. C. Cobbold, Basic limitations of ISFET and silicon pressure transducers: Noise theory, models and device scaling, Sensors & Actuators, Vol. 4, 1983, pp. 426-438.

[18] J. Janata, Thirty years of CHEMFETs – a personal view, Electroanalysis 16 (2004) 1831–1835.

[19] H. Suzuki, T. Hirakawa, S. Sasaki, I. Karube, Micromachined liquid-junction Ag/AgCl reference electrode, Sensors and Actuators B: Chemical 46 (1998) 146–154.

[20] K. M. Chang, C. T. Chang, K. Y. Chao, J. L. Chen, Development of FET-type reference electrodes for pH-ISFET applications, Journal of the Electrochemical Society 157 (2010) J143–J148.

[21] W. Vonau, W. Oelssner, U. Guth, J. Henze, An all-solid-state reference electrode, Sensors and Actuators B: Chemical 144 (2010) 368–373.

[22] R. E. G. van Hal, J. C. T. Eijkel, P. Bergveld, A novel description of ISFET sensitivity with the buffer capacity and double layer capacitance as key parameters, Sens. Actuators B 24/25 (1995) 201–205.

[23] R. E. G. van Hal, J. C. T. Eijkel, P. Bergveld, A general model to describe the electrostatic potential at electrolyte/oxide interfaces, Adv. Coll. Interf. Sci. 69 (1996) 31–62.

[24] B. S. Kang, H. T. Wang, F. Ren, B. P. Gila, C. R. Abernathy, S. J. Pearton, et al., pH sensor using AlGaN/GaN high electron mobility transistors with Sc_2O_3 in the gate region, Applied Physics Letters 91 (2007).

[25] G. Steinhoff, M. Hermann, W. J. Schaff, L. F. Eastman, M. Stutzmann, Eickhoff, pH response of GaN surfaces and its application for pH-sensitive field-effect transistors, Applied Physics Letters 83 (2003) 177–179.

[26] A. B. Encabo, J. Howgate, M. Stutzmann, M. Eickhoff, M. A. Sanchez-Garcia, Ultrathin GaN/AlN/GaN solution-gate field effect transistor with enhanced resolution at low source-gate voltage, Sensors and Actuators B: Chemical 142 (2009) 304–307.

[27] A. Podolska, M. Kocan, A. M. G. Cabezas, T. D. Wilson, G. A. Umana-Membreno, B. D. Nener, et al., Ion versus pH sensitivity of ungated AlGaN/GaN heterostructure-based devices, Applied Physics Letters 97 (2010).

[28] S. S. Kocha, M.W. Peterson, D. J. Arent, J. M. Redwing, M. A. Tischler, J. A. Turner,Electrochemical investigation of the gallium nitride-aqueous electrolyte interface, J.Electrochem. Soc. 142 (12) (1995) L238–L240.

[29] G. Steinhoff, M. Hermann, W. J. Schaff, L.F. Eastman, M. Stuztmann, M. Eickhoff, pH response of GaN surfaces and its application for pH-sensitive field-effect transistors, Appl. Phys. Lett. 83 (177) (2003).

[30] W. M. Siu, R. S. C. Cobbold, Basic properties electrolyte–SiO–Sisystem: physical theoreticalaspects, IEEE Trans. Electron Devices ED-26 (1979)1805.

[31] B. Baur, G. Steinhoff, J. Hernando, O. Purrucker, M. Tanaka, B. Nickel, M. Stutzmann, M. Eickhoff, Chemical functionalization of GaN and AlN surfaces, Appl.

Phys. Lett. 87 (2005) 263901.

[32] B. Baur, J. Howgate, H.-G. von Ribbeck, Y. Gawlina, V. Bandalo, G. Steinhoff, M.Stutzmann, M. Eickhoff, Catalytic activity of enzymes immobilized on AlGaN／GaN solution gate field-effect transistors, Appl. Phys. Lett. 89 (2006) 183901.

[33] G. Steinhoff, O. Purrucker, M. Tanaka, M. Stutzmann, M. Eickhoff, AlxGa1–xN—A New Material System for Biosensors, Adv. Funct. Mater., 13 (2003) 841.

[34] G. Steinhoff, B. Baur, G. Wrobel, S. Ingebrandt, A. Offenhäusser, A. Dadgar, A.Krost, M. Stutzmann, M. Eickhoff, Recording of cell action potentials with AlGaN／GaN field-effect transistors,Appl. Phys. Lett., 86 (2005) 033901.

[35] I. Cimalla, F. Will, K. Tonisch, M. Niebelschütz, V. Cimalla, V. Lebedev, AlGaN/GaN biosensor-effct of device processing steps on the surface properties and biocompatibility, Sensors &Act., 123 (2007) 740–748.

[36] M. Bayer, C. Uhl, P. Vogl, Theoretical study of electrolyte gate AlGaN/GaN field effect transistors, Journal of Applied Physics, 97, 033703 (2005).

[37] St. Linkohr, W. Pletschen, S. U. Schwarz, J. Anzt, V. Cimalla, O. Ambacher, CIP (cleaning-in-place) stability of AlGaN/GaN pH sensors, Journal of Biotechnology, 163 (2013) 354– 361.

[38] Niketa Sharma, Shivanshu Mishra, Kuldip Singh, Nitin Chaturvedi, Ashok Chauhan, C. Periasamy Dheeraj Kumar Kharbanda, Priyavart Parjapat, P. K. Khanna, and Nidhi Chaturvedi, High-Resolution AlGaN/GaN HEMT-Based Electrochemical Sensor for Biomedical Applications, IEEE Transactions on Electron Devices, Issue 1, Jan. 2020, pp. 289 – 295.

[39] Dongyang Xue, Heqiu Zhang, Aqrab ul Ahmad, Hongwei Liang, Jun Liu, Xiaochuan Xia, Wenping Guo, Huishi Huang, Nanfa Xu, Enhancing the sensitivity of the reference electrode free AlGaN/GaN HEMT based pH sensors by controlling the threshold voltage, Sensors & Actuators: B. Chemical 306 (2020) 127609.

[40] Anna Podolska, Daniel Broxtermann, Joerg Malindretos, Gilberto A. Umana-Membreno, Stacia Keller, Umesh K. Mishra, Angela Rizzi, Brett D. Nener, and Giacinta Parish, Method to Predict and Optimize Charge Sensitivity of Ungated AlGaN/GaN HEMT-Based Ion Sensor Without Use of Reference Electrode, IEEE Sensors Journal, Vol. 15, No. 9, Sept 2015.

[41] Y. Maeda, K. Niigata, K. Narano, L. Wang, and J. -P. Ao, Surface Dependence of pH Sensors on AlGaN/GaN Heterostructure, ECS Transactions, 61 (19) 65-71 (2014).

[42] Kazutaka Niigata, Kazuhiro Narano, Yutaro Maeda, and Jin-Ping Ao, Temperature dependence of sensing characteristics of a pH sensor fabricated on AlGaN/GaN heterostructure, Japanese Journal of Applied Physics 53, 11RD01 (2014).
[43] Lei Wang, Yuyu Bu, Jin-Ping Ao, Effect of oxygen plasma treatment on the performance of AlGaN/GaN ion-sensitive field-effect transistors, Diamond & Related Materials 73 (2017) 1–6.
[44] Lei Wang, Yuyu Bu, Liuan Li, Jin-Ping Ao, Effect of thermal oxidation treatment on pH sensitivity of AlGaN/GaN heterostructure, Applied Surface Science 411 (2017) 144–148.
[45] Liuan Li, Xiaobo Li, Taofei Pu, Yang Liu, Jin-Ping Ao, Normally off AlGaN/GaN ion-sensitive field effect transistors realized by photoelectrochemical method for pH sensor application, Superlattices and Microstructures 128 (2019) 99–104.

Chapter 2：Dependence of Al-content on AlGaN/GaN ISFET with AlGaN barrier layer

§2.1. The necessary of high Al-content AlGaN barrier layer

AlGaN/GaN-based ISFETs are promising candidates for biochemistry sensing [1] and environment monitoring owing to their high-temperature operation, chemical stability and sensitivity to pH, multi-ions, DNA, enzyme and so on [2-4]. Besides, the ISFETs possess the advantage of compatibility with the conventional CMOS technology and other related semiconductor technologies, so that they can be fabricated through the micro-nano processes and integrated with electric circuits easily. Generally, in a AlGaN/GaN heterostructure, the piezoelectric and spontaneous polarization effects will generate a two-dimensional electron gas (2DEG) with a high electron mobility and a high electron density at the AlGaN/GaN interface. When the surface of the AlGaN/GaN heterostructure is in contact with solutions, the surface potential variation in different solutions causes the band bending of AlGaN/GaN heterostructure, resulting in the modulation of 2DEG channel [5]. The mechanism is believed to be the interaction between the surface of the AlGaN/GaN heterostructure and the solutions through the surface binding sites on the semiconductor surface. A higher surface binding site density for H_3O^+ and a higher 2DEG concentration are beneficial for enhancing the sensitivity of the AlGaN/GaN ISFETs.

The metal oxides on the AlGaN surface are regarded as the origination of the binding site. To increase the surface binding site density, extensive efforts have been carried out to modify the AlGaN surface with different dielectrics such as Si_3N_4, PdO, Al_2O_3, and HfO_2 [6-8]. In our previous work, we modified the AlGaN surface by various methods such as ozone or O_2 plasma treatment, thermal oxidation, wet oxidation and so on [9-11]. It demonstrates that an Al_2O_3-rich surface can not only provide a relatively smooth surface, but also improve the sensitivity to 57.7 mV/pH, which is close to the Nernstian limit. In this case, the AlGaN barrier with relatively high Al content is another potential approach to enhance the sensitivity. For one hand, higher Al content can introduce higher 2DEG concentration in the channel to sensing the surface electric charges. For the other hand, more Al_2O_3 will be formed in the native oxide of the AlGaN surface with a higher Al content [12]. It is found that the sensitivity of the pH sensor increases significantly with the increase of Al content in

the AlGaN barrier layer. However, the growth of high Al content AlGaN barrier encounters larger lattice mismatch and results in higher dislocation density [13], which increasing the risk of device degradation, especially for pH sensors work in alkaline environment. Besides, it is also difficult to realize good ohmic contact on this layer. In this work, as pH sensor, an AlGaN/GaN ISFET with stacked high Al-content AlGaN barrier (SB-ISFETs) has been fabricated to evaluate the surface sensing ability and reliability.

§2.2. Sample fabricating process

All samples were fabricated in lab in Tokushima University. The procedures were almost same as following:

1. Clean the wafer (bought from outside)
   a. H_2SO_4:H_2O_2=4:1, 100℃ 10 minutes (to remove the Inorganic substance)
   b. Acetone 100℃ 10 minutes, ultrasound 3 minutes (to remove organic substance)
   c. Methanol rinsing
   d. Deionized water rinsing
2. Photolithography (MESA)
   a. Coating
      (1) Drying 100℃ 1 minute
      (2) Coating (AZP4210, fully cover with the wafer) 3000r/min 15s
      (3) Drying 100℃ 6 minutes
   b. Photolithography
      (1) Mask clean: Acetone, Methanol, deionized water
      (2) Exposure 150 counts
      (3) Image develop: developing liquid (AZ400K): deionized water=1:4.5, 1 minute in developing liquid and 30s in the deionized water
      (4) Drying 105℃ 8 minutes
3. ICP (MESA)
   a. UV-plasma stripper (80℃ 10 minutes)
   b. ICP 26# (program restored in ICP) 100nm
   c. Removing photoresist

(1) Remover (liquid specially) 150℃ 10 minutes, ultrasound 3 minutes depend on the surface check by the microscope

(2) Acetone, Methanol and deionized water rinsing

4. Photolithography and ICP like step 2 and 3 if recess or other structure is necessary
5. Removing Si caused by the ICP step

   HF: HNO_3=1:1,5 minutes,→ remover 150℃ 10 minutes, ultrasound 1-3 minutes→ Acetone rinsing→Methanol rinsing→deionized water rinsing
6. Photolithography (Ohmic contact)
   a. Coating
      (1) Drying 100℃ 1 minute
      (2) Coating (AZP4210, fully cover with the wafer) 3000r/min 15s
      (3) Drying 100℃ 6 minutes
   b. Photolithography
      (1) Mask clean: Acetone, Methanol, deionized water
      (2) Exposure 150 counts
      (3) Image develop: developing liquid (AZ400K): deionized water=1:4.5, 1 minute in developing liquid and 30s in the deionized water
   c. Removing of redundant photoresist
      (1) Drying 105℃ 8 minutes
      (2) UV-plasma stripper (80℃ 3 minutes)
7. Ohmic contact sputtering
   a. Sputtering
      (1) HCl: H_2O=1:1, 5 minutes
      (2) Sputtering: Ti/Al/Ti/Au=50/200/40/40
   b. Lift-off
      (1) remover 150℃ 10 minutes, ultrasound 1-3minutes
      (2) Acetone rinsing
      (3) Methanol rinsing
      (4) Deionized water rinsing
   c. Annealing: 850℃ 100s
   d. Measure the I-V curve and adjust the annealing condition
   e. Repeat step7.c-d until good I-V curve obtained

8. Photolithography (Gate)

a. Coating

(1) Drying 100℃ 1 minute

(2) Coating (AZP4210, fully cover with the wafer) 3000r/min 15s

(3) Drying 100℃ 6 minutes

b. Photolithography

(1) Mask clean: Acetone, Methanol, deionized water

(2) Exposure 150 counts

(3) Image develop: developing liquid (AZ400K): deionized water=1:4.5, 1 minute in developing liquid and 30s in the deionized water

c. Removing of redundant photoresist

(1) Drying 105℃ 8 minutes

(2) UV-plasma stripper (80℃ 3 minutes)

9. Gate contact sputtering (if necessary)
10. Tests to verify the process (see section 2.3)
11. Dicing

§2.3. Evaluation of the fabricating process

§2.3.1 Film resistance

In order to test the resistance of the thin film (metal, semiconductor), the test pattern with different width (W =3, 6, 9, 12, 15 μm) as shown in Figure 2-1 is formed on the insulating (or semi insulating) substrate. Let the current (I_{14}) flow between electrodes 1 - 4, measure the voltage difference ((V_{23}) between electrodes 2 – 3, and obtain the resistance R. Then, the block resistance ρ_s can be calculated by the resistance R and the formula $R = \frac{V_{23}}{I_{14}} = \rho_s \frac{L}{W}$. The fabrication error of linewidth W is assumed to be ΔW, then $R = \rho_s \frac{L}{W+\Delta W}$. The line length L is set to be long (400 μ m), and the fabrication error can be ignored.

$$\frac{1}{R} = \frac{1}{\rho_s L}(W + \Delta W) = \frac{W}{\rho_s L} + \frac{\Delta W}{\rho_s L}. \qquad (2\text{-}1)$$

The block resistance ρ_s can be obtained by the slope of $\frac{1}{R}\sim W$ characteristic, andΔW can be obtained by the intercept. If the thickness t of the film is known, the volume resistivity of the film can be further calculated, $\rho = \rho_s t$.

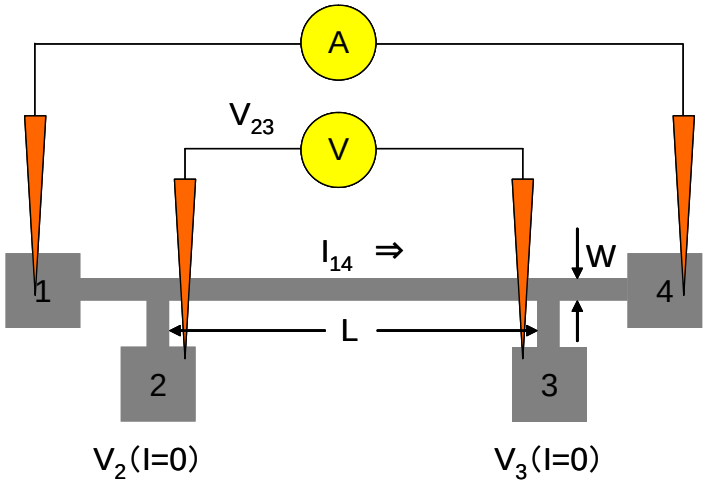

Figure 2-1 Film resistance test

§2.3.2 Schottky contact characteristics

From the forward current voltage characteristic (I-V characteristic) of Schottky contact, the ideal factor n and Schottky barrier height φ can be obtained by using the thermionic emission model:.

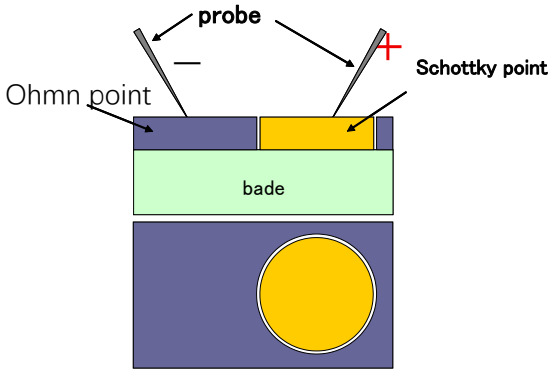

Figure2-2 Schottky contact testing pattern

$$I = A_e A^* T^2 \, exp\left(-\frac{q\varphi_b}{kT}\right)\left[exp\left(\frac{qV}{nkT}\right) - 1\right]. \quad (2\text{-}2)$$

$$A^* = \frac{4\pi q m^* k^2}{h^3} . \quad (2\text{-}3)$$

Here A^* is Richard's constant, n is the ideal factor, A_e is the area of Schottky contact. For n-GaN, A^* = 24.0 (acm-2k-2).

For the forward voltage of $qV \geq 3kT$, $\exp\left(\frac{qV}{nkT}\right) \geq 1$, the Schottky contact current is simplified as

Current:

$$I = A_e A^* T^2 \, exp\left(-\frac{q\varphi_b}{kT}\right) exp\left(\frac{qV}{nkT}\right). \tag{2-4}$$

Current density:

$$J = A^* T^2 \, exp\left(-\frac{q\varphi_b}{kT}\right) exp\left(\frac{qV}{nkT}\right). \tag{2-5}$$

Logarithm of current density on both sides

$$ln\, J = \frac{qV}{nkT} + ln\,(A^* T^2) - \frac{q\varphi_b}{kT}. \tag{2-6}$$

Here $J(= I / A_e)$ is the current density of the Schottky contact. The ideal factor n can be obtained from the slope of the line, and the barrier height φ_b can be obtained from the intercept of the line. Note: the low or high pressure field is not linear.

§2.3.3 Ohmic contact characteristics

Using TLM (transmission line model) graph, Ohmic contact resistance and block resistance of semiconductor can be measured. As shown in the figure below, make two ohmic electrodes on the semiconductor film, measure the resistance between the two electrodes, and then calculate the block resistance and contact resistance of the semiconductor. In order to eliminate the contact resistance of the probe and the series resistance of the wire and improve the test accuracy, the four-probe method can be used (refer to the test method of thin film resistance). Change the distance d between electrodes, the resistance is proportional to the distance (d) and inversely proportional to the electrode width (W), as follows:

$$R = \frac{\rho_S d}{W} + \frac{2R_C}{W}. \tag{2-7}$$

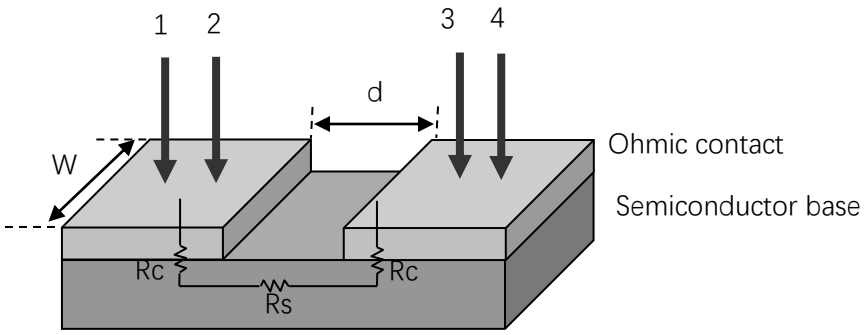

Figure 2-3 Ohmic contact test

Here R=Resistance（Ω）, d=Distance between electrodes（μm）, W=Width of electrode（mm）, ρ_s=block resistance（Ω/□）Rc=contact resistance（Ω・mm）。

The distance between electrodes is the X axis, the resistance is the Y axis, the slope of the straight line can calculate the square resistance (Rs), and the intercept of the Y axis can calculate the contact resistance (Rc). Generally, d = 5, 10, 15, 20, 25 μ m, w = 200 μ m.

Note: there will be some errors in the line width due to the manufacturing process. ΔW can be ignored, and Δd can be measured by ohmic contact metal pattern (refer to the test method of thin film resistance). In addition, this kind of figure needs to be isolated from the process; otherwise the line width W cannot be defined.

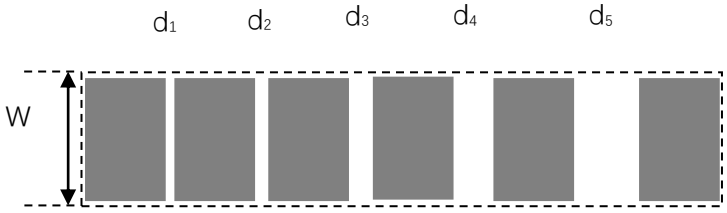

Figure 2-4 TLM drawing

§2.3.4 Circular TLM

The inner diameter and outer diameter of the design figure are r_1 and r_2 respectively, so the resistance from the inner circle to the outer circle is:

$$R = \frac{\rho_S}{2\pi}\ln\left(\frac{r_2}{r_1}\right) + \frac{R_C}{2\pi}\left(\frac{1}{r_1} + \frac{1}{r_2}\right). \quad (2\text{-}8)$$

Here R=Resistance（Ω）, r_1 and r_2=inner diameter and outer diameter（mm）, ρ_s=block resistance of semiconductor（Ω/□）, Rc=contact resistance（Ω・mm）。

Setting $\left(\frac{1}{r_1}+\frac{1}{r_2}\right)$ a constant，$R \propto \ln\left(\frac{r_2}{r_1}\right)$ is linear。The block resistance can be obtained from the slope of the fitting line, and the contact resistance can be obtained from the intercept.

§2.4. Surface sensibility for AlGaN/GaN with different Al-contents

The AlGaN/GaN heterostructure used in this experiment was grown on a sapphire substrate. From the bottom to the top, the structure consists of a transition layer, a 3 μm u-GaN (unintentionally-doped GaN). The following stacked barrier layer includes a 16 nm AlGaN barrier layer with 25% Al composition and finally an 8 nm AlGaN barrier layer with 35% Al composition. A 24 nm conventional AlGaN barrier (CB) with 25% Al composition is also adopted as reference. The device fabrication process begins with device isolation. An etching depth of 600 nm was formed by inductively-coupled plasma system. Next, Ti/Al/Ti/Au (50/200/40/40 nm) was deposited by magnetron sputtering for the source and drain electrodes followed by annealing process at 850 ℃ for 1 min in a N_2 ambient. After that, the samples were diced and mounted on a Teflon substrate. Finally, all the conducting area was covered with silicone resin to avoid contact with the solutions except at the open-gate region. The open-gate region is of width of 200 μm and length of 600 μm.

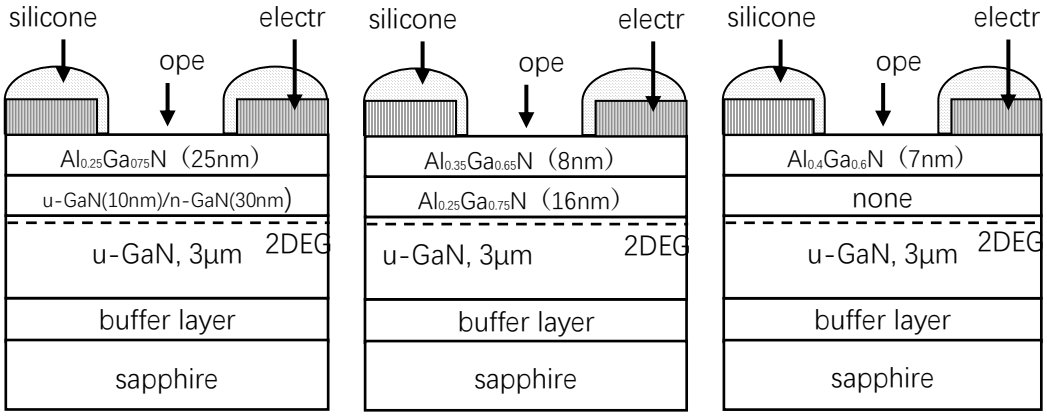

Figure 2-5 Structure of pH sensors with different Al content

To achieve good performance of pH sensor we fabricated sensors with different Al content with structure as in Figure 2-5. We did basic tests to assure the fabricating process correct, such as Ohmic test (Figure 2-6), HEMT Vd-Id test (Figure 2-7), Vg-Ig (Figure 2-8) test and Vg-Id test (Figure2-9).

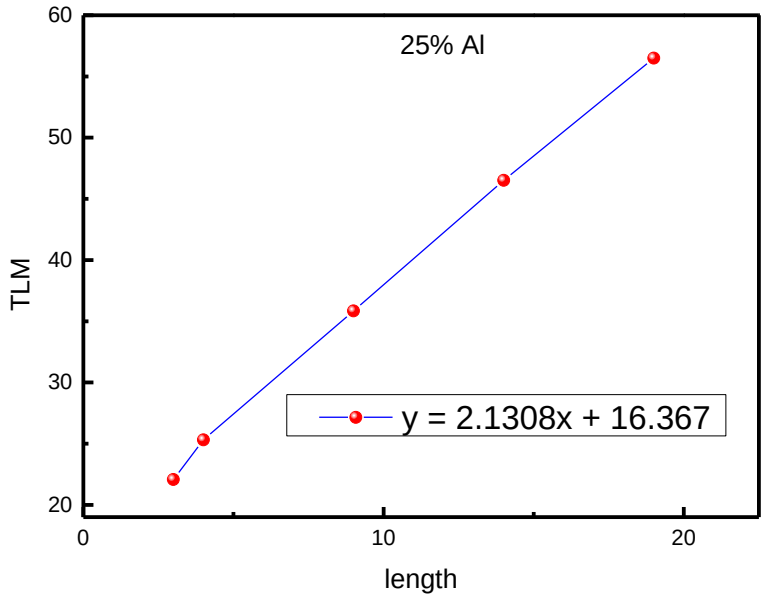
25% Al
TLM
length
y = 2.1308x + 16.367
60
50
40
30
20
0
10
20

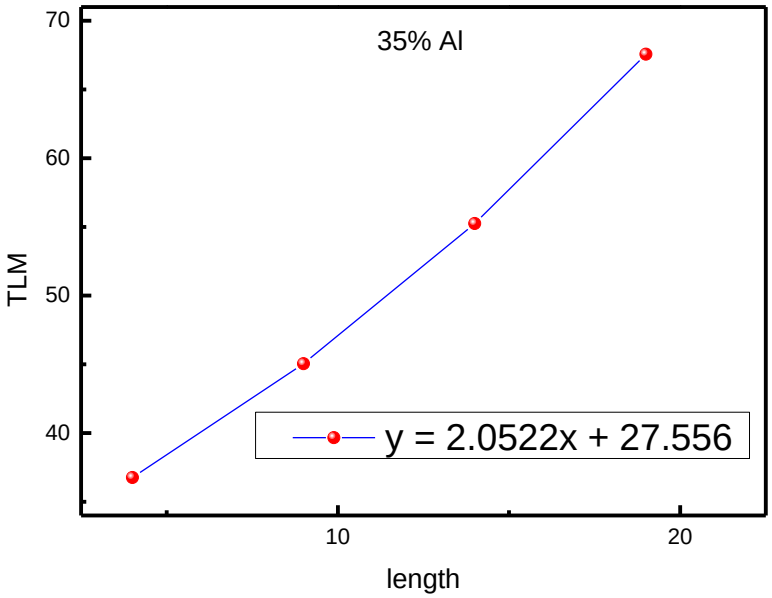
35% Al
TLM
length
y = 2.0522x + 27.556
70
60
50
40
10
20

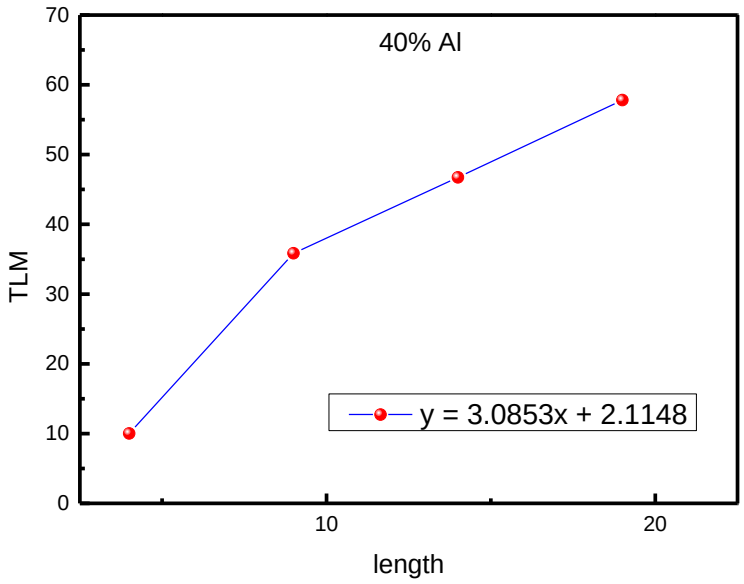

Figure 2-6 Ohmic test with Al content 25%,35% and 40%

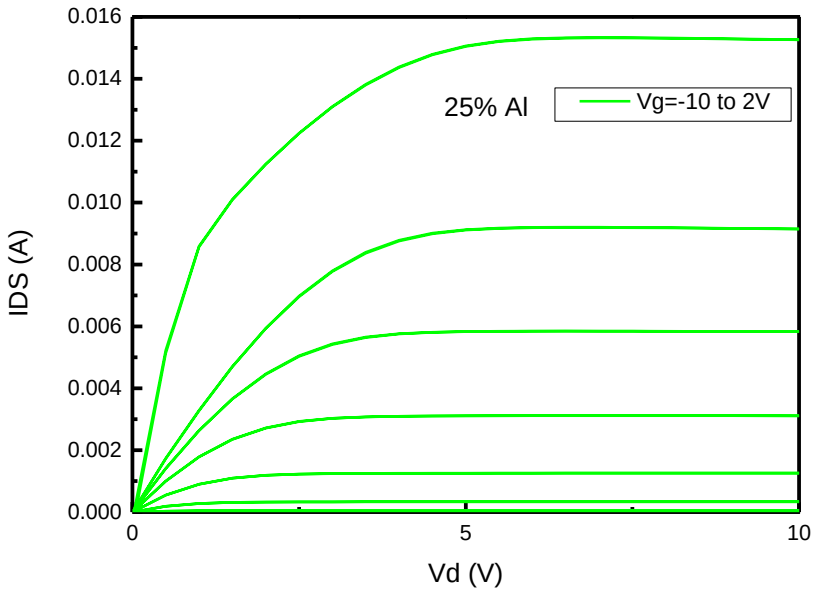

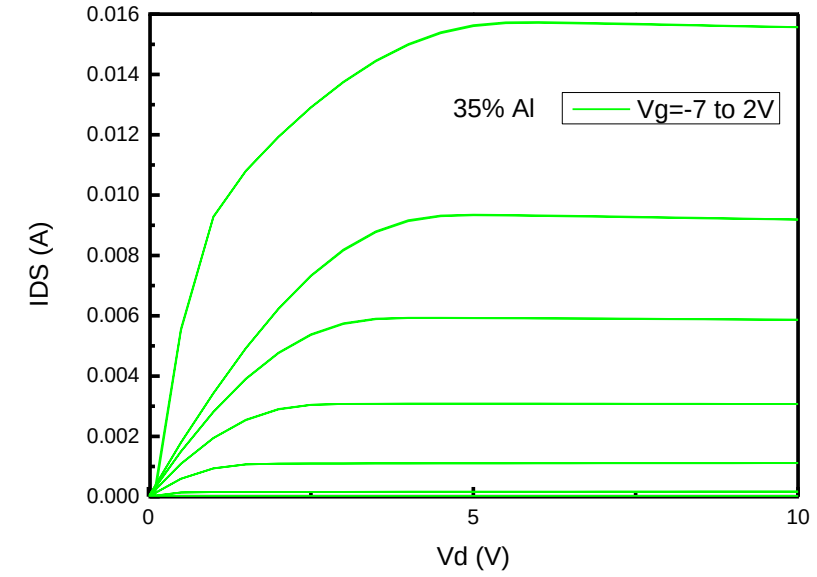

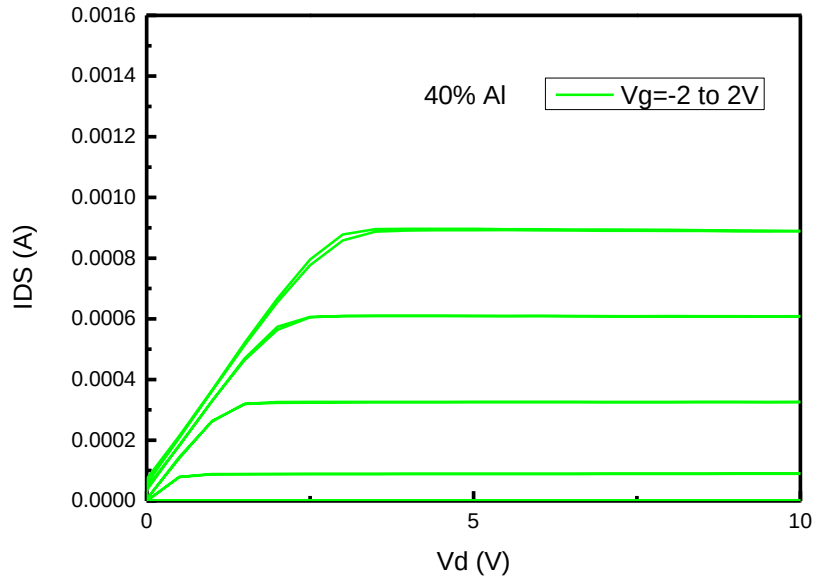

Figure 2-7 HEMT Vd-Id test with Al content 25%,35% and 40%

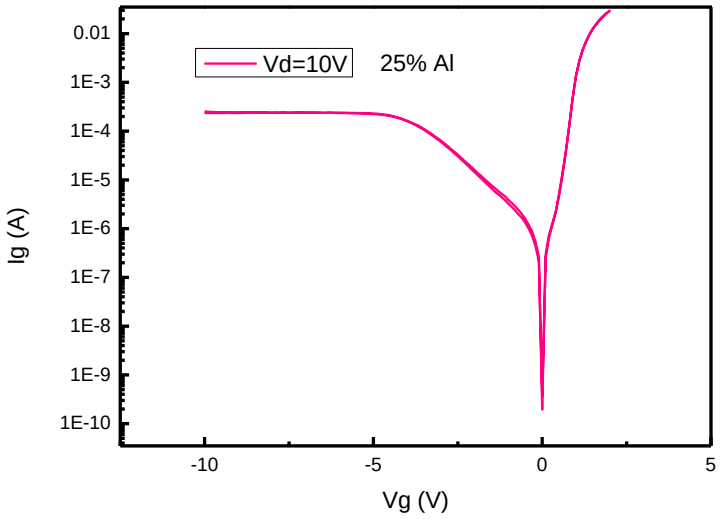
Vd=10V
25% Al
Ig (A)
0.01
1E-3
1E-4
1E-5
1E-6
1E-7
1E-8
1E-9
1E-10
-10
-5
0
5
Vg (V)

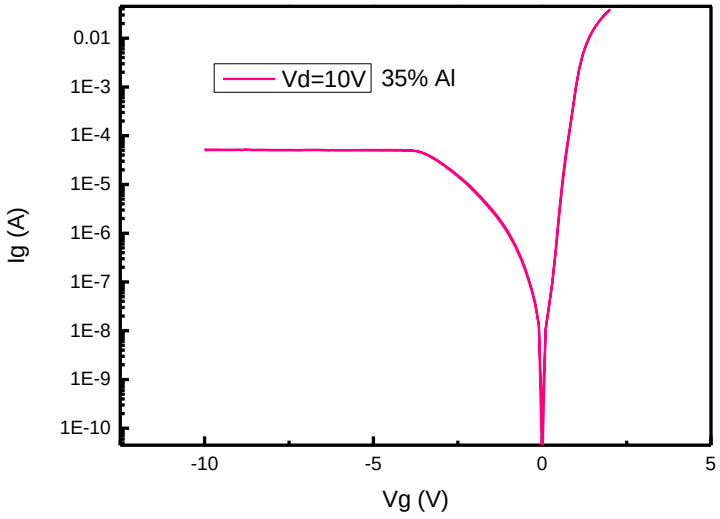
Vd=10V
35% Al
Ig (A)
0.01
1E-3
1E-4
1E-5
1E-6
1E-7
1E-8
1E-9
1E-10
-10
-5
0
5
Vg (V)

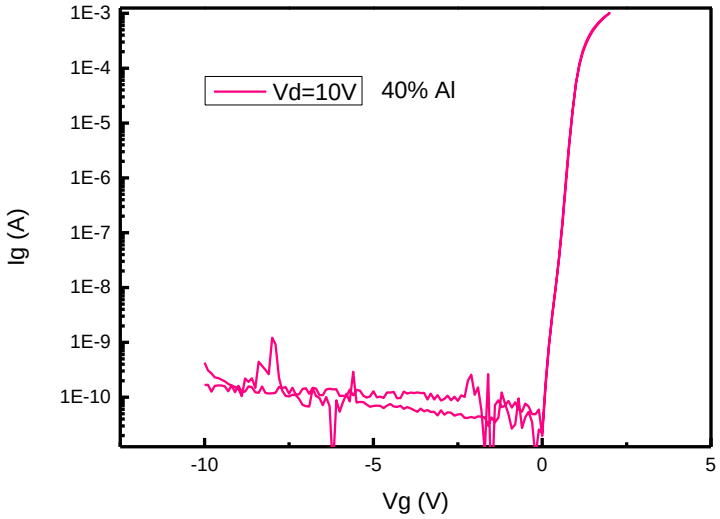
Vd=10V
40% Al
Ig (A)
1E-3
1E-4
1E-5
1E-6
1E-7
1E-8
1E-9
1E-10
-10
-5
0
5
Vg (V)

Figure 2-8 HEMT Vg-Ig test with Al content 25%, 35% and 40%

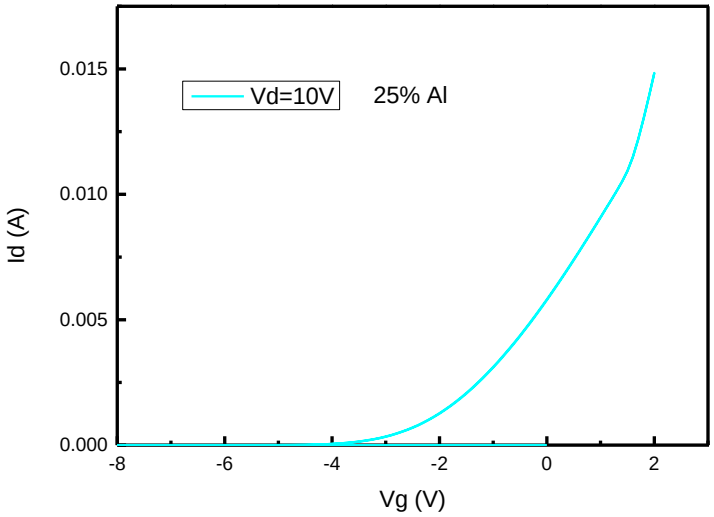

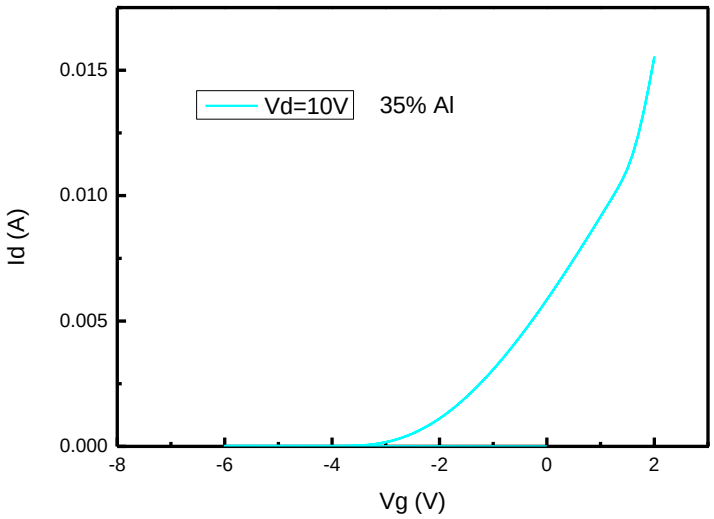

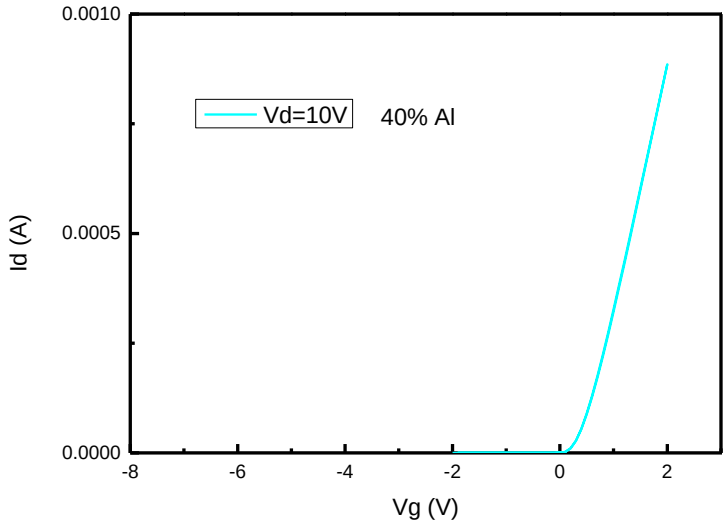

Figure 2-9 HEMT Vg-Id test with Al content 25%, 35% and 40%

After packaging the device (Figure 2-10), we set up a pH sensing system shown in Figure 2-11. We tested the Id-Vd curves (Figure 2-12) and the sensing performance of the sensors with different Al content in different solutions (Figure 2-13):

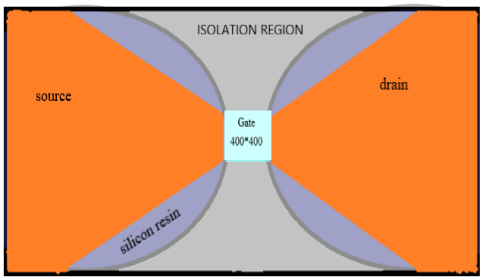

Figure 2-10 Packing structure of pH sensor

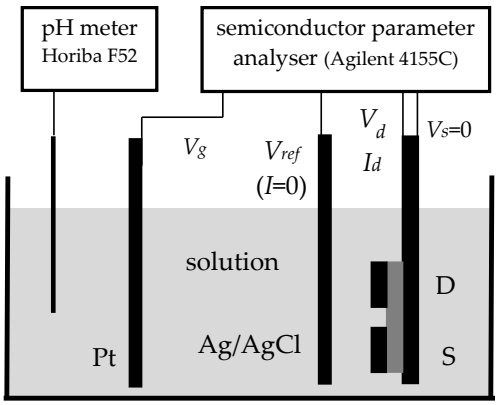

Figure 2-11 The pH sensing system

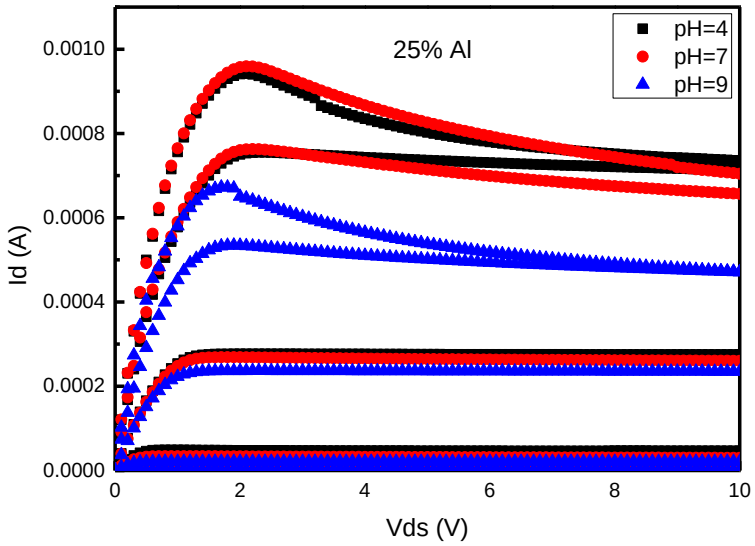
25% Al
pH=4
pH=7
pH=9
Id (A)
Vds (V)
0.0000
0.0002
0.0004
0.0006
0.0008
0.0010
0
2
4
6
8
10

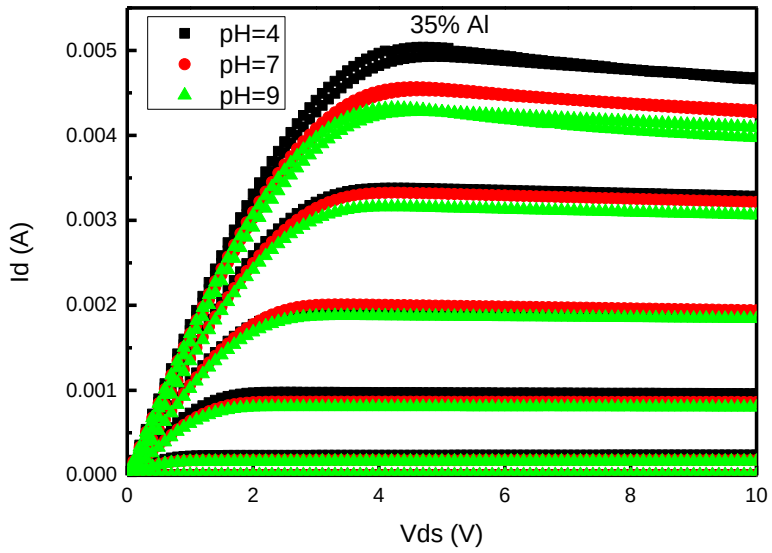
35% Al
pH=4
pH=7
pH=9
Id (A)
Vds (V)
0.000
0.001
0.002
0.003
0.004
0.005
0
2
4
6
8
10

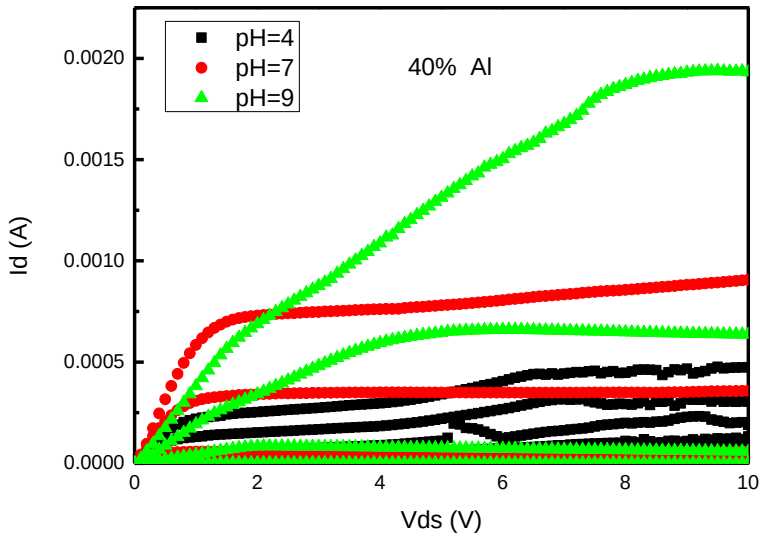

Figure 2-12 Id-Vd test of sensors with Al content 25%,35% and 40%

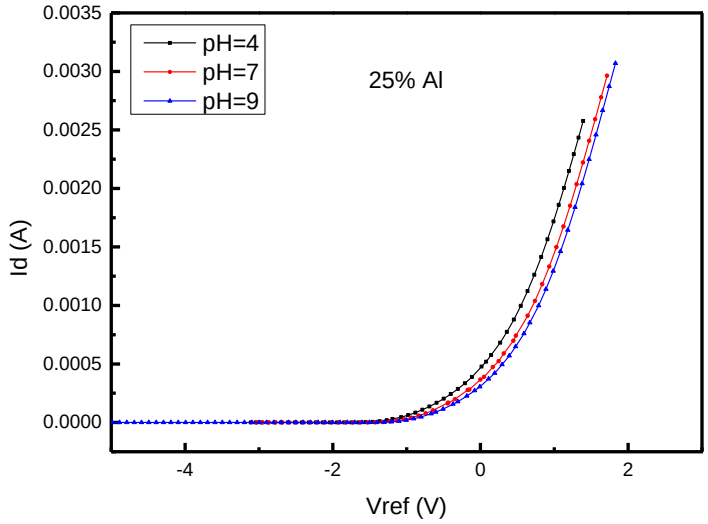

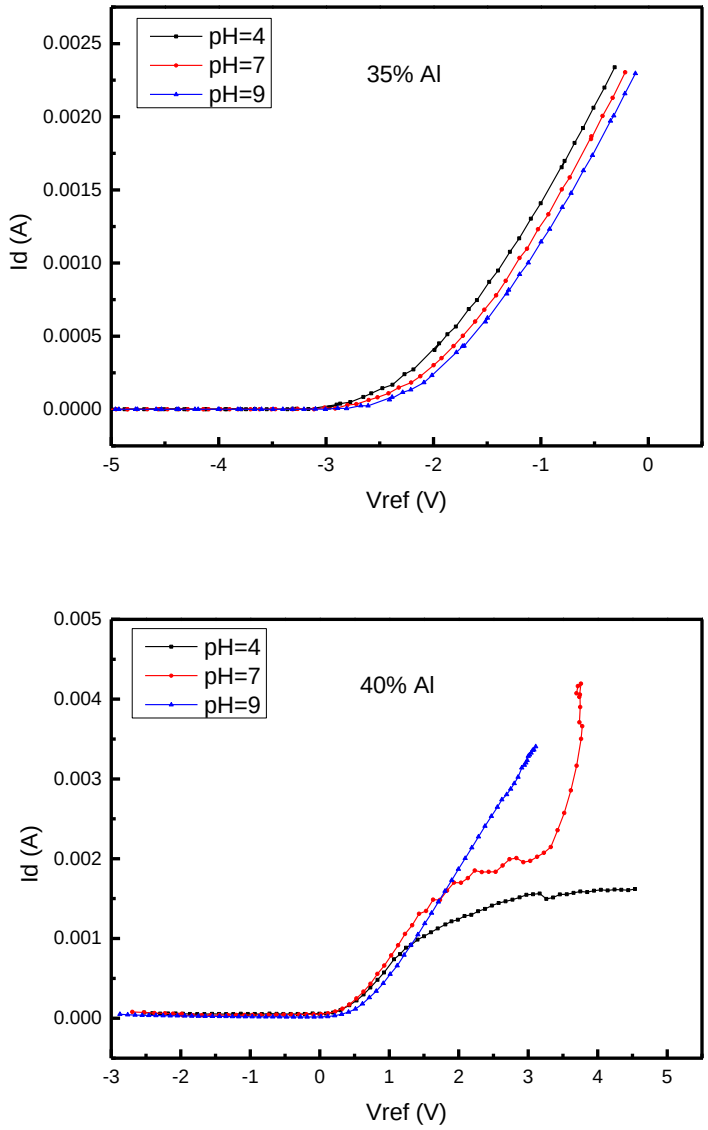

Figure 2-13 Sensing performance test of sensors with Al composition 25%, 35% and 40%

All the HEMT samples have good Vds-Id curves. 25% and 35% Al content sensor samples have good Vg-Ig curve while 40% Al content sensor sample has bad Vg-Ig curve (Figure 2-13) due to the different structures. There is only a 7 nm $Al_{0.4}Ga_{0.6}N$ layer without any transition layer in 40% Al content samples so that the lattice mismatch is much and the 2DEG concentration is too low. We compared the characteristics of sensors with 25% and 35% Al content only.

The pH surface sensitivity (S_V) is defined as the measured surface potential change divided by the pH value change ($\triangle V/pH$). From the transfer characteristics of the sensor at the drain voltage of 10 V in the different solution, we extracted the sensitivity of the pH sensor. The voltage vs the Ag/AgCl electrode can be extracted at

the same drain current such as Id=300 μA for 35% Al composition and Id=120 μA for 25 Al composition under different pH values. From the slope of the V-pH plot, we can obtain the pH surface sensitivity.

We also obtained the current sensitivity defined as $S_A=S_V*G_M$. We read the currents at the same voltage to find the maximum current difference. (V_{ref}=-1.0 V for 35% Al composition and V_{ref}=1.3 V for 25% Al composition).

The pH sensor based on AlGaN/GaN heterostructure with high Al content (35%) in the barrier layer with a 16 nm transition layer of 25% Al content shows better surface sensitivity (S_V) of 56.01 mV/pH, which is bigger than that (53.94 mV/pH) of the sensor with 25% Al content, but worse current sensitivity S_A (-0.09544 mA/pH Vs -0.10166 mA/pH).

Both this pH surface sensitivity S_V and current sensitivity S_A are obtained in the lab test with analyzer by voltage sweeping. In the actual measuring application, it is not easy to scan the voltage to make the same current. Therefore, we need to use other characteristic to realize the measurement.

In general, we can fix the gate voltage (not Vref) and the drain voltage to find the relationship between the drain-source current and the pH value of the solution. As in figure 2-12, we get the curve without the reference electrode, therefore, if we can find the relationship between the current and the pH, we can get a method to measure the pH of solution in application. As in figure 2-12, if we chose Vg=0 V and Vd=2 V, even the biggest pH (14) would be in linear region. Read these three current values, we can obtain the relationship between the current and the pH value. We find the relationship between the drain current and the pH value is linear. We define a NEW sensitivity S, which describes the relationship between the drain current and the pH of the solution in the linear region of the sensor as the reference electrode useless. S=-0.058 mA/pH when the drain voltage is 2.0 V and gate voltage (electrode in the solution) is 0V. It is very useful in application.

If we shift the drain voltage to 2.8V, the relationship is still linear, we can get a bigger S (absolute value) =-0.084 mA/pH (figure 10). Only if we assure it is still in linear region even the biggest pH=14, we can continue to shift the drain voltage to get bigger S.

§2.5. Surface stability in the alkaline solution

The effect of the SB (stack barrier) structure on the electrical properties of 2DEG channel was evaluated by the Schottky-gated heterostructure field-effect transistors (HFET) device. The nominate length and width of the Ni/Au gate are 8 and 50 μm, respectively. Figure 2-14 shows the output *I-V* and transfer characteristics of HFETs with CB and SB structures. Both kinds of device present good pinch-off characteristics when the gate voltage range from -5 to 1 V (1 V/step). Compared with the CB-HFET, the SB-HFET shows a relatively high maximum drain current density at the same gate-source voltage (Figure 2-14a), while the threshold voltages are comparable (Figure. 2-14b). Therefore, we assume that the SB structure shows slight influence on the 2DEG density (threshold voltage) and the discrepancy between output current is ascribed to the slightly difference in uniformity and/or source/drain ohmic contact resistance.

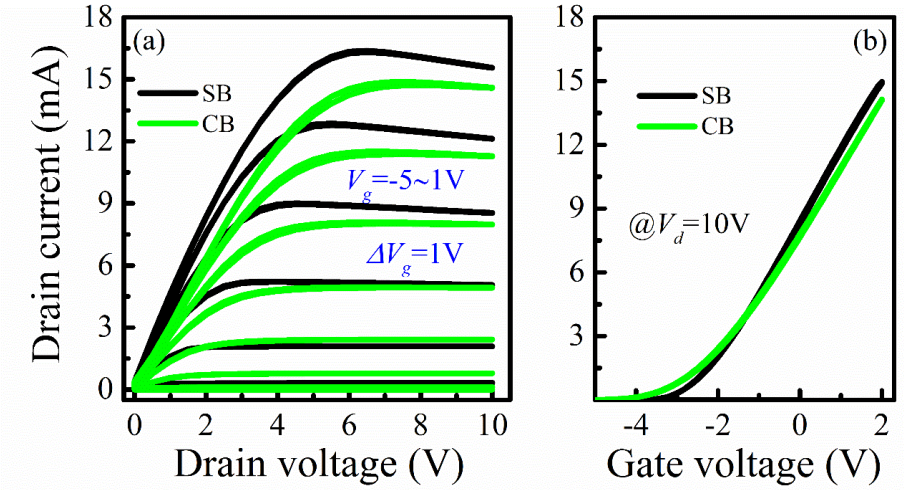

Figure 2-14 Drain current-voltage (a) and transfer (b) characteristics of the CB- and SB-HFET with metal gate under different gate voltage.

Figure 2-15 shows the output *I-V* and transfer characteristics of ISFETs with stacked barrier structure. The *I-V* curves were measured in three kinds of solutions (pH values of approximately 4, 7 and 9, respectively) with different reference-voltages (V_{ref}). The SB-ISFETs present good pinch-off characteristics when the V_{ref} ranges from -5 to 0 V (1 V/step), with the output current decreasing with the pH value increasing. The possible reason is ascribed to the slightly positive shift of the threshold voltage, which is consistent with the transfer characteristics shown in Figure.2-15b. It demonstrates that the variation of pH value of the detection solution modulates the surface potential, resulting in the change of 2DEG density (threshold voltage) of the ISFETs pH sensor [14]. In addition, the pH sensitivity of the ISFETs is defined as the voltage shift versus pH value at a current level of 4 mA, which can be calculated from the pH dependent transfer characteristics (inset of Figure. 2-15b). The deduced sensitivity is approximately 55.5 mV/pH, which is very close to the room temperature Nernstian limit of 58.7 mV/pH.

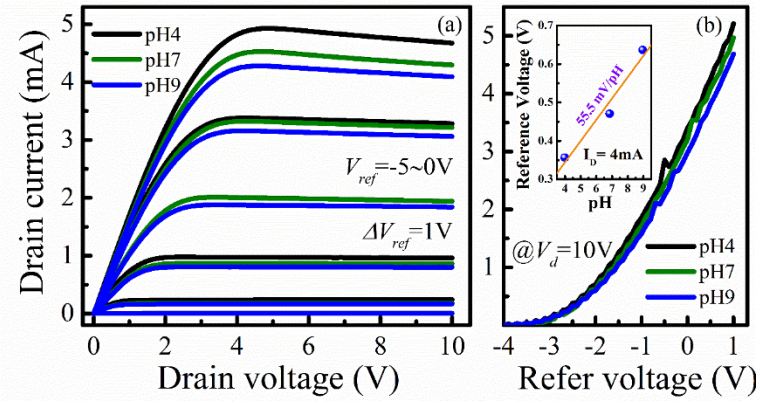

Figure 2-15 The output (a) and transfer (b) characteristics for ISFETs. Inset of (b) the corresponding pH sensitivity deduced at a drain current of 4 mA.

The above measurements could be repeated in the acid and neutral solutions except alkaline solutions. To reveal the surface reliability of the AlGaN/GaN pH sensors, the transfer characteristics of the sensor were recorded in alkaline solution for five times. Obviously, the transfer curve presents an obvious positive shift with the increasing test time (Figure 2-16a). In addition, the drain current also shows a decrease trend along with the increasing test time. The threshold voltage of the device (defined at the current level of 1 mA) was recorded and plotted versus test time, as shown in Figure 2-16b. The variation of threshold voltage increases from approximately -1.6 V to approximately -0.8 V, which doubly confirms the positive shift of transfer curve (Figure 2-16a). Generally, the positive shift of threshold voltage for an AlGaN/GaN structure is caused by the reduce of 2DEG density [15, 16] The absorption of surface negative charge as well as the decrease of AlGaN thickness are the possible reasons for this phenomenon.

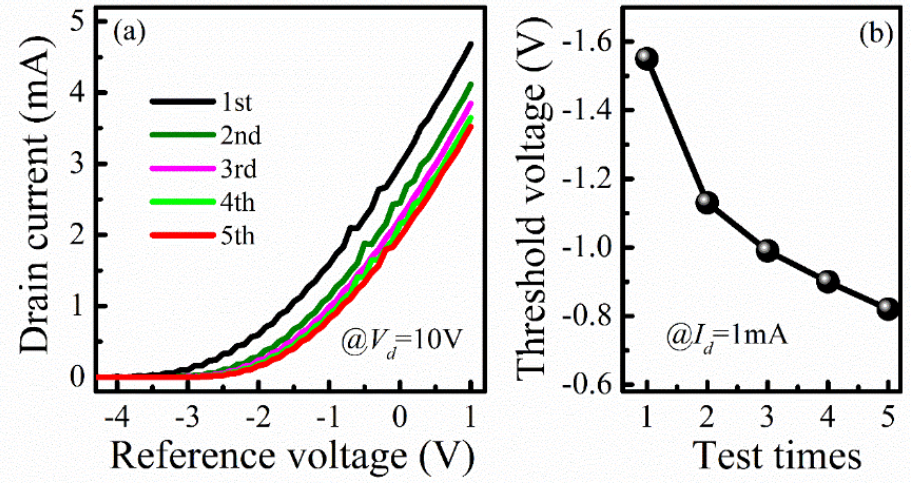

Figure 2-16 The transfer curves of pH sensor recorded for five different times (a). The deduced threshold voltages at drain current of 1 mA were plotted versus test times (b)

Test results showed the bulk voltage fluctuation in alkaline solution, while the voltage applied to the click is unidirectional. The Vref-time curve obtained in tests also showed obvious fluctuation in alkaline solution. As shown in Figure 2-17, the frequency and amplitude of Vref fluctuation increased significantly with the increase of pH value. There should be some kind of reaction, which is related to the concentration of hydroxyl ion.

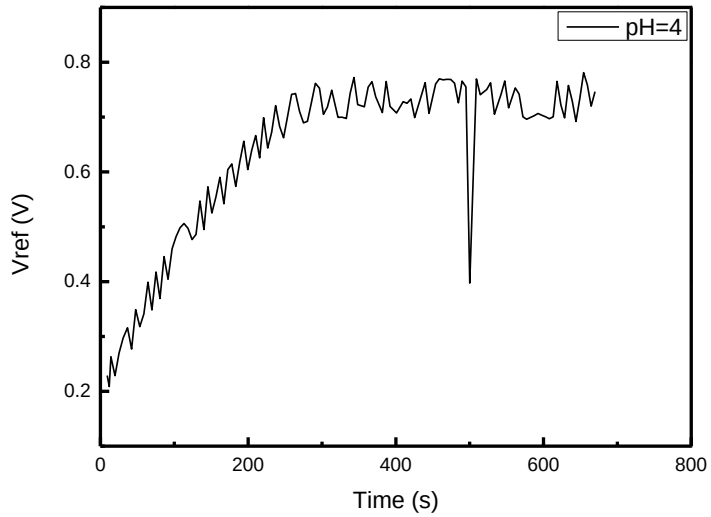

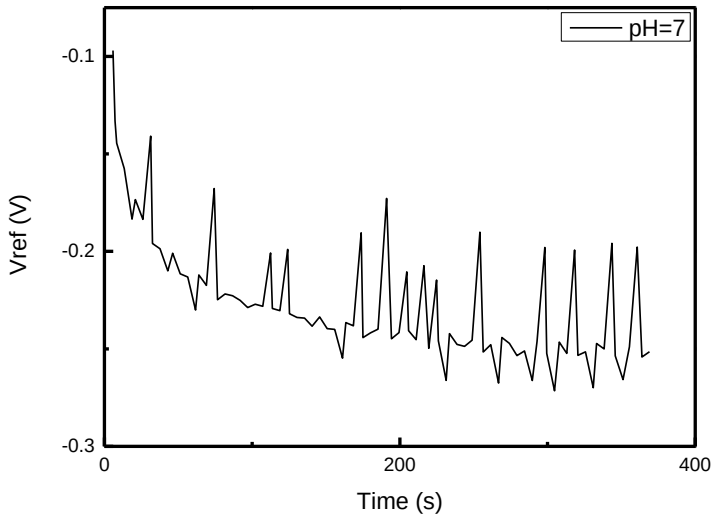

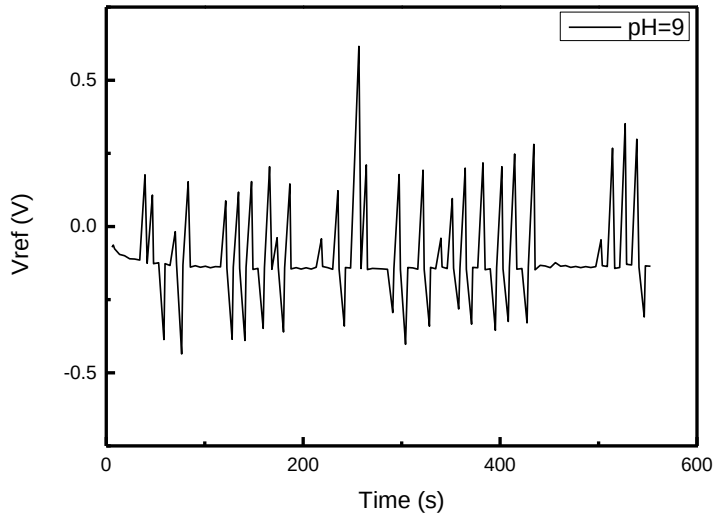

Figure 2-17 The frequency and amplitude of Vref fluctuation in different solutions

To further evaluate the mechanism of the shift on threshold voltage in alkaline solutions, we firstly measured the surface morphologies of the device before and after alkaline sensing by high-resolution scanning electron microscopy (SEM), as shown in Figure 2-18. It is clearly observed that the device shows a homogeneous and smooth surface before alkaline sensing, excepting a few thin Au nanoparticles sprayed to enhance the electrical conductivity for SEM measurement. On the other hand, the sample after the alkaline sensing displays a poor surface with many reaction residuals. Obvious pits with hexagonal shape were observed on the surface after cleaning (inset of Figure 2-18b), which can be attributed to the wet etching on the surface. Generally, there are three main types of morphologies correlated with different dislocations in GaN-based materials. After etched by alkaline solution, the pure screw-type (α-type), pure edge-type (β-type), and mixed-type dislocations (γ-type) present a trapezoidal shape, triangular shape, and combination of triangular and trapezoidal shapes, respectively [17]. All the three kinds of shapes are clearly observed in our experiment, which confirms the etching effect of the dislocations during alkaline sensing.

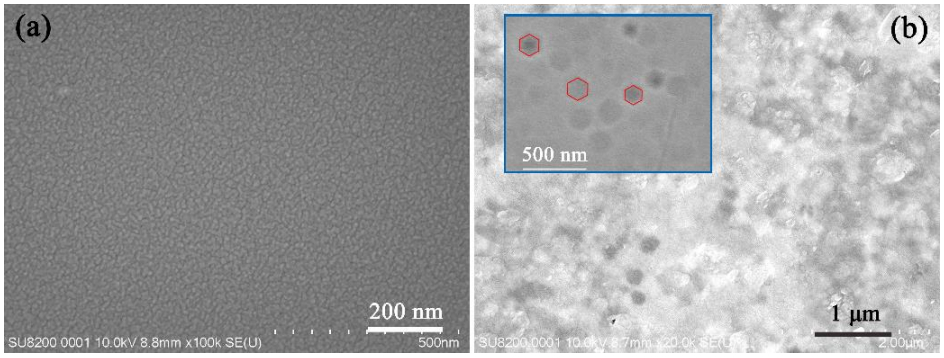

Figure 2-18 SEM images of device surface before (a) and after (b) pH sensing. Inset of (b) is the zoom-in view of the etched dislocations. The typical dislocations were marked with red hexagonal

X-ray photoelectron spectroscopy (XPS, ESCALAB 250Xi, made in USA) was tested on the sensing region by using an incident monochromatic X-ray beam from the Al target. The C-C bond peak of 284.8 eV as a reference and the spot size is about 900 μm. The core level (CL) spectra of Ga3d as well as the Al2p for GaN material is shown in Figure.2-19. Three peaks can be fitted in Ga3d spectrum before and after alkaline sensing (Figure 2-19a), including N2s (at around 17.4 eV), Ga-N (at around 19.6 eV) and Ga-O (at around 19.8 eV) bonding [18]. However, the intensity of the Ga3d spectrum decreases slightly after alkaline sensing measurement. In addition, the Ga-N bonding dominates the spectrum of the sample before alkaline sensing while Ga-O became domination after alkaline sensing as shown in inset of Figure 6a. On the other hand, drastic intensity decrease was observed for the CL spectra of Al2p (Figure 2-19b). Therefore, the decrease of Al element is much significant than that of Ga. Taking into accounting that the detection depth of XPS is approximately 10~20 nm, the variation of chemical component mainly occurs in the upper AlGaN thin layer.

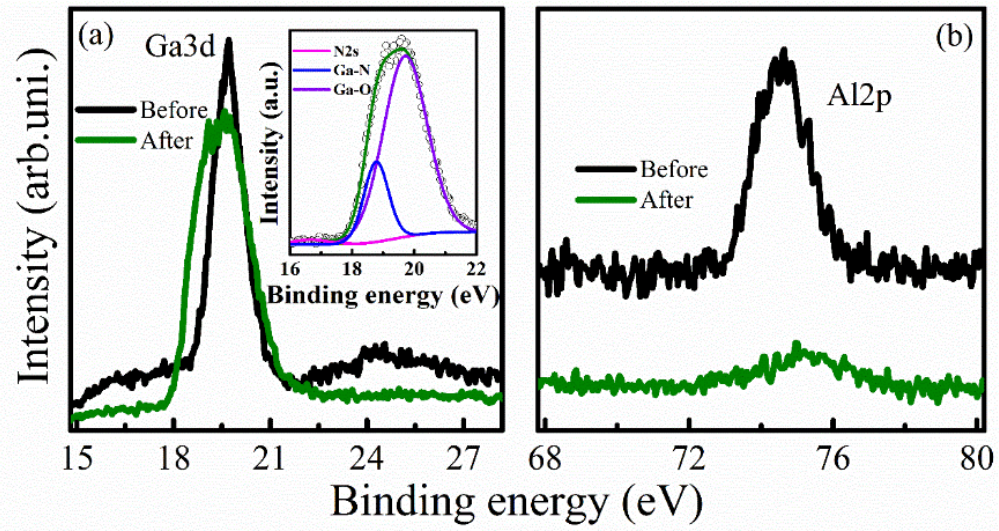

Figure 2-19 The Ga3d and Al2p XPS spectra of the AlGaN/GaN pH sensor before and after pH sensing. Inset of (a) shows the fitting curve of Ga3d spectrum after pH sensing

The sensing region after 5 times measurements was further investigated by transmission electron microscopy (TEM) and energy dispersive X-ray spectroscopy (EDX). It is clearly observed that many voids with a size of approximately 100 nm present on the cross-section of device (Figure 2-20a). It worth noting that the size of the void is comparable with that of the etched dislocation in the SEM picture. The typical void (marked as region 1) was enlarged and shown in Figure 2-20b. The AlGaN/GaN interface exhibits excellent abruptness with the thickness of AlGaN barrier is approximately 25 nm, which is consistent with the nominate thickness of our structure. Furthermore, the element distribution of the device is displayed in Fig2-20c-f. Obviously, the generation of voids will cause the loss of Ga and Al, which is attributed to the decrease intensity of XPS spectra as shown in Figure 2-19. Especially, the Al content only residual on the un-etched barrier region. Then, the intensity of the Al spectrum nearly disappears after alkaline sensing. Furthermore, the oxygen segregates in the void region, implying the oxidation of GaN-based material before dissolution.

Combining the electrical and material characteristics above, the possible degradation mechanism can be discussed as follows. In previous works, the electrochemical (EC) method was adopted to realize a recessed-gate scheme for obtaining normally-off GaN power device [19, 20]. The AlGaN barrier can be etched away by the cyclic anodic oxidation and subsequent dissolution of the resulted oxide in an electrolyte [21]. Generally, the dislocation terminal on the surface introduces high density of dangling bonds and lattice defects compared with the perfect lattice.

Then, the chemical activity around the dislocation is much higher and more easily oxidized when contact with the electrolyte [22, 23]. During the alkaline sensing measurements, the electrical stress on drain and sensing region enhance the transformation of AlGaN around dislocation region into oxide. Then, the alkaline solution dissolves the oxide and generates the void in GaN-based material. Therefore, the surface electrochemical reactions can destroy the 2DEG channel, resulting in the positive threshold voltage shift and the decreasing output current.

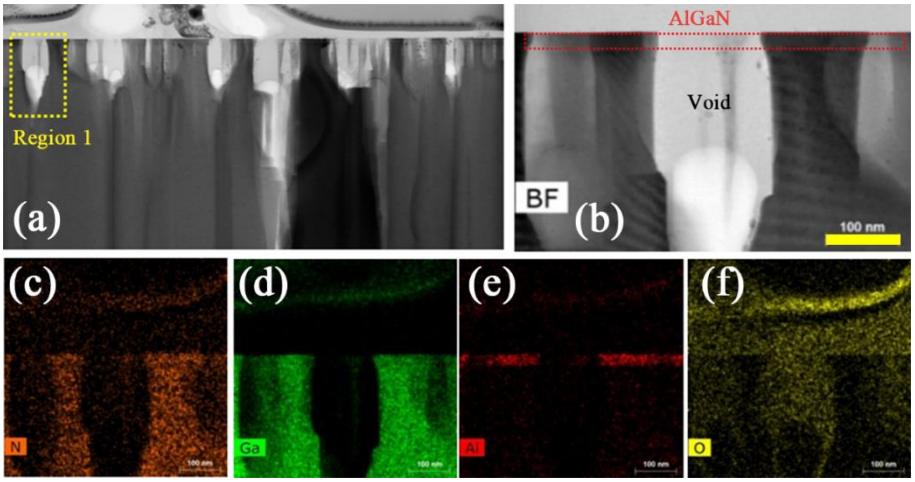

Figure 2-20 The cross-section TEM image (a) and the zoom-in picture of region 1 of the device after 5 times pH sensing. (c)-(f) are the EDX mapping images of the N, Ga, Al, and O content.

The device performance and degradation mechanism of the AlGaN/GaN ISFETs with stacked high Al-content AlGaN barrier have been investigated. It demonstrates that the AlGaN/GaN ISFETs present good pinch-off characteristics in three kinds of solutions, showing a sensitivity of approximately 55.5 mV/pH. However, threshold voltage increases from approximately -1.6 V to approximately -0.8 V when measured in alkaline solution for 5 times, along with a decreasing output current. The high-resolution SEM photos show that there are high density hexagonal pits with the size of approximately 100 nm on the device surface, presenting the etching effect of the dislocations during alkaline sensing. The XPS demonstrated that the intensity of the Ga3d and Al2p spectra decreases after pH sensing measurement, implying the variation of chemical component occurs in the upper AlGaN thin layer. Furthermore, many voids with a size of approximately 100 nm were observed from the TEM pictures, which is comparable with that of the SEM. Combining with the EDX, the degradation in electrical performance can be attributed to the transformation of AlGaN into oxide as well as the followed alkaline solution dissolve.

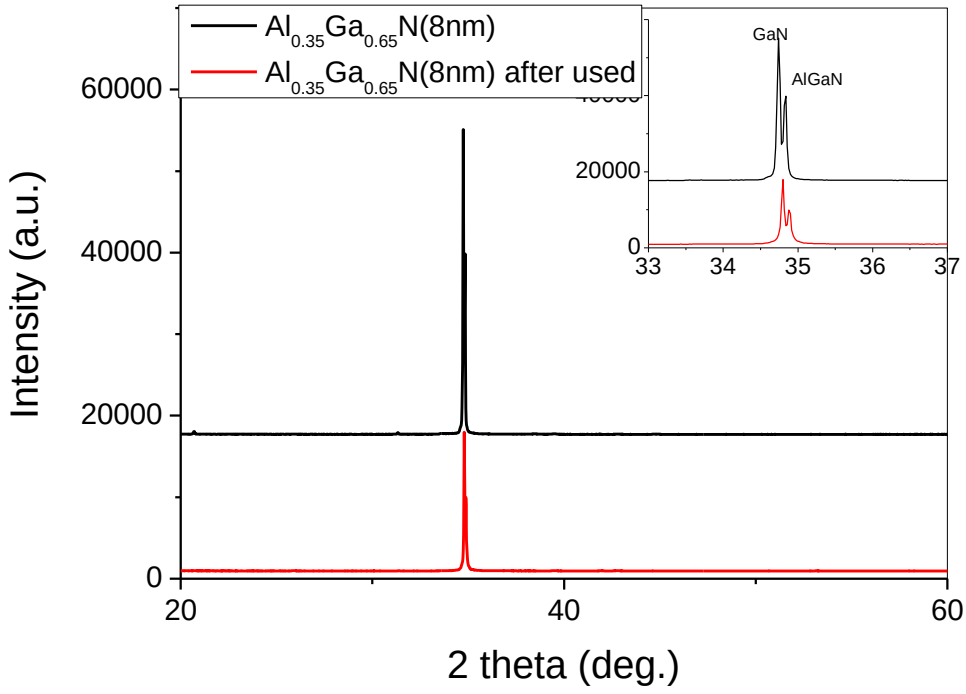

Figure 2-21 XRD patterns of $Al_{0.35}Ga_{0.65}N$(8nm)/$Al_{0.25}Ga_{0.75}N$(16nm) before and after used.

As can be seen in Figure 2-21, a peak located at ~34.8° was identified in both the samples, corresponding to the (002) plane of GaN or AlGaN. Furthermore, the peak is made up of two sharp peaks (see the insert), of which the right one could be assigned to AlGaN due to its smaller lattice distance than GaN. Even after used, the phase of AlGaN could be observed clearly in the XRD pattern of the sample. It demonstrates that AlGaN remains in the sample, although a small part of Al might be dissolved into the solution.

We have the following analysis on the material reaction process. AlN component within AlGaN layer of the electrode eroded in H_2O through intricated hydrolyzed procedures according initially with Equation A [24],

(A: $AlN + 2H_2O \rightarrow AlOOH(amorphous) + NH_3$

An amorphous porous boehmite layer with stoichiometry similar to AlOOH was formed on the surface of the electrode; Ammonia molecules ($NH_3 \bullet H_2O$) originated from Equation B

(B: $NH_3 + H_2O \rightarrow NH_3 \bullet H_2O$)

Ammonia molecules ionize in water as Equation C

(C: $NH_3 \bullet H_2O \rightarrow NH_4^+ + OH^-$)

So a certain amount of hydroxide ions is generated in solution. Therefore, along with these two reactions go on the concentration of the OH^- of the system turn gradually higher and higher, as long as the concentration of the hydroxide reach/over a certain threshold (e.g. $[OH]^-$ amount larger than three times of Al component perhaps) the AlOOH(amorphous) above-mentioned coverage on the electrode surface is transformed possibly followed Equation D

(D: $AlOOH_{amporo} + H_2O \xrightarrow{OH^-} Al(OH)_3$) into $Al_2O_3 \cdot 3H_2O$

hydrated alumina as the following of bayerite, gibbsite, nordstrandite etc. The electrode surface is constantly impacted and rinsed by water molecules a part of AlOOH and $Al(OH)_3$ small paticles positioned on the electrode wash off into solution forming Alumina hydrate sol [25, 26, 27]. As time goes by the AlN constitutes of AlGaN of the surface film is gradually eroded and loses its protective effect on the surface. In turn, the AlN among AlGaN directly contacted with water molecules, and the above processes again and again to form aluminum hydroxide colloid in the aqueous electrolyte solution [28]. As we know that the surface of $Al(OH)_3$ nanoparticles with much positive charges, this means that in water series when pH is higher than 7 the overmuch hydroxide ion makes the $Al(OH)_3$ colloid sol-gel process. Given adequate pH value $Al(OH)_3$ gelatin may precipitate out from the solution [29].

§2.6. Conclusions

As pH sensors, AlGaN/GaN ion-sensitive field-effect transistors (ISFETs) with stacked and high Al-content AlGaN barrier have been fabricated to evaluate the sensing ability and surface reliability. It demonstrates that the stack barrier shows mild influence on the two-dimensional electron gas channel. In addition, the AlGaN/GaN ISFETs present good pinch-off characteristics in three kinds of solutions with different pH values, showing a sensitivity of approximately 55.5 mV/pH. However, threshold voltage shifting as well as the output current decreasing was observed after worked in alkaline solution. The surface analysis results confirm that the surface was electrochemical etched into many voids, resulting in a positive shift on the threshold voltage. This etching process is related to the surface oxide and dislocation on the high Al-content AlGaN barrier layer. Therefore, the degradation in electrical performances can be attributed to the transformation of AlGaN into surface oxide as well as the followed dissolution in alkaline solution.

§2.7. References

[1] P. Bergveld, Development of an Ion-Sensitive Solid-State Device for Neurophysiological Measurements, IEEE Trans. Biomed. Eng. BME-17 (1970) 70-71.

[2] L. Chiang, Y. C. Chen, J. -C. Chou, Simulation and Experimental Study of the pH-Sensing Property for AlN Thin Films, Jpn. J. Appl. Phys. 40 (2001) 5900-5904.

[3] J. Schalwig, G. Muller, M. Eickhoff, O. Ambacherand, M. Stutzmann, Gas sensitive GaN/AlGaN-heterostructures, Sens. Actuat. 87 (2002) 425-430.

[4] M. Eickhoff, J. Schalwig, G. Steinhoff, O. Weidemann, L. Görgens, R. Neuberger, M. Hermann, B. Baur, G. Müller, O. Ambacher, M. Stutzmann, Electronics and sensors based on pyroelectric AlGaN/GaN heterostructure, phys.stat.solidi. 0 (2003) 1908-1918.

[5] R. E. G. van Hal, J. C. T. Eijkel, P. Bergveld, A general model to describe the electrostatic potential at electrolyte oxide interfaces, Adv. Colloid Interface Sci.69 (1996) 31-62

[6] H. Y. Liu, W. C. Hsu, W. F. Chen, C. W. Lin, Y. Y. Li, C. S. Lee, W. C. Sun, S. Y. Wei, S. M. Yu, Investigation of AlGaN/GaN Ion-Sensitive Heterostructure Field-Effect Transistors-Based pH Sensors with Al2O3 Surface Passivation and Sensing Membrane, IEEE Sens. J., 16 (2016) 3514–3522.

[7] N. Maeda, M. Hiroki, N. Watanabe, Y. Oda, H. Yokoyama, T. Yagi, T. Makimoto, T. Enoki, T. Kobayashi, Systematic study of insulator deposition effect (Si_3N_4, SiO_2, AlN, and Al_2O_3) on electrical properties in AlGaN/GaN heterostructures, Jpn. J. Appl. Phys., 46 (2007) 547-554.

[8] R. M. Lin, F. C. Chu, A. Das, S. Y. Liao, V. C. Su, Improved device performance of GaN/AlGaN high-electron-mobility transistor using PdO gate interlayer, Jpn. J. Appl. Phys., 52 (2013) 111002.

[9] L. Wang, Y. Bu, J. -P. Ao, Effect of oxygen plasma treatment on the performance of AlGaN/GaN ion-sensitive field-effect transistors, Diam. Relat. Mater., 73 (2017) 1–6.

[10] L. Wang, Y. Bu, L. Li, J. -P. Ao, Effect of thermal oxidation treatment on pH sensitivity of AlGaN/GaN heterostructure ion-sensitive field-effect transistors, Appl. Surf. Sci. 411 (2017) 144–148.

[11] L. Wang, L. Li, T. Zhang, X. Liu, J.-P. Ao, Enhanced pH sensitivity of AlGaN/GaN ion-sensitive field effect transistor with Al2O3 synthesized by atomic layer deposition, Appl. Surf. Sci. 427 (2018) 1199–1202.

[12] Y. Maeda, K. Niigata, K. Narano, L.Wang, J.-P. Ao, Surface Dependence of pH Sensor on AlGaN/GaN Heterostructure, ECS Trans. 61 (2014) 65-71.

[13] K. Jones, T. Chow, M. Wraback, M. Shatalov, Z. Sitar, F. Shahedipour, K. Udwary, G. S. Tompa, AlGaN devices and growth of device structures, J. Mater. Sci., 50 (2015) 3267–3307.

[14] D. E. Yates, S. Levine, T. W. Healy, Site-binding model of the electrical double layer at the oxide/water interface, J. Chem. Soc. 70 (1974)1807-1818.

[15] L. He, F. Yang, L. Li, Z. Chen, Z. Shen, Y. Zheng, Y. Yao, Y. Ni, D. Zhou, X. Zhang, L. He, Z. Wu, B. Zhang, Y. Liu, High threshold voltage uniformity and low hysteresis recessed-gate Al2O3/AlN/GaN MISFET by selective area growth, IEEE Trans. Electron Devices 64 (2017) 1554.

[16] Q. Wang, Y. Jiang, J. Zhang, K. Kawaharada, L. Li, D. Wang, J. P. Ao, Effects of recess process and surface treatment on the threshold voltage of GaN MOSFETs fabricated on a AlGaN/GaN heterostructure, Semicond. Sci. Technol. 30 (2015) 065004.

[17] L. Sang, B. Ren, M. Sumiya, M. Liao, Y. Koide, A. Tanaka, Y. Cho, Y. Harada, T. Nabatame, T. Sekiguchi, S. Usami, Y. Honda, H. Amano, Initial leakage current paths in the vertical-type GaN-on-GaN Schottky barrier diodes, Appl. Phys. Lett., 111 (2017) 122102.

[18] L. Li, W. Wang, L. He, X. Zhang, Z. Wu, Y. Liu, Determination of band offsets between p-NiO gate electrode and unintentionally doped GaN for normally-off GaN power device, J. Alloys Compd. 728 (2017) 400-403.

[19] C. -T. Lee, Y. -S. Chiu, Gate-recessed AlGaN/GaN ISFET urea biosensor fabricated by photoelectrochemical method, IEEE Sensors J., 16 (2016) 1518-1523.

[20] F. Horikiri, H. Ohta, N. Asai, Y. Narita, T. Yoshida, T. Mishima, Excellent potential of photo-electrochemical etching for fabricating high-aspect-ratio deep trenches in gallium nitride, Appl. Phys. Exp. 11 (2018) 091001.

[21] L. Li, X. Li, T. Pu, Y. Liu, J. -P. Ao, Normally off AlGaN/GaN ion-sensitive field effect transistors realized by photoelectrochemical method for pH sensor application, Superlattices and Microstructures, 128 (2019) 99–104

[22] I. Arslan, N.D. Browning, Role of oxygen at screw dislocations in GaN, Phys. Rev. Lett. 91 (2003) 165501.

[23] M.E. Hawkridge, D. Cherns, Oxygen segregation to dislocations in GaN, Appl. Phys. Lett. 87 (2005) 201.

[24] Chung- daw Young, Jenq-gong Dhu, Corrosion of aluminum nitride substrates in acid alkaline solutions and water, J. Mater. Sci., 1995, 30, 185-195.

[25] Paul Bowen, James G. Highfield, Alain Mocellin, and Terry A, Rin Degradation of Aluminum Nitride Powder in an Aqueous Environmet, J Am. Ceram. Soc., 1990, 73 [3] 724-28.

[26] Alain C. Pierre, Donald R. Uhlmann, Gelation of Aluminum Hydroxide Sols, J. Am. Cerum. Soc., 1987 70 [I] 28-32.

[27] T. N. Wittberg, J. Douglas Wolf, Senpu Wang, Aluminium hydroxide growth on aluminiun surface exposes to an air 1% NO mixture, J. Mater. Sci., 1998, 23, 1745-1747.

[28] S. Fukumoto, T. Hookabe, H. Tsubakino, Hydrolysis behavior of aluminum nitride in various solutions, J. Mater. Sci., 2000, 35 2743 – 2748.

[29] James G. Highfield and Paul Bowen, Diffuse-Reflectance Fourier Transform Infrared Spectroscopic Studies of the Stability of Aluminum Nitride Powder in an Aqueous Environment, Anal. Chem. 1989, 61, 2399-2402.

Chapter 3：Enhanced sensitivity of AlGaN/GaN ISFETs with recessed structure

§3.1. The necessary of recess structure

For AlGaN/GaN-based pH sensors, oxides and nitrides naturally formed on the AlGaN surface can be used to detect H^+ in solution [1]. The sensing mechanism of the solid-state pH sensor is widely accepted as site-dissociation model [2], in which an electrochemical reaction occurs between the surface of the oxides or the native oxides and the solution. In the literature, surface potential sensitivity (Sv) has been used to evaluate the performance of AlGaN/GaN-based pH sensors. Ample reports on increasing S_V by the ways such as H_2O_2 treatment, oxygen plasma treatment [3], thermal oxidation treatment [4], Al_2O_3 synthesized by atomic layer deposition [5], use planar dual gate [6], increasing Al components in AlGaN [7], photoelectrochemical method, and so on. However, according to Nernst theory [8], the limit value of S_V at room temperature is 59.5 mV/pH. In practical applications, the current output and transconductance (G_M) are more effective parameters to integrate with subsequent circuits, where current sensitivity (S_A) is important. And when S_A is used as the evaluation parameter, the reference electrode can be omitted. As we know that $S_A = S_V \times G_M$, when S_V reaches the limit, it is the key to improve G_M. In HEMT devices, the threshold voltage is also an important factor, which can adjust the voltage value corresponding to the maximum transconductance. Recess process is a good way to increase transconductance and adjust V_T both.

§3.2. The fabrication of recess structure pH sensor

New samples were fabricated as in Figure 3-1, the AlGaN/GaN ISFET pH sensor was based on the AlGaN/GaN HEMT structure, which was formed on a Si substrate, followed by a 2.5 μm transition layer, a 1.2 μm GaN:C high resistance layer, a 300 nm GaN channel layer, a 1 nm AlN spacer layer, a 22 nm AlGaN barrier layer with Al content of 24% and a 3 nm GaN cap layer on top. The fabrication process is based on a standard photolithography and lift-off technology [9]. In order to cut off the 2DEG effectively between devices and reduce the surface leakage, BCl_3 /Cl_2 gas was used in the inductively coupled plasma (ICP) system to form mesa isolation. Next, the

Ti/Al/Ni/Au (20/160/55/45 nm) metal stacks were deposited by electron beam evaporation (EBE) as the source (S) and drain (D) electrodes. The ohmic contact was then formed after rapid thermal process (RTP) at 860℃ for 60 s in a nitrogen atmosphere. Finally, a groove with a width of 2 μm and a depth of about 14 nm was etched in the middle of the gate region using BCl_3 /Cl_2 gas in the ICP system. To perform the ammonium hydroxide treatment, some samples were immerged in the ammonium hydroxide for 15 min at 30℃. The devices were packaged on the designed printed circuit boards (PCBs). The source and drain electrodes were led out through the silver wires. Finally, all the conducting areas, except the sensing area, were covered with thick silicone resin to prevent them from contacting the liquid solutions. The sensing area is an open-gate structure with a length of approximately 800 μm and width of 800 μm. The top view is shown in Figure 3-1(b). To avoid the reaction of surface Al with solution, a 3nm GaN cap layer was added. To get higher threshold voltage and G_M, a recessed gate with a width of 2 μm and a depth of about 14 nm was performed.

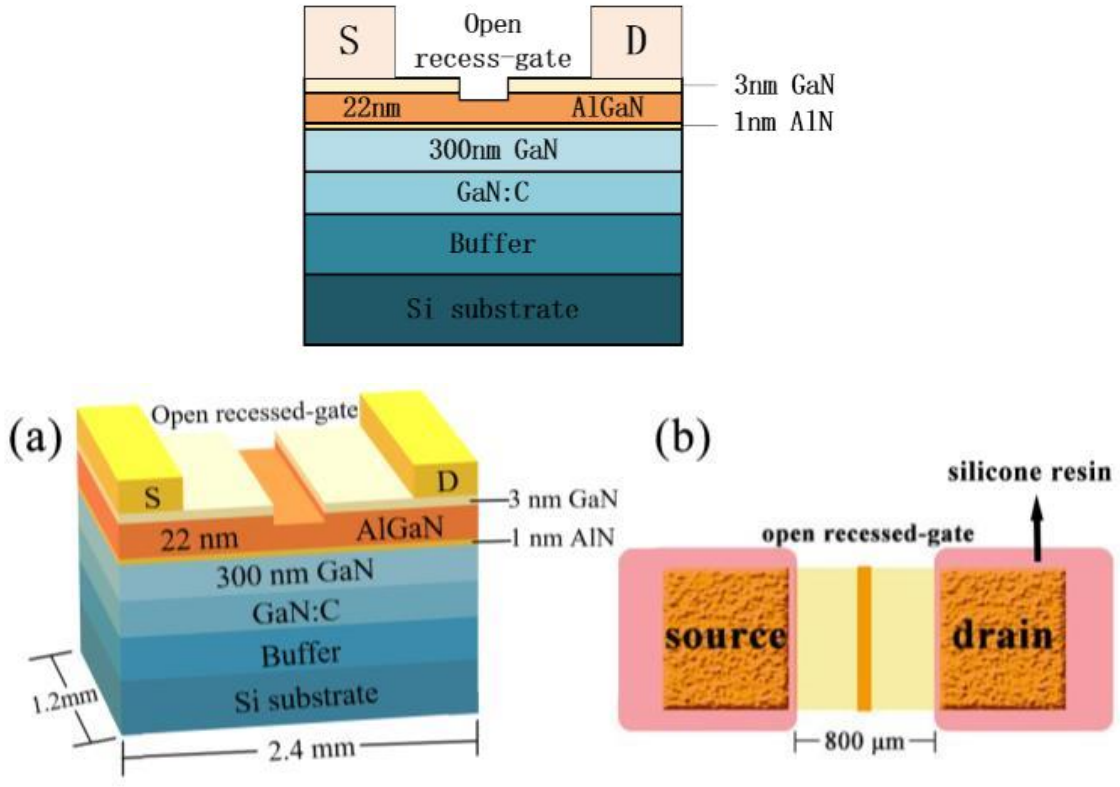

Figure 3-1 (a) Cross-sectional view of a pH sensor on AlGaN/GaN heterostructure; (b) Top view of a pH sensor with silicone resin protection cover.

Three kinds of samples were fabricated without recessed-gate, with

recessed-gate and with both recessed-gate and NH_4OH treatment, respectively. And the basic electrical parameters of the samples were compared such as threshold voltage, G_M, etc. The transfer characteristics of the devices in the same phosphate buffer solutions (PBSs, pH=7) were examined by monitoring I_{DS} with V_G sweeping from -4 to 2 V, and V_{DS} was kept at 10 V. The G_M was calculated from the differential of the transfer curve. The threshold voltage (V_{TH}) of the AlGaN/GaN device was also obtained by the intercept of the curve.

§3.3. Results and Discussion

Figure 3-2 shows the transfer characteristics of the ISFETs in the solutions and the G_M of samples under three different conditions with the drain voltage set at 10 V and the gate voltage scanned from -5 V to 2 V. Compared with the device without recessed-gate, the threshold voltage of the device with recessed-gate has a significant positive shift from -3.33 to -0.31 V, and the maximum transconductance is greatly improved about 150% from 0.8 to 2 mS. The recess process reduced the thickness of the AlGaN gate barrier layer, and the 2DEG concentration below the recess region became lower [10]. Then it needs less voltage to deplete the 2DEG, leading to a positive shift of V_T. Besides, the thinner AlGaN barrier layer increased the gate capacity, which improves the gate control ability and the transconductance G_M. After performing ammonium hydroxide treatment, the threshold voltage has a shift about 0.17 V from -0.31 to -0.14 V, and the transconductance does not change significantly. The etching damage in the dry process often introduces a large number of interface states on the etched AlGaN surface [11]. The interface states are usually n-type defects (such as nitrogen vacancy, V_N). This damage could eventually lead to a negative shift of the threshold voltage. Therefore, the threshold voltage shift after the ammonium hydroxide treatment could account on the remove of the damage.

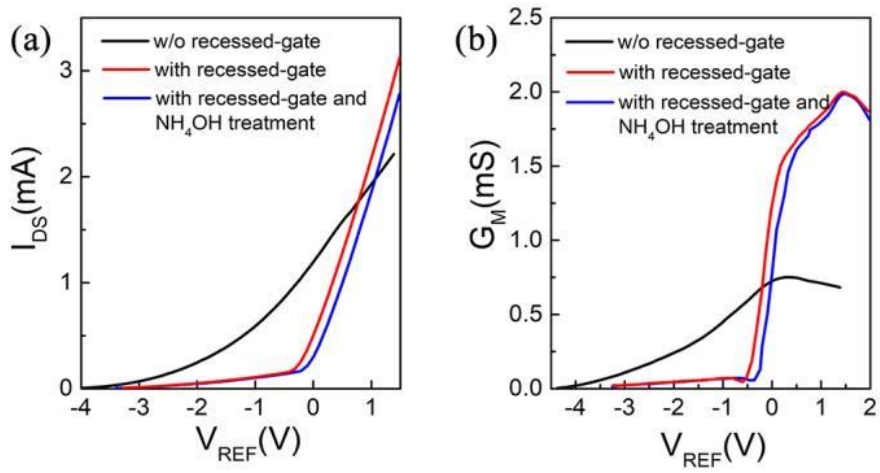

Figure 3-2 (a) The transfer characteristic curve (Id -Vref) of the samples under three different conditions when Vd was at 10V; (b) The G_M -Vref curve of the devices when Vd was at 10 V.

Figure 3-3 shows the transfer characteristics of three types of samples in different pH solutions when the drain voltage is set at 10 V. Three types of devices show a good response to different pH solutions. As the pH value increases, the drain current decreases and the threshold voltage has a positive shift.

To analyze the sensing mechanism of AlGaN/GaN ISFET pH sensors, the site-dissociation model [12] is now generally accepted. Metal oxides and metal nitrides, such as Al_2O_3, Ga_2O_3, AlN etc., will be formed on the surface of AlGaN. The protonation and deprotonation of hydroxyl groups on the gate oxide results in its pH sensing capability.

Generally, the sensitivity of an ISFET is defined by the change in surface potential. The calculation formula is defined as [13]

$$s_v = \frac{\partial \varphi}{\partial pH} = -2.3\frac{kT}{q}\frac{1}{\frac{2.3kTC_{dif}}{q^2\beta_{\text{int}}}+1} = -2.3\frac{kT}{q}\bullet\alpha \quad , \qquad (2\text{-}1)$$

where C_{dif} is the capacitance of different electric double layers, β_{int} the intrinsic buffer capacity, T the absolute temperature, α the sensitivity coefficient, ranging from 0 to 1 determined by the absolute temperature, and k Boltzmann's constant. The essence of the above formula is the Nernst limit formula.

The current sensitivity is a more effective parameter for evaluating the devices. The S_A is defined as

$$S_A = S_V \bullet G_M = \frac{\partial \varphi}{\partial pH}\bullet G_M = \frac{\partial I}{\partial pH} \quad . \qquad (2\text{-}2)$$

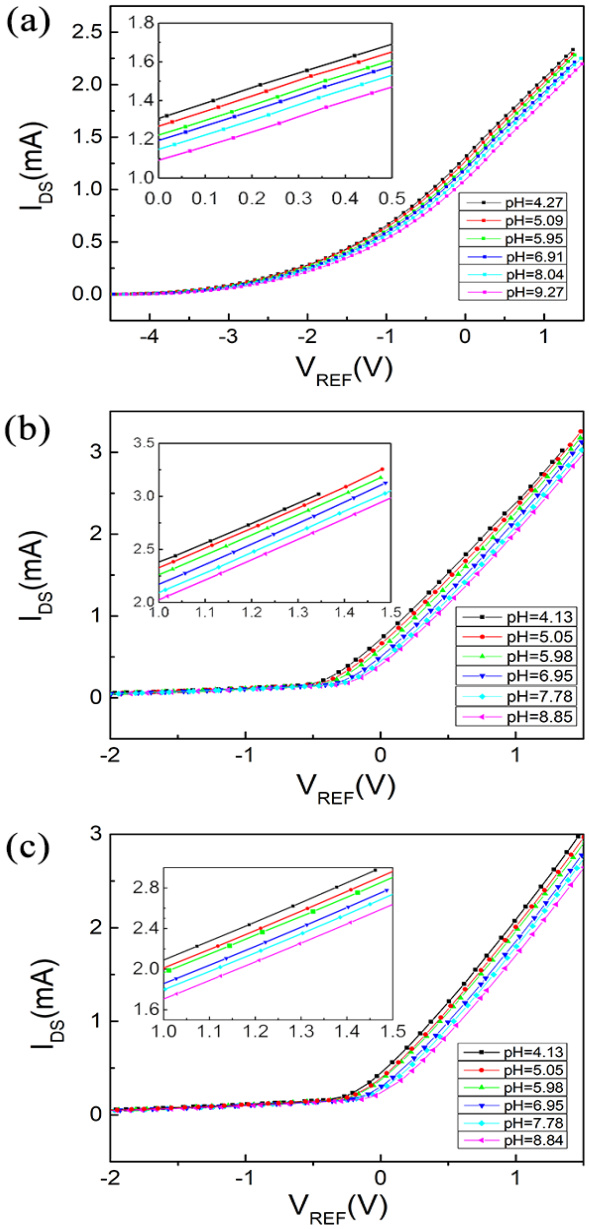

Figure 3-3. (a) The transfer characteristic curve (Id -Vref) of the sample without recessed-gate in different pH solutions; (b) I d -Vref of sample with recessed-gate in different pH solutions; (c) Id -Vref of the sample with recessed-gate and NH_4OH treatment in different pH solutions.

Figure 3-4 shows the pH-current sensitivity and the pH-potential sensitivity characteristics of three samples. All the samples show a good linearity under different conditions. The current sensitivity increased from 52.25 μA/pH of the no recessed-gate device to 78.86 μA/pH of the recessed-gate device, and finally increased to 84.39 μA/pH after NH_4OH treatment, which improved the performance by 61%. The Sv decreased from 55.81 mV/pH of the no recessed-gate device to 39.59 mV/pH of the recessed-gate device, and finally increased to 44.14 mV/pH after NH_4OH treatment. This situation is similar to the problems caused by dry etching in

recessed-gate AlGaN/GaN HEMT devices [14]. The etching damage in the dry process often introduces a large number of interface states on the etched AlGaN surface. The charges near the solution/AlGaN interface will reduce S_V. And the NH_4OH treatment can ameliorate this disadvantage, improving Sv without affecting G_M, hence S_A was increased again.

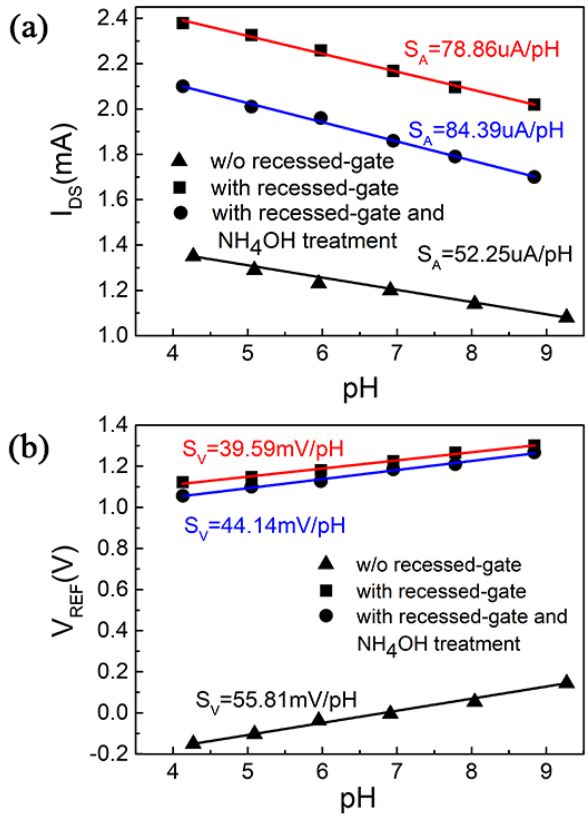

Figure 3-4 The current sensitivity (S_A) (a) and the potential sensitivity (S_V) (b) of the samples without recessed-gate, with recessed-gate and with recessed-gate and NH_4OH treatment.

To investigate the mechanism of the S_A increasement after dry etching and NH_4OH treatment, XPS results of the sensing surface were shown to supplement and explain the above result. In Fig 3-5, the core level spectrum of Ga3d, and Al2p under three different conditions were revealed. The Ga3d peak was fitted into Ga-O (20.20 eV) [14] and Ga-N (19.40 eV) [15] bonds. It can be calculated that the proportion of Ga-N are 99%, 76%, and 92% on the surface of sample without recessed-gate, sample with recessed-gate, and the sample with recessed-gate and NH_4OH treatment. The intensity ratio between the Ga-N peak and Ga-O peak of the recess devices had an obvious decreasing compared with that in the untreated one. After further NH_4OH treatment, the ratio increased a lot. For the Al2p peak, it was fitted into Al-O (74.10 eV) [16] and Al-N (73.50 eV) [15] bonds. The proportion of Al-N are calculated to be

79%, 69%, and 86% on the surface of sample without recessed-gate, sample with recessed-gate, and the sample with recessed-gate and NH_4OH treatment. The intensity ratio between Al-N and Al-O has the same change as that of Ga-N. Therefore, the above results mean that the content of N atoms on the surface of the sensing area changes significantly after different steps of treatment. During the dry etching process, a large number of nitrogen atom vacancies were introduced. When the voltage is scanned forward, a large amount of charge is trapped under the gate, forming a virtual gate [17], which leading to a more negative threshold voltage and a smaller S_V. During the process of ammonium hydroxide treatment, some nitrogen vacancies are filled. Hence, a higher S_A and S_V can be obtained.

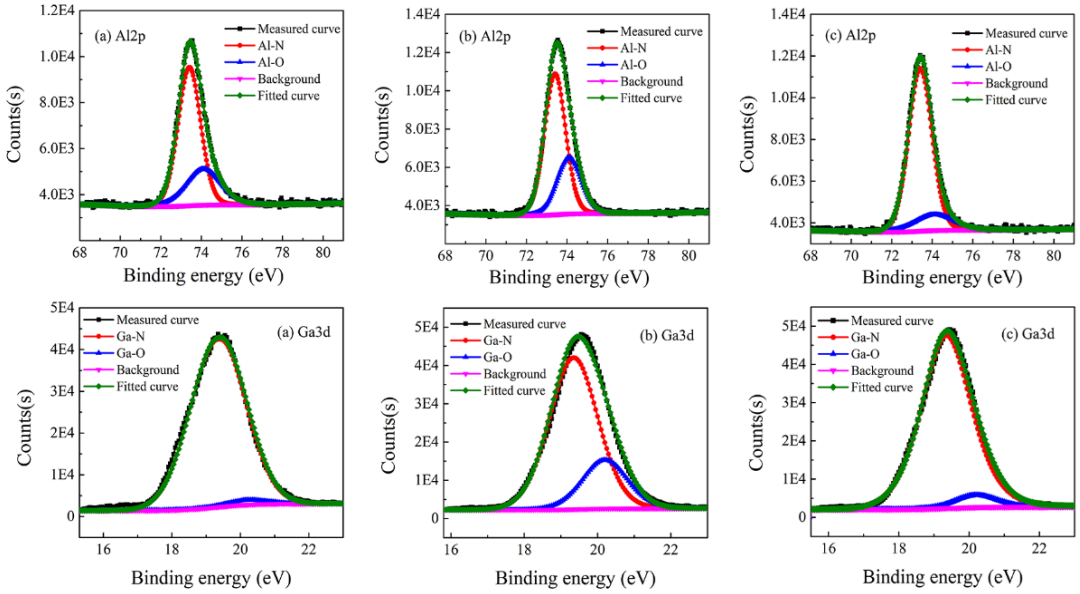

Figure 3-5 The XPS results of (a) the sample without recessed-gate, (b) the sample with recessed-gate and (c) the sample with recessed-gate and NH4OH treatment.

Figure 3-6 shows the energy band diagram of the sample with recessed-gate. From the XPS results, more nitrogen atom vacancies were introduced by the damage of the recess process, which is equivalent to an n-type doping on the surface. The recess process changes the bending direction of the conduction band of AlGaN, leading to a depletion region and potential barrier φ_B. In this work, instead of a metal, the electrolyte became the gate of the ISFET. Different from the Schottky contact between metal and semiconductor, there are two curved barrier φ_A and φ_B between the electrolyte and the AlGaN surface. φ_A is the surface potential barrier of the electrolyte interface, and φ_B is the surface potential barrier of the open-gate interface [18]. When AlGaN is in contact with the electrolyte, metal atoms on the surface due to native

nitrogen atom vacancies are easily to combine OH bond of H_2O and form electroneutral MOH (M is metal atom), reducing the negative charge in AlGaN, leading to a higher φ_B on the AlGaN side. After the OH bonds of H_2O are taken by metal atoms in AlGaN, H atoms with negative charges are left on the electrolyte surface, leading to a φ_A on the electrolyte side. The pH value change in the electrolyte would lead the potential change in the electrolyte. Part of the potential change would drop in potential φ_A and φ_B, leading to a less potential change in the 2DEG channel. This is the reason why the actual S_V cannot reach the ideal value. However, the NH_4OH treatment was effective in removing the dry-etching damage. Hence, compared to that of the sample with recessed-gate only, the φ_B and the change on φ_B become lower, which accounts for higher Sv in the sample after NH_4OH treatment.

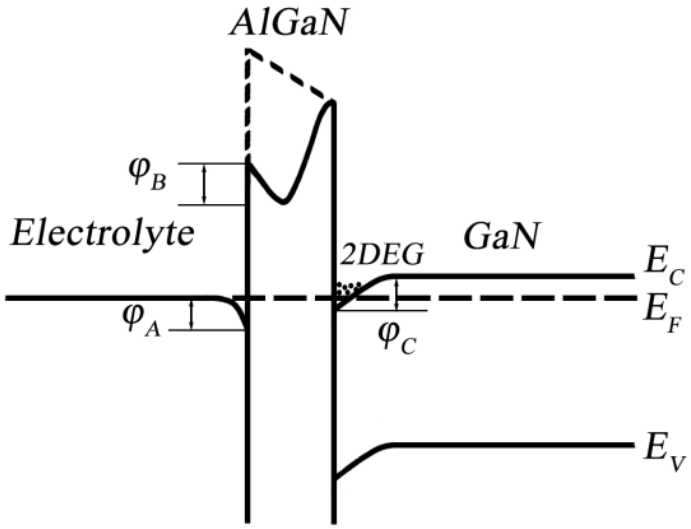

Figure 3- 6. The energy band structure of the sample with recessed-gate

§3.4. Conclusions

The top layer of GaN effectively prevents the reaction of aluminum on the surface with the solution. The current sensitivity of AlGaN/GaN-based ISFET pH sensors has been improved by 61% from 52.25 to 84.39 μA/pH by recessed-gate structure and ammoniate water treatment. The key factors to improve the current sensitivity of AlGaN/GaN-based sensors are potential sensitivity and transconductance. The dry etching recess process can be used to improve the transconductance. But the surface defects introduced during the dry etching decreases potential sensitivity slightly. Then, ammonium hydroxide treatment can be used to improve surface condition, that is, to increase potential sensitivity.

§3.5. References

[1] G. Steinhoff, M. Hermann, W. Schaff, L. Eastman, M. Stutzmann and M. Eickhoff, pH response of GaN surfaces and its application for pH-sensitive field-effect transistors, Appl. Phys. Lett., Vol. 83, No. 1, pp.177-179, 2003.

[2] D. Yates, S. Levine, T. Healy, Site-Binding Model of the Electrical, Vol. 70, No.70, pp. 1807-1818, 1974.

[3] L. Wang, Y. Bu, J. Ao, Effect of oxygen plasma treatment on the performance of AlGaN/GaN ion-sensitive field-effect transistors, Diam. Relat. Mater, Vol. 73, pp. 1-6, 2017.

[4] L. Wang, Y. Bu, L. Li, J. Ao, Effect of thermal oxidation treatment on pH sensitivity of AlGaN/GaN heterostructure ion-sensitive field-effect transistors, Appl. Surf. Sci., Vol. 411, pp. 144-148, 2017.

[5] L. Wang, L. Li, T. Zhang, X. Liu, J. Ao, Enhanced pH sensitivity of AlGaN/GaN ion-sensitive field effect transistor with Al 2 O 3 synthesized by atomic layer deposition, Appl. Surf. Sci., Vol. 427, pp. 1199-1202, 2018.

[6] Q. Cheng, M. Wang, M. Tao, R. Yin, Y. Li, N. Yang, W. Xu, C. Gao, Y.Hao, and Z. Yang, Planar Dual Gate GaN HEMT Cascode Amplifier as a Voltage Readout pH Sensor with High and Tunable Sensitivities, IEEE Electron Device Lett., Vol. 41, No. 3, pp. 485-488, March 2020.

[7] Y. Maeda, K. Niigata, K. Narano, L. Wang, and J. Ao, Surface Dependence of pH Sensors on AlGaN/GaN Heterostructure, ECS Transactions, Vol. 61, No. 19, pp. 65-71, 2014.

[8] P. Bergveld, ISFET, theory and practice, IEEE Sensor Conference Toronto, p.1, 2003.

[9] J. Ao, D. Kikuta, Y. Naoi, Y. Ohno, Copper gate AlGaN/GaN HEMT with low gate leakage current, IEEE Electr. Device L., Vol. 24, pp. 500–502, 2003.

[10] N. Shrestha, Y. Li, T. Suemitsu, Senior, and S. Samukawa. Electrical Characteristic of AlGaN/GaN High-Electron-Mobility Transistors with Recess Gate Structure, IEEE T. Electron Dev., Vol, 66, No. 4, pp.1694-1698, April 2019.

[11] Q. Wang, K. Tamai, T. Miyashita, S. Motoyama, D. Wang, J. Ao and Ohno Y, Influence of dry recess process on enhancement-mode GaN metal-oxide-semiconductor field-effect Transistors, Jpn. Appl. Phys. Vol. 52, No. 1S, 2013.

[12] D. Yates, S. Levine, T. Healy, Site-Binding Model of the Electrical Double Layer at the Oxide/Water Interface, J. Chem. Soc. Faraday Trans., Vol. 70, No.7 0, pp. 1807-1818, 1974

[13] N. Yang, W. Henson, J. Hauser, J. Wortman, Estimation of the effects of remote charge scattering on electron mobility of n-MOSFETs with ultrathin gate oxides, IEEE T. Electron Dev., Vol. 47, No. 2, pp. 440–447, 2000.

[14] J. Epp and J. Dillard, Adsorption of nitric oxide, nitrous oxide, and oxygen on ion-bombarded gallium arsenide (100), Chem. Mater., Vol. 2, No. 4, pp. 449-454, 1990.

[15] R. Gordon, D. Hoffman, U. Riaz, Atmospheric Pressure Chemical Vapor Deposition of Gallium Nitride Thin Films, Volume 204 (Symposium E–Chemical Perspectives of Microelectronic Materials II), p. 95, 1990.

[16] S. Seal, S. Krezoski, T. Barr, Application of photoelectron spectroscopy in inorganic and organic material systems, Experimental Methods in the Physical Sciences. Vol. 38, pp. 111-190, 2001.

[17] T. Narita, D. Kikuta, N. Takahashi, K. Kataoka, Y. Kimoto, T. Uesugi and M sugimoto, Study of etching-induced damage in GaN by hard x-ray photoelectron spectroscopy, Phys. Status Solidi A, Vol. 208, pp. 1541–1544, 2011.

[18] Y. Dong, H. Zhang, A. Ahmad, H. Liang, J. Liu, X. Xia, W. Guo, H. Huang and N. Xu, Enhancing the sensitivity of the reference electrode free AlGaN/GaN HEMT based pH sensors by controlling the threshold voltage, Sens. Actuators B, Chem., Vol. 306, p. 127609, 2020.

Chapter 4：Application of AlGaN/GaN ISFETs pH sensor

§4.1. The design principle of pH sensor circuit

The ISFET is in fact nothing else than a MOSFET with the gate connection separated from the chip in the form of a reference electrode inserted in an aqueous solution which is in contact with the gate oxide [1].The general application principle is shown in the Figure 4-1.

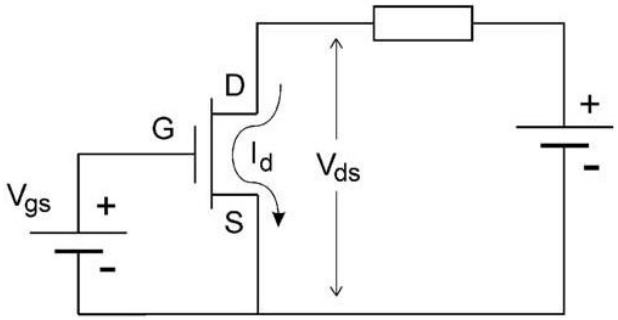

Figure 4-1 Basic principle of MOSFET (ISFET)

The general expression for the drain current of the MOSFET and thus also of the ISFET in the non-saturated (as 0-A in figure 2-3) mode is

$$I_d = C_{ox}\mu\frac{W}{L}\left[\left(V_{gs} - V_t\right)V_{ds} - \frac{1}{2}{V_{ds}}^2\right], \qquad (4\text{-}1)$$

with C_{ox} is the oxide capacity per unit area, W and L the width and the length of the channel, respectively , and the μ electron mobility in the channel. In the saturated region of operation, the expression is different, but this is not of any influence for a clear apprehension of the matter.

In both cases, the drain current I_d is a unique function of the input voltage V_{gs} , only when the geometric sensitivity parameter $\beta = C_{ox}\mu\frac{W}{L}$, as well as the applied drain-source voltage V_{ds} and the threshold V_t are constant. The parameter β is a design constant and V_{ds} is kept constant by the applied electronic circuit. In addition, the fabrication processes for MOSFET devices are so well under control that V_t is also a constant, which manifests itself only as a certain threshold voltage, hence its name. Thus, V_{gs} is the only input variation. In case of the ISFET, it was initially debated whether the observed ion sensitivity should be described as an additional

input variable in terms of a modification of V_{gs} or a modification of V_t . Defining the metal connection of the reference electrode as a remote gate, as shown in Figure 1b, suggests that any interfacial potential in the input circuit should be described in terms of V_t. Therefore, the second important MOSFET equation is that of the threshold voltage:

$$V_t = \frac{\emptyset_M - \emptyset_{Si}}{q} - \frac{Q_{ox}+Q_{ss}+Q_B}{C_{ox}} + 2\emptyset_f, \qquad (4\text{-}2)$$

where the first term reflects the difference in work function between the gate metal ($\emptyset_M$) and the silicon ($\emptyset_{Si}$), the second term is due to accumulated charge in the oxide(Q_{ox}), at the oxide–silicon interface (Q_{ss}) and the depletion charge in the silicon (Q_B), whereas the last term determines the onset of inversion depending on the doping level of the silicon. All terms are purely physical in nature.

In case of the ISFET, the same fabrication process is used, resulting in the same constant physical part of the threshold voltage (Eq. (5-2). However, in addition to this, two more contributions manifest themselves: the constant potential of the reference electrode, E_{ref} , and the interfacial potential $\psi + \chi^{sol}$ at the solution/oxide interface of which ψ is the chemical input parameter, shown to be a function of the solution pH and χ^{sol} is the surface dipole potential of the solvent and thus having a constant value. Hence the expression for the ISFET threshold voltage becomes

$$V_t = E_{ref} - \psi + \chi^{sol} - \frac{\phi_{Si}}{q} - \frac{Q_{ox}+Q_{ss}+Q_B}{C_{ox}} + 2\phi_f. \qquad (4\text{-}3)$$

Note that the parameter $\emptyset_M$ in Eq. (2), being the work function of the gate metal seems now to be disappeared, but this is not true, because it is ‘‘buried’’ by definition in the term E_{ref} .

In case the ISFET is treated as a MOSFET and connected to a curve tracer with the reference electrode connected to the V_{gs} port, I_d -V_{ds} curves can be recorded as function of V_{gs} as is usually done with MOSFETs. However, with the reference electrode connected to the source (V_{gs}=0) similar curves can be achieved by changing the pH of the solution.

Bousse [2] developed for the first time a rather simple theory with two parameters, derived from the already existing site-dissociation and double-layer

models. These parameters are the pH_{pzc}, being the value of the pH for which the oxide surface is electrically neutral and β, determining the final sensitivity. The resulting equation for the surface potential ψ as given in Eq. (4-3) for relatively large values of β is

$$\psi = 2.3\frac{kT}{q}\frac{\beta}{\beta+1}(pH_{pzc} - pH). \quad (4\text{-}4)$$

From Eq. (4-4) it can be seen that the sub-Nernstian response can now easily be explained by means of a not too large value of β for the oxide under investigation. The value of β can be expressed in terms of the acidic and basic equilibrium constants of the related surface reactions, for which a parameter $[H^+]_s$ has been introduced, which represents the surface concentration of H^+ ions, being related to the $[H^+]$ bulk value by Boltzmann statistics. This parameter has since the introduction of the site-dissociation model served as a mathematical quantity for many further models with different type of surface sites, even including a PSPICE model of the group of Grattarola [3], but the chemico/physical significance was rather unclear.

Van Hal and Eijkel introduced a new model [4,5] which is in fact nothing else than the, for electrical engineers, well-known equation for capacitors Q=CV, where Q is the surface charge in the form of protonized (OH_2^+) or deprotonized (O^-)OH groups of the oxide surface, C is the double-layer capacitance at the interface and V is the resulting surface potential, denoted as ψ in Eqs. (4-3) and (4-4). The surface charge acts as a source or sink for protons, whereas the load of this source is the double-layer capacitance. The surface proton buffer capacity as well as the value of the double-layer capacity determine together the final value of the potential ψ which can be expressed in a sensitivity factor α, resulting in the simple equation:

$$\Delta\psi = -2.3\alpha\frac{RT}{F}\Delta pH_{bulk}. \quad (4\text{-}5)$$

With

$$\alpha = \frac{1}{\left(\frac{2.3kT}{q^2}\right)\left(\frac{C_s}{\beta_s}\right)+1}, \quad (4\text{-}6)$$

where β_s symbolises the surface buffer capacity, e.g. the ability of the oxide surface to deliver or take up protons, and C_s is the differential double-layer capacitance, of which the value is mainly determined by the ion concentration of the bulk solution via the corresponding Debye length.

Eq. (4-5) shows that only in case α approaches 1, the maximum Nernstian sensitivity of 58.2 mV per decade (at 20℃) can be obtained, whereas for oxides

having a value α < 1 a sub-Nernstian response can be expected. Eq. (4-6) shows that α=1 is reached for oxides with a large value of the surface buffer capacity β_s and a low value of the double- layer capacity C_s.

Therefore, all studies tried to change the materials, structures or surface treatments of the GaN based ISFETs so that they could improve the parameter α to increase the surface sensitivity (voltage). On account of the limit of Nernst equation, the improvement of the sensitivity is limited. This is very limited to improve the actual measurement. If we consider the sensitivity of current, we may have more methods to improve the sensitivity and resolution of measurement.

As well known, in the non-saturation region of MOSFET, the drain current is Eq (5-1),

$$I_d = C_{ox}\mu\frac{W}{L}\left[(V_{gs} - V_t)V_{ds} - \frac{1}{2}{V_{ds}}^2\right].$$

So, if V_{ds} is constant,

$$\Delta I_d = V_{ds}C_{ox}\mu\frac{W}{L}\Delta V_{gs}. \quad (4\text{-}7)$$

According to Eq (5-5),

$$\Delta I_d = -2.3\alpha V_{ds}C_{ox}\mu\frac{W}{L}\Delta pH. \quad (4\text{-}8)$$

If we define a current sensitivity,

$$\frac{\Delta I_d}{\Delta pH} = -2.3\alpha V_{ds}C_{ox}\mu\frac{W}{L}. \quad (4\text{-}9)$$

We found that we have many ways to improve this sensitivity, increasing the V_{ds} *or* $\frac{W}{L}$, *not only* α.

It must be noted that the increase of drain voltage must be within the range of non-saturated region, because if it reaches the saturated region, it will become the following equation,

$$I_{Dsat} = C_{ox}\mu\frac{W}{2ML}(V_{gs} - V_t)^2. \quad (4\text{-}10)$$

Then,

$$\Delta I_{Dsat} = 2C_{ox}\mu\frac{W}{2ML}(V_{gs} - V_t)\,\Delta V_{gs}. \quad (4\text{-}11)$$

The relationship between the drain current and the gate voltage is no longer linear.

As for AlGaN/GaN structure, the current flowing between the drain and source contacts can be written as follows (rate at which the 2DEG charge moves across the gate):

$$I_D = qn_s V_{eff} W_G, \qquad (4\text{-}12)$$

where V_{eff} is the effective velocity of the electrons in the channel, n_s is the 2DEG charge density and W_G is the gate width.

The 2DEG carrier density can vary from a maximum value of n_{s0} to a minimum value of zero depending on the gate bias:

$$n_s = \frac{\varepsilon_{AlGaN}}{q(d_{AlGaN} + \Delta d)}(V_G - V_T), \qquad (4\text{-}13)$$

where d_{AlGaN} is the thickness of the AlGaN barrier layer, Δd is the effective distance of the 2DEG from the hetero-interface, and V_G is the gate bias. V_T is the threshold voltage, the gate bias required to pinch-off the channel, which is determined by the composition and doping profile of the AlGaN layer.

When HFETs are biased at low drain voltages ($V_D < V_G - V_T$), the devices are said to be operating in a linear regime, where the electron velocity is linearly related to the electric field strength. However, at high drain biases ($V_D > V_G - V_T$), the effective electron velocity saturates and becomes independent of bias or the electric field strength. Velocity saturation (V_{sat}) occurs due to scattering of electrons with the semiconductor lattice. For practical purposes, devices are

$$I_D = \frac{\varepsilon_{AlGaN} W_G V_{sat}}{(d_{AlGaN} + \Delta d)}(V_G - V_T). \qquad (4\text{-}14)$$

In reality, I_D is not totally independent of V_D. At high values of V_D, high electric fields exist between the drain and gate contacts and may cause electrons to be injected into the GaN buffer or captured by electron traps. A parallel conduction path may exist between the drain and source contacts. The high drain-to-gate field may also result in an increase in parasitic gate leakage current into the channel. The I_D-V_D curves may also exhibit negative differential resistance at high drain bias voltages, which is characteristic of self-heating effects. These effects cause I_D to be slightly dependent on V_D.

§4.2. The prototype of sensor

In actual measurement practice, we will give a fixed gate voltage and source voltage to observe the change of source current in different pH solutions. Because the output characteristics are different in different regions, different Vds (1.8 V, 3.3 V) are used to compare the results.

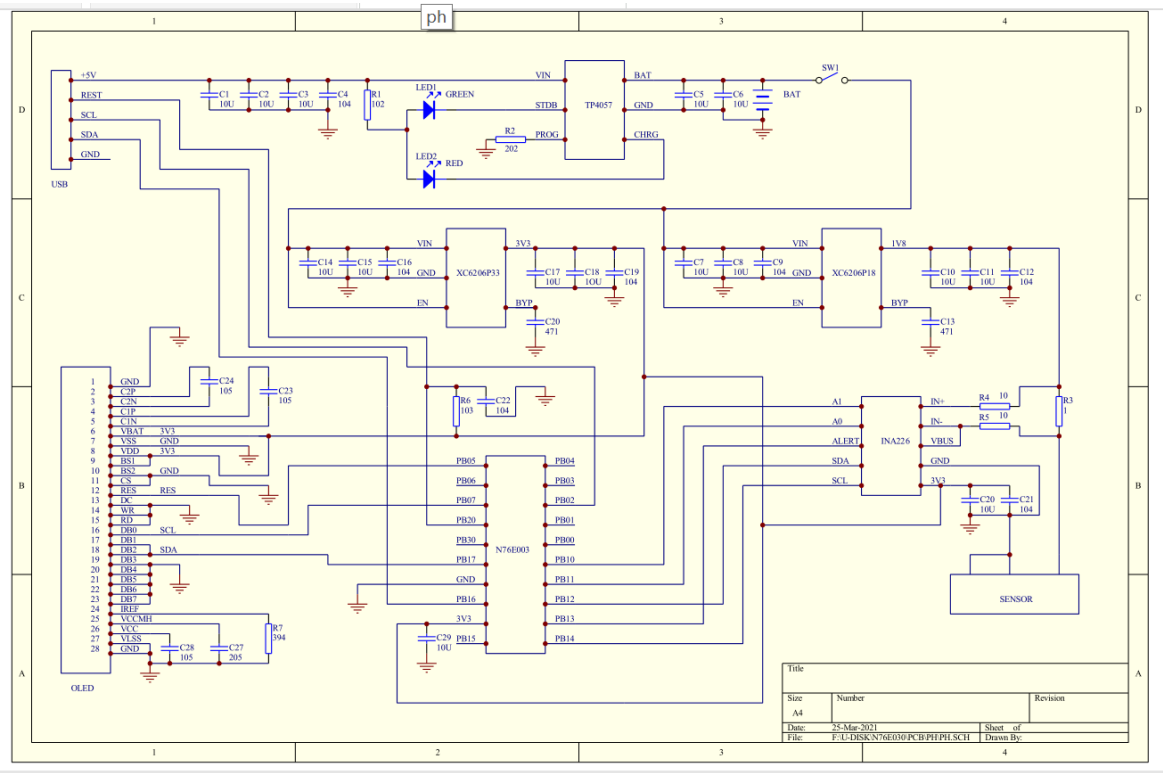

Figure 4-2 The circuit principle diagram of samples made of AlGaN/GaN pH sensor

The whole design is realized by using the output characteristics of the sensor. A voltage of 1.8V, 3.3V applied between the source and the drain to make it work in different regions. The platinum strip connected with zero voltage provides normal conduction voltage to the gate surface. The voltage changes with the change of pH. The calibration algorithm can be given by comparing with the standard pH meter.

At present, the overall size is 130mm * 50mm.The voltage between the drain and the source (Vds) and the current between them (Ids) are displayed while the pH value not. To know the exact pH value, we have to find the relationship between current and pH. We have reserved a mini USB interface to facilitate battery charging and upgrade embedded software.

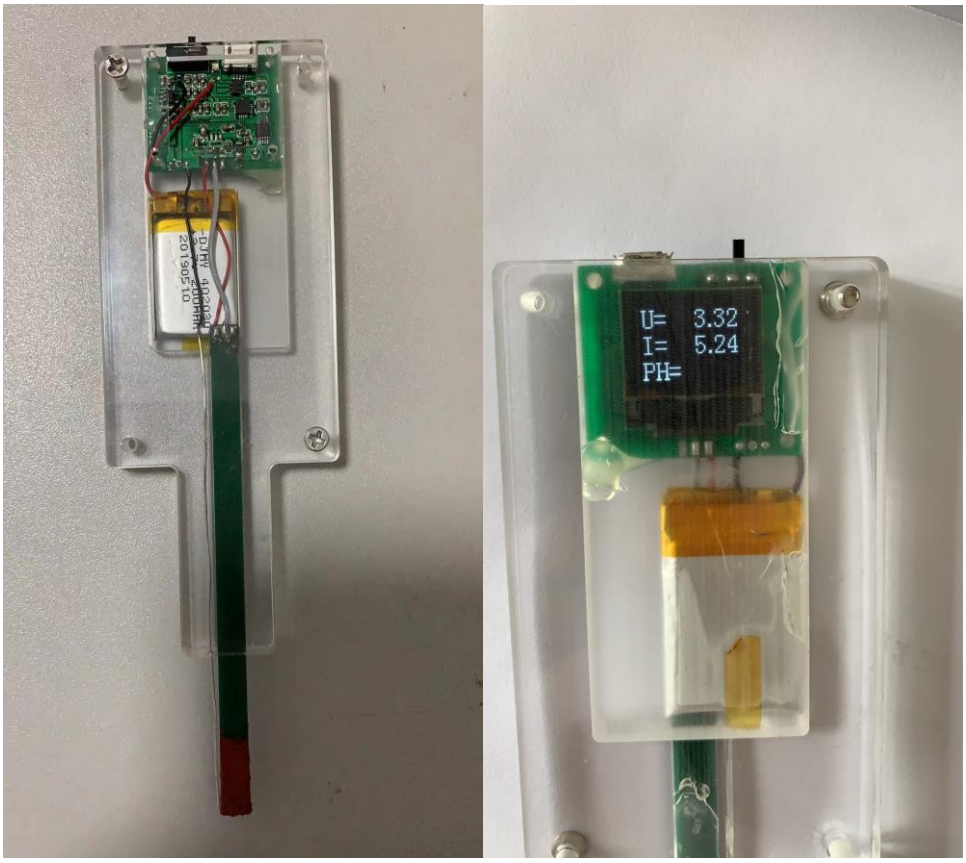

Figure 4-3 The photos of finished sample made of AlGaN/GaN pH sensor

§4.3. Results and discussion

We test the pH meter of Vd=3.3 V first. Turn on the meter but not put into the solution, it is found that the current continuously drops rapidly from a bigger value (about 6.00 mA) to a smaller one (about 5.20 mA) and then decreases with more and more slower velocity until it reaches 4.30mA at a relative status (hold on more than 20 seconds). While put the meter into the solution and turn it on, a similar phenomenon can be found but the initial current and the final stable current are much smaller, which are 4.30 V or even lower and 3.90 V or even lower respectively, and the velocity of the drop is slower than that before putting into the solution. Figure 4-4 shows the Id-time curve of sample #2 in solution with pH=3.95.

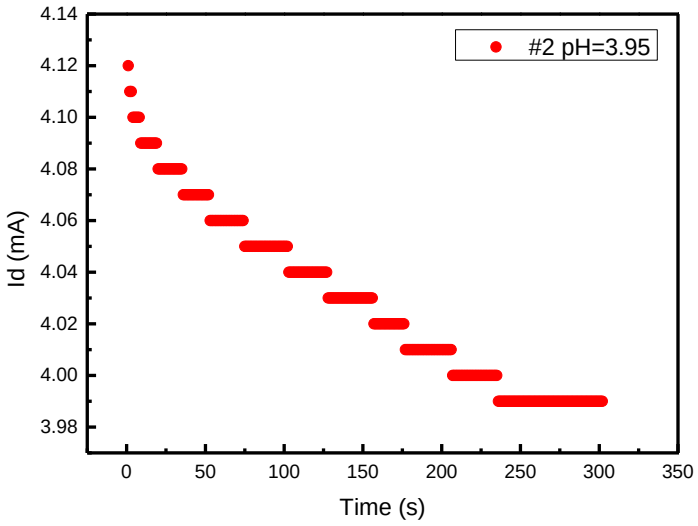

Figure 4-4 Id-time curve of sample #2@pH=3.95

The initial current before putting into the solution is higher than that after putting into the solution, because the gate is in suspension state before putting into the solution, and the gate voltage should be at 0V or higher, and the gate voltage will be lower than 0V after putting into the solution, which is consistent with the output characteristic curve of ISFET. After the circuit is turned on, the current will make the junction temperature of ISFET increase, which will make the electron mobility decrease and the resistivity increase. The current will naturally drop. The slowing down decreasing speed is due to the constant trend of heat dissipation and current heating towards heat balance. Before putting into the solution, the heat dissipation can only be the radiation in the air, and the heat dissipation in the solution is the heat exchange with the solution, so the heat dissipation speed is much faster. So in solution, the current drops much more slowly.

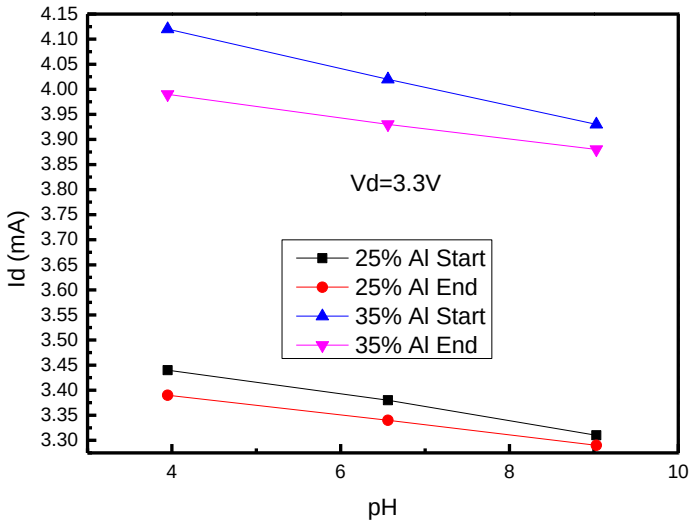

Figure 4-5 Id-pH curve in different solutions @ Vd=3.3V

Figure 4-5 shows the result of start and end currents in different solutions. All the results show good linear between the current and the pH value of solution, which is consistent with the equation 5-14. According to the result, the sensitivity of sample #1(25% Al) at the start time is -25.6 μA/pH and the sensitivity at the end is -19.7 μA/pH. The sensitivity of sample #2 (35% Al) at the start is -37.4 μA/pH and the sensitivity at the end is -21.7 μA/pH. Therefore, the sensor with higher Al content shows higher sensitivity in application and the lower junction temperature means the higher sensitivity.

In order to verify the stability and repeatability, put a sample into the solution. When the current is relatively stable (3.34ma), turn off the circuit and turn it on immediately, the current will return to 3.34ma from 3.36ma immediately (within 3 seconds) and remain relatively stable (more than 5 seconds). The experiment was repeated 100 times, each time with the same result. In other words, the pH measurement circuit is stable and repeatable.

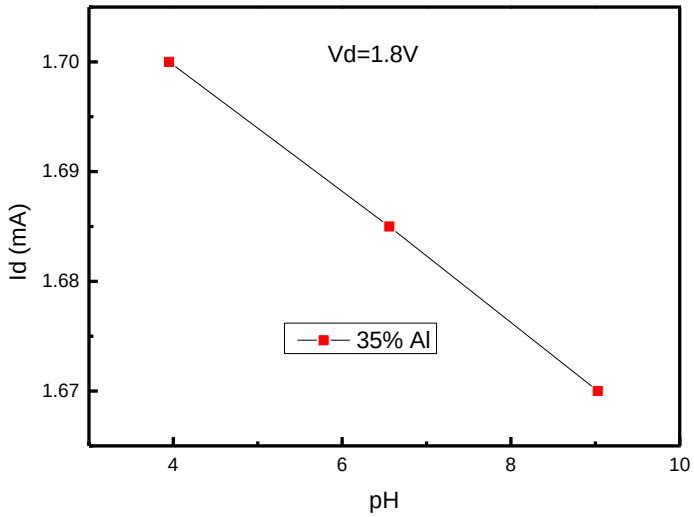

Figure 4-6 Id-pH curve in different solutions @ Vd=1.8V

We change the drain voltage (Vd) of one of the samples to 1.8V. The current is 2.19 mA in the suspended state (before putting into solution), and it is very stable. When it is putted into the solution with different pH, the stable current (1.67-1.70mA) will be displayed. This shows that our previous explanation of heating and heat dissipation is reasonable. Because the current is very small, basically it will not lead to the rise of junction temperature. Similarly, because the gate voltage at suspension is higher than the gate voltage putted into the solution, the current at suspension is relatively larger. But because the drain voltage of 1.8V makes the device work in the linear region, the current is very small, so although the state is stable, the sensitivity is not high, only -5.9 μA/pH. This is also consistent with the equation 5-12 and 5-13.

The same experiments to verify the stability and repeatability also prove that the measurement itself is stable and repeatable.

§4.4. Conclusion

These results can lead to the following conclusions: 1. GaN based ISFET can measure the pH value of solution with similar circuit, whether working in the linear region or saturated region; 2. The measurement is stable and repeatable; 3. The small current in the linear region can make the measurement stable and fast, but the resolution is very low. High resolution can be obtained in the saturated region, but the measurement is unstable due to excessive current; 4. The measurement accuracy and

speed are related to the junction temperature.

§4.5. References

[1] P. Bergveld, Thirty years of ISFETOLOGY What happened in the past 30 years and what may happen in the next 30 years, Sensors and Actuators B 88 (2003) 1–20

[2] L. J. Bousse, N. F. de Rooij, P. Bergveld, Operation of chemically sensitive field effect sensors, as function of the properties of the insulator/electrolyte interface, IEEE Trans. Electron Devices ED-30 (1983) 1263–1270.

[3] M. Massobrio, S. Martinoia, M. Grattarola, Use of SPICE for modelling silicon-based chemical sensors, Sens. Mater. 6 (2) (1994) 101.

[4] R. E. G. van Hal, J. C. T. Eijkel, P. Bergveld, A novel description of ISFET sensitivity with the buffer capacity and double layer capacitance as key parameters, Sens. Actuators B 24/25 (1995) 201–205.

[5] R. E. G. van Hal, J. C. T. Eijkel, P. Bergveld, A general model to describe the electrostatic potential at electrolyte/oxide interfaces, Adv. Coll. Interf. Sci. 69 (1996) 31–62.

Chapter 5：GaN-based temperature sensors for integration

§5.1. Advantage of SBD temperature sensor

When the GaN based pH sensor is applied, its current is not only related to the pH value of the solution, but also related to the temperature. If the temperature signal can be obtained at the same time, the accuracy of measurement will be greatly improved. Similarly, GaN based sensors will make the integration of devices easier. The lateral configuration AlGaN/GaN heterostructure field-effect transistors (HFETs) with two-dimensional electron gas (2DEG) channel enables the high-density integration of devices. Besides the high-voltage power transistors and rectifiers, various low voltage transistors, diodes, resistors, and capacitors can also be fabricated on AlGaN/GaN platform for peripheral circuits.

Gallium nitride (GaN) with wide bandgap, low intrinsic carrier concentration, and high saturation velocity is a promising candidate for high-power and high-temperature applications [1, 2]. Generally, the high temperature environment as well as the self-heating effect will obviously affect the junction temperature (Tj) of a power device. The accurate measuring of Tj is critical for thermal management and can be obtained by both direct and indirect methods [3–5]. As found in Chapter 4, even in GaN based pH sensor application, the junction temperature also has a great influence on the measurement. Among those technologies, an in-situ temperature sensor with a significantly faster dynamic response is proposed by using a small p-n junction diode or Schottky barrier diode (SBD). The quasi linear dependency of current-voltage characteristic on the temperature is utilized to Tj sensing. To achieve this purpose, the anode electrode of the diode requires a good thermal stability.

The most common electrode used as anode for GaN SBD is Ni metal [6, 7]. However, the existence of interface reaction between Ni and GaN results in the degradation of the rectification characteristics [8]. On the other hand, the refractory metal nitride usually presents good thermal stability, which can be regarded as a candidate to alternate the conventional metal anode [9]. Liuan Li et al. found that good Schottky properties are maintained even after the ohmic annealing at 800°C when the reactively-sputtered TiN was used as the gate material for AlGaN/GaN HFETs [10, 11]. Furthermore, the TiN anode GaN SBD with a low turn-on voltage to

breakdown voltage ratio is also attractive to develop microwave power rectification. They demonstrated that GaN Schottky barrier diode (SBD) and pn diode (PND) with a thermally stable anode electrode have the possibility of temperature monitoring. The forward voltage of the diode decreases with the increasing temperature linearly with a sensitivity of around 2.0 mV/K. The conventional planar AlGaN/GaN SBD can be easily realized by using a metal anode, but it exhibits an undesired high onset voltage (Von). Various techniques such as recessed-anode, thin barrier, p-GaN cap layer, and fluorine ion implantation have been proposed for achieving low Von. Among those methods, the recessed-anode scheme is the most promising one because its simple structure and no requirement of extra process. However, there is rarely report on the design and fabrication of temperature sensor block for the AlGaN/GaN platform.

Herein, the conventional planar and recessed anode AlGaN/GaN SBDs were fabricated to evaluate the feasibility of temperature sensor application. The recessed anode SBD show a relatively lower V_{on} and better Schottky contact characteristics from 298 to 473 K. The forward voltage appears good linear dependence on temperature when the sensor is biased at different current levels, implying the good potential in temperature sensor application.

§5.2. Fabrication of recessed-anode AlGaN/GaN SBD

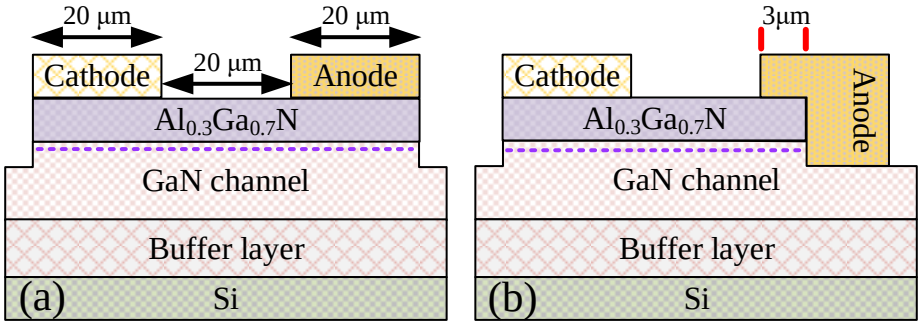

. Figure 5-1 The cross-section view of the conventional planar (a) and recessed anode (b) SBD. The corresponding dimensions are also marked

The AlGaN/GaN HFETs wafers used in this experiment are grown on a 2-in. Si(111) substrate by metal organic chemical vapor deposition. From bottom to top, the heterostructure consists of a 20 nm high-temperature AlN nucleation layer, a 1.0 μm undoped semi-insulating GaN layer, a 400 nm GaN channel layer, and a 25 nm thick undoped AlGaN layer. The nominal Al mole fraction of the AlGaN layer was set to 30%, resulting in a sheet carrier density and mobility of 1.0×10^{13} cm^{-2} and 1200 cm^2/Vs, respectively.

The fabrication of the conventional (Figure.5-1a, labeled as Refer) and recessed anode (Figure.5-1b, labeled as Recess) diodes adopts a standard lift-off technology. Firstly, the mesa isolation was formed by Cl_2/BCl_3 mixture gas dry etching with an etch depth of about 100 nm. The anode recessing process is also accomplished simultaneously during isolation. After cleaned by sulfuric peroxide mixture (SPM) and diluted HCl solution, the Ti/Al/Ni/Au (15/80/25/60 nm) stack was deposited and annealed at 870 °C for 30 s in nitrogen ambient as cathode electrode (width and length are 100 and 20 μm). After opened the anode area (width and length are 100 and 20 μm), Ni/Au (25/65 nm) is deposited as the anode electrode. The anode to cathode distance was set to 20 μm. The anode electrode of the refer diode locals above the AlGaN barrier as a planar structure. While the anode of the Recess diode composes a 3 μm overlapped planar structure and a recessed sidewall Schottky contact.

§5.3. The sensitivity and mechanism of AlGaN/GaN SBD

To evaluation the feasibility of temperature sensor application, the current-voltage (I-V) characteristics of the SBDs (Figure 5-2 for refer diode and Figure 5-3 for recess diode) were recorded at various temperature ranging from 298 to 473 K with a step of 25 K.

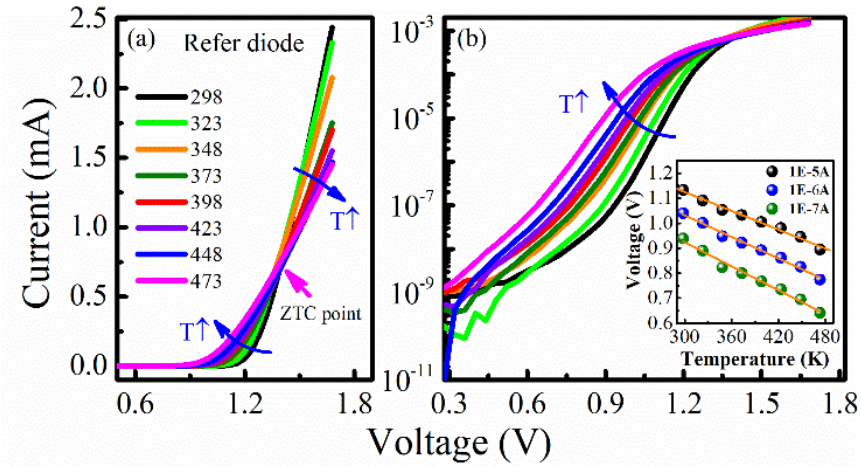

Figure 5-2. The temperature dependent I-V characteristics of SBD (refer diode) in linear (a) and semi-log (b) scale with temperature. Inset of (b) is the relationship between forward voltage and temperature at different current levels.

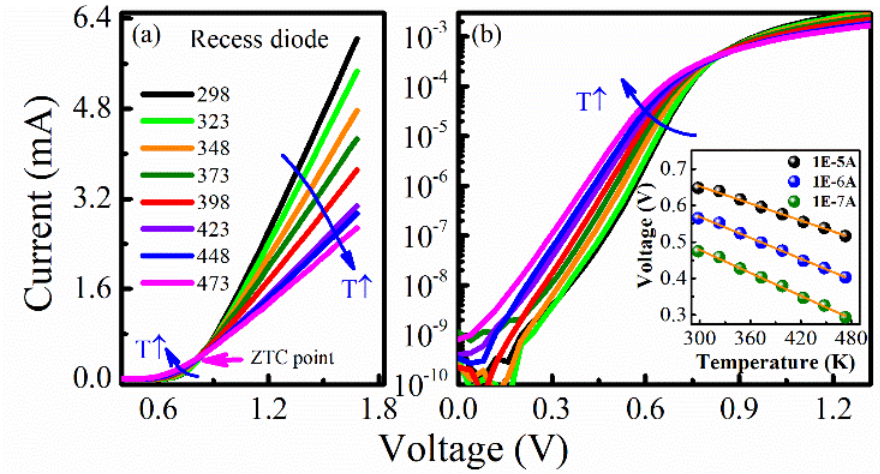

Figure 5- 3. The temperature dependent I-V characteristics of SBD (recess diode) in linear (a) and semi-log (b) scale with temperature. Inset of (b) is the relationship between forward voltage and temperature at different current levels.

For the Refer SBD (as shown in Figure 5-2a), the I-V curves at all temperature show typical rectification characteristics. In addition, a zero-temperature coefficient (ZTC) bias point (approximately 1.4 V in our experiment) was observed on the curves. As reported in our previous work, the current below the ZTC bias point (sub-threshold region) increases gradually with the increasing temperature due to the decrease of turn-on voltage. Generally, the electrons can gain higher thermal energy to surmount the Schottky barrier at a high temperature, resulting in the negative shift of turn-on voltage. While the forward current decreases with the increasing temperature above the ZTC bias point (fully turn-on region) due to the mobility degradation and the increasing series resistance. Furthermore, observed from the semi-logarithmic plot of the sub-threshold region, the I-V characteristics are linear and shift negatively with the increasing temperature (Figure 5- 2b), implying that the transportation follows the thermionic emission (TE) model. The temperature dependent I-V curves of the Recess SBD (as shown in Figure 5-3) present similar characteristics with that of the Refer diode. However, the turn-on voltage of the diode decreases to a smaller value along with a much obvious variation in the fully turn-on region.

To reveal the temperature dependent electrical behavior in detail, we fitted the *I-V* curves by using the *TE* model (Figure 5-4a). Theoretically, the forward current (I_D) when $V_F > 3kT/q$ is represented as

$$I_D = A_e A^* T^2 \exp\left(-\frac{q\phi_B}{kT}\right)\exp\left(\frac{q\left(V_F - I_D R_s\right)}{nkT}\right) \tag{5-1}$$

The forward voltage is solved as

$$V_F = n\varphi_b + \frac{nkT}{q}\left[\ln\left(\frac{I_D}{A_e A^*}\right) - 2\ln(T)\right] + I_D R_s = \frac{1}{K_2}\left(\ln\frac{I+K_1}{K_1} + K_3 I\right), \quad (5\text{-}2)$$
$$K_1 = A_e A^* T^2 \exp\left(-\frac{q\varphi_b}{kT}\right), K_2 = \frac{q}{nkT}, K_3 = \frac{qR_s}{nkT}$$

where A_e, T, q, n, k, A^* and R_s are the Schottky anode area, Kelvin temperature, electronic charge, ideality factor, Boltzmann constant, Richardson constant (26.9 $Acm^{-2}K^{-2}$ in our calculation) and series resistance, respectively.

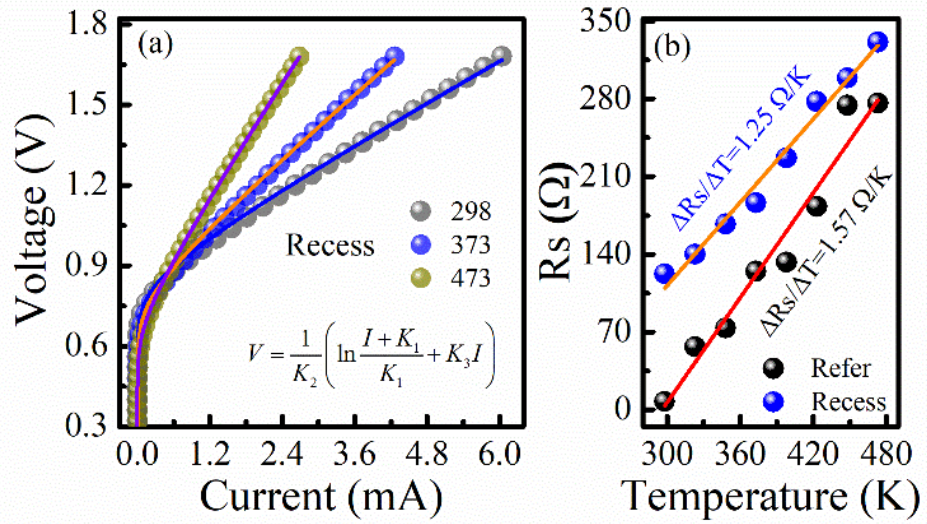

Figure 5-4 The typical fitted forward-biased I-V characteristics (a) based on the TE model. The comparison of deduced Rs for two kinds of SBDs (b).

The typical forward-biased *I-V* characteristics of the Recess SBD as well as the fitting lines based on *TE* model are plotted in Figure 5-4a, indicating that all the curves show good agreement with the experimental data at different temperature. It worth noting that the Rs increases obviously with the increasing temperature (Figure 5-4b), showing a positive slope (dRs/dT) of approximately 1.57 and 1.25 Ω/K for the Refer and Recess SBD, respectively. The Rs of the Recess SBD is relatively higher than that of the Refer one because of the smaller area. However, it shows a weaker temperature dependency, which can be ascribed to the directly contact between the anode and 2DEG channel. The dRs/dT values are much higher compared with the lateral or vertical SBDs fabricated on n-GaN (around the order of mΩ/K) in our previous works. This may be ascribed to that the increasing temperature enhances the scattering and degrades the mobility of the 2DEG channel. When considering the temperature sensor application, although the relatively large Rs at the fully-turn-on region results in an obvious variation of voltage to obtain a higher sensitivity (as

represented in Eq.5-2), the series resistance would degrade the temperature error and linearity along with a larger loss. Therefore, the fully-turn-on region of the AlGaN/GaN based SBD is not suitable.

Observed from Figure 5-5a, the deduced Φ_b of Refer SBD increased from 0.76 eV to approximately 1.16 eV linearly versus 1/T. On the other hand, although shows a similar trend versus temperature with the Refer diode, the Φ_b of the Recess SBD is relatively smaller in the range from 0.69 eV to approximately 1.01. In addition, the n values show a strong negative correlation with the Φ_b (Figure 5-5b) indicating that the n decreased with the increasing temperature. The variation of Φ_b and n versus temperature can be explained by the barrier height non-homogeneous effect, namely, the spatial fluctuation of the barrier height at the metal/AlGaN interface. It assumes that some lower barrier contacts were embedded on the uniform barrier. Therefore, the current is dominated by the low barrier regions at relatively low temperature, presenting a relatively lower Φ_b. With the temperature increasing, the carrier gains high enough energy and crosses over the high barrier regions.

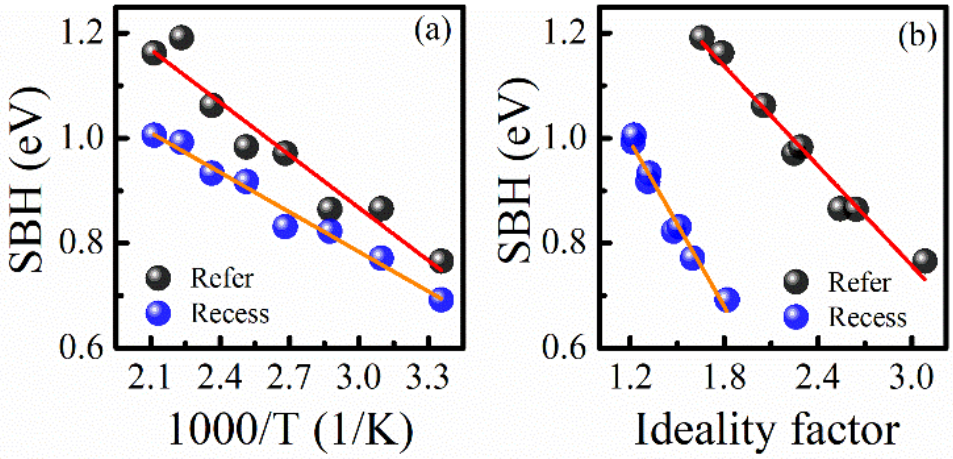

Figure 5-5. The temperature dependency of Φb (a) and the relationship between Φb and n (b) for the SBDs.

To evaluate the sensing ability, the forward voltage at the sub-threshold region was plotted versus temperature as shown in inset of Figure 5-2b and inset of Figure 5-3b. Under the three typical current levels, the forward voltage of both kinds of diodes shows good linearity versus temperature, indicating the promising potential for sensor applications. The temperature sensitivities at current levels of 1×10^{-5}, 1×10^{-6}, and 1×10^{-7} A for the Refer SBD are calculated to be approximately 1.26, 1.44, and 1.61 mV/K, respectively. While for the Recess SBD (Figure 5-3b), the sensitivities are

calculated to be approximately 0.78, 0.95, and 1.05 mV/K, respectively. The sensitivity shows a decreasing trend with the increasing current level, which is in agreement with our previous works. Generally, the sensitivity of a diode sensor in sub-threshold region should show a relationship with the increasing effective current density decreases as represented as follows:

$$\frac{dV_F}{dT} \propto \frac{nKT}{q} \ln\left(\frac{I_D}{A_e A^*}\right). \quad (5\text{-}3)$$

Based on equation (5-3), a smaller current level at a specific anode area increases the absolute value of $\ln(I_D/A_e)$, resulting in a higher sensitivity. Therefore, the sensitivity should be proportional to the logarithms of current density.

We plotted the corresponding sensitivity versus the effective current density as shown Figure 5-6. The good linearity between sensitivity and $\ln(I_D/A_e)$ confirms the discussion above. In addition, the sensitivity of the Refer SBD is higher than that of the Recess SBD, which can be attributed to the relatively larger n value of the Refer SBD.

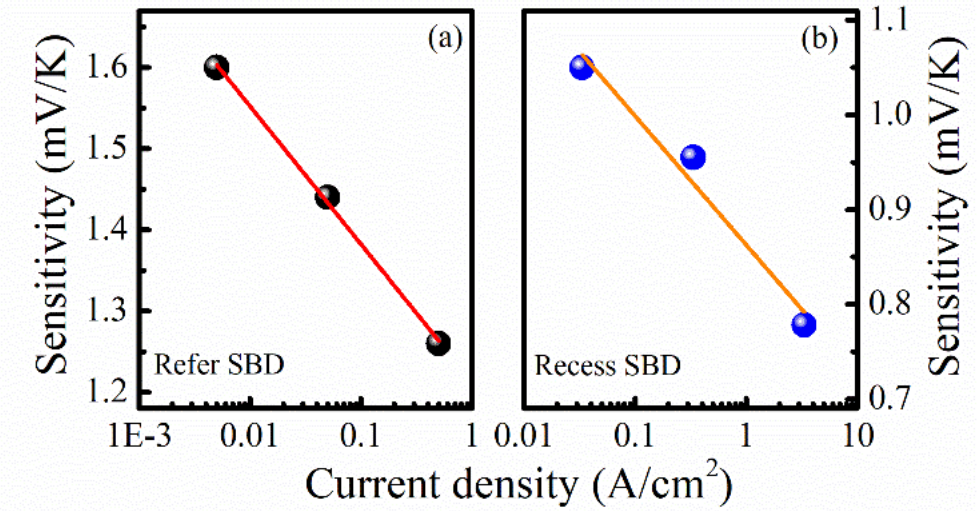

Figure 5-6. the sensitivity versus current density for the Refer (a) and Recess SBD(b), respectively.

The AlGaN/GaN Schottky barrier diode temperature sensor was fabricated by using the recessed anode structure. Compared with the conventional planar diode, the recessed anode SBD show a relatively lower turn-on voltage and better Schottky contact characteristics. The I-V curves at all temperature show typical rectification characteristics along with a ZTC bias point. Above ZTC point (fully-turn-on region), the relatively large series resistance would degrade the temperature error and linearity

along with a larger loss, which is not suitable for temperature sensor application. Below ZTC point (sub-threshold region), the I-V characteristics are linear and shift negatively with the increasing temperature, following the TE model. The temperature dependent forward voltage at a fixed current shows good linearity, resulting in a sensitivity of approximately 1.0 mV/K. The sensitivity shows a decreasing trend with the increasing current level, which is in agreement with the thermionic emission model. Those results indicate that the recessed anode AlGaN/GaN SBD is suitable to integrate with GaN-based power device for temperature sensor application.

§5.4. Development of vertical SBD temperature sensor

GaN-based material is promising for power electronic applications because of its superior Baliga's figure-of-merit than SiC and Si [12-14]. Especially, along with the development of low dislocation density free-standing GaN substrate, vertical GaN power rectifiers including Schottky barrier diode (SBD) and p-n diode (PND) have been demonstrated with record high performance in recent years [15,16]. Compared with PND, the SBD presents a typically low on-state voltage (Von) and no storage of minority carriers, resulting in a high-efficiency rectifier in the breakdown voltage (BV) of less than 1 kV range [17, 18]. However, when the device is biased at a larger reverse voltage, the image force causes a serious energy barrier lowering effect [19], which significantly increases the leakage current and leads to a reduced breakdown voltage. A higher Schottky barrier height (SBH, ϕ_b) helps to reduce the leakage current but at the cost of an unfavorable increase of Von. On the other hand, edge termination techniques, such as guard ring, p-n junction termination extension (JTE) and junction barrier Schottky diode (JBS), are beneficial for attenuating the field crowding effect at the junction periphery and reducing the reverse leakage [20-22]. Patterned p-type doping region plays a key role in those approaches, which is still a big challenge for GaN through implantation, diffusion and selective area growth/etching [23, 24]. For the p-GaN grown by metal-organic chemical vapor deposition (MOCVD), the low solubility and high activation energy of Mg dopants are the main problems. While for p-GaN obtain through ion implantation route, the GaN surface will decompose during high temperature activation process. Generally, the forward voltage (V_F) under a constant current, as well as the reverse saturation current (I_S) under a constant voltage for the diode, shows strong dependence on

temperature. Good linearity is helpful to simplify the pre-calibration procedure by using only two temperature points. In our previous study, we fabricated GaN-compatible temperature sensors based on thermally stable TiN anode SBD and p-NiO/n-GaN PND. In the temperature range from 25 to 200 °C, both the SBD and PND present good linearity with the sensitivity of 1.0-2.0 mV/K. However, all the GaN SBD and PND diodes were fabricated on a lateral or quasi-vertical structure. The temperature sensor with vertical GaN device is rarely reported.

We have demonstrated that the nickel oxide (NiO) is a natural p-type semiconductor by using low-temperature reactive sputtering, implying that it can be a simple method to form area-selectively deposition without any etching or activation process [25, 26]. Besides, the lateral p-NiO/n-GaN heterojunction diode presents excellent rectifying behavior and good interface quality. However, the vertical GaN diode with p-NiO as guard ring structure has not yet been reported. Herein, the NiO is area-selectively deposited to serve as a termination structure for TiN-anode SBDs, which is potential to combine the advantages of both SBD and PND devices. The effect of the p-NiO guard ring length on the properties of the vertical GaN Schottky barrier diodes was investigated extensively.

The vertical SBDs (Figure 4-7) without (reference device) and with p-NiO guard ring were fabricated on a free-standing GaN wafer. A 14 μm n-GaN drift layer was grown on a 350μm thick commercial free-standing GaN substrate by MOCVD with resistivity of 0.05 Ωcm and doping concentration of approximately 1×10^{18} cm^{-3} . The net doping concentration of the drift layer is close to 2×10^{16} cm^{-3} as extracted from the capacitance-voltage curve, as reported in our previous works [27]. After cleaning, ohmic contact of a multi-layer Ti/Al/Ti/Au (50/200/40/40 nm) cathode was sputtered on the backside of the wafer and annealed in N_2 ambient at 800℃ for 1 min. The multi-layer ohmic electrode and the annealing condition are usually adopted for AlGaN/GaN heterostructure device. Fortunately, the on-resistance of the vertical diode by using this annealing process without further optimization is comparable with that of other works [27]. Then, a thick gold layer with a thickness of about 1μm was electroplated to form a probe pad. The NiO guard ring (100 nm) was formed by reactive sputtering with an Ar:O_2 (Ar:O_2 = 15:5 sccm) mixed gas ambient using a Ni metal target. As reported in our previous work [15], the hole concentration and mobility of the NiO were approximately 1.16×10^{18} cm^{-3} and 0.85 cm^2 V^{-1} s^{-1},

respectively. After cleaning in a BHF and a diluted HCl solution, the TiN Schottky anode was prepared with an Ar:N_2 (Ar:N_2 = 15:3 sccm) mixed gas ambient using a Ti metal target. After that, a cap layer of Ni/Au (30/70 nm) was deposited on the TiN layer in Ar ambient to form a probe pad. Finally, post metallization annealing was conducted at 300℃ for 10 min to improve the contact quality and homogeneity between the sputtered metal layers and the metal/GaN interface.

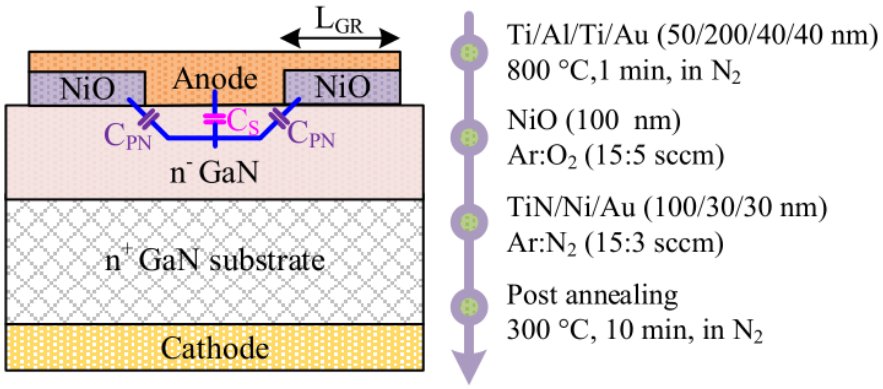

Figure 5-7 The schematic structure of vertical GaN Schottky barrier diode without (a) and with (b) p-NiO guard ring. The main fabrication process steps are also listed.

To evaluate the effect of the guard ring length (L_{GR}) on the electrical performance of the SBDs, current-voltage (I–V) characteristics were recorded at room temperature firstly. Following the thermionic emission (TE) theory, when the forward bias V_F>3kT/q, the forward current (I_D) can be represented as [28] equation (5-1), and the forward voltage is solved as equation (5-2).

Based on equation (5-2), we fitted the forward-biased I–V characteristics of the diodes with different guard ring length (Figure 5-8a). All the experimental curves show good agreement with the TE model, implying that the forward conduction is dominated by the Schottky contact region. This can be also confirmed with the deduced parameters, as plotted in Figure 5-8b. The obtained ideality factor n and Schottky barrier height ϕ_b values are nearly the same for all the diodes with different L_{GR}. On the other hand, we also observed that the Rs increased by nearly two times when the L_{GR} increased to 40μm. The possible reason is ascribed to that the p-NiO guard ring forms a PN junction with the beneath n-GaN, resulting in a depletion region that will then compress the SBD conduction path.

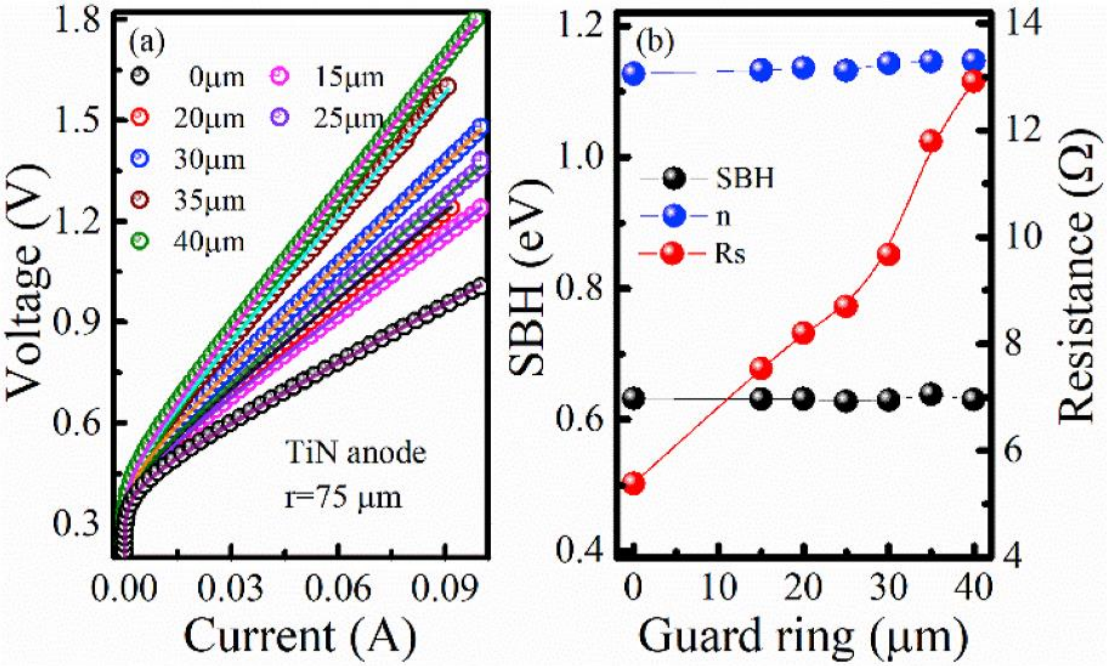

Figure 5-8 (a) The room temperature I–V characteristics of SBDs with different L_{GR}. (b) The corresponding ideality factor, SBH, and R s are deduced by TE model.

The typical temperature-dependent I–V characteristics of the reference device and SBD with a 25μm guard ring were measured from 25 to 200℃, as shown in Figure 5-9. Both devices show obvious rectification characteristics at all temperatures. The relatively low work function of TiN (4.7 eV) is beneficial for decreasing the turn-on voltage, but also resulting in a relatively high reverse leakage current, compared with the conventional Ni/Au or Pt/Au anode. When the temperature increases, the two kinds of SBDs show comparable leakage current as well as similar temperature dependence trend. This result confirms that the electrical properties of the SBDs are mainly determined by the Schottky contact region under relatively small reverse bias even though there is a PN junction guard ring.

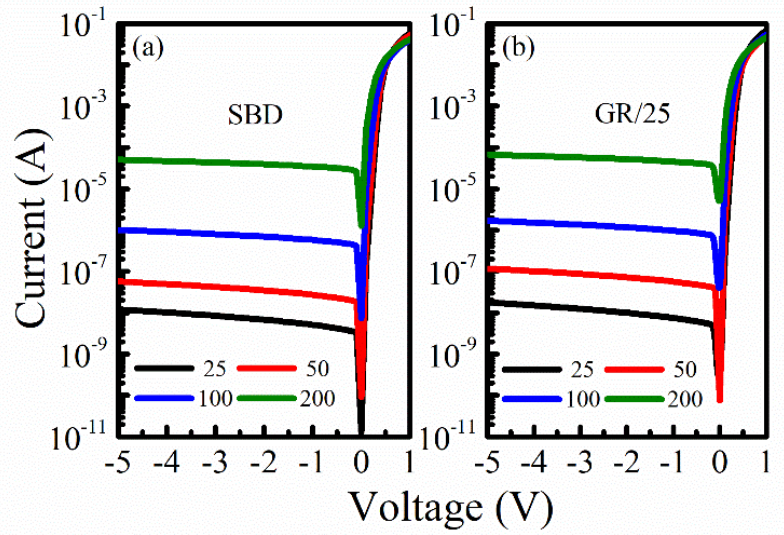

Figure 5-9. The typical temperature-dependent I–V characteristics of SBDs without (reference device) and with a 25μm guard ring measured from 25 to 200 ◦ C.

The capacitance-voltage (C-V) curves (@1 MHz) of the circular diodes with different L_{GR} are shown in Figure 5-10. The capacitance decreases with the negative bias due to the increasing depletion width (Figure 5-10a). The frequency-dependent C-V measurements ranging from 1 kHz to 1 MHz were further investigated to evaluate the interface status (Figure 5-10b). It demonstrates that no obvious capacitance dispersion appears even at a high reverse voltage and a frequency of 1 MHz, implying relative weak frequency dispersion. Theoretically, the trapping/de-trapping process occurs when the interface states close to the Fermi level. However, this process cannot follow up the variation of frequency if the interface states possess a relatively large time constant, resulting in a frequency dispersion effect. Especially, the external electric field down shifts the Fermi level in the GaN side when the Schottky contact under a relatively high reverse bias. Then, the trapping/de-trapping process occurs between the deep interface states and Fermi level, which cannot follow up the variation of frequency [29, 30]. In this work, the free-standing GaN substrate with low dislocation density as well as the good TiN/GaN interface is beneficial for suppressing the dispersion effect.

It worth noting that the capacitance at zero voltage (Figure 5-10a) decreases gradually with the increasing L_{GR} compared with the SBD diode (L_{GR} = 0 μm). In our diodes with a NiO guard ring, the capacitance consists a Schottky contact part (SBD) and a PN junction part (PND). Owing to the low average sputtering rates of 0.6 and 1.7 nm/min for the TiN and NiO deposition, respectively, we can assume that the

anode electrode is homogeneously deposited and the capacitance at zero voltage is proportionally to the area. However, as shown in the inset of Figure 5-10a, the calculated capacitance of the Schottky contact part is much smaller than the measured total capacitance at zero voltage. This means that the PN junction part also contributes to the capacitance. By subtracting the capacitance of the Schottky contact region from the total one, the obtained capacitance presents a good linearity versus the area of the PN junction region (inset of Figure 5-10b). Based on those results, we can conclude that the total capacitance results from the shunt of SBD and PND capacitance.

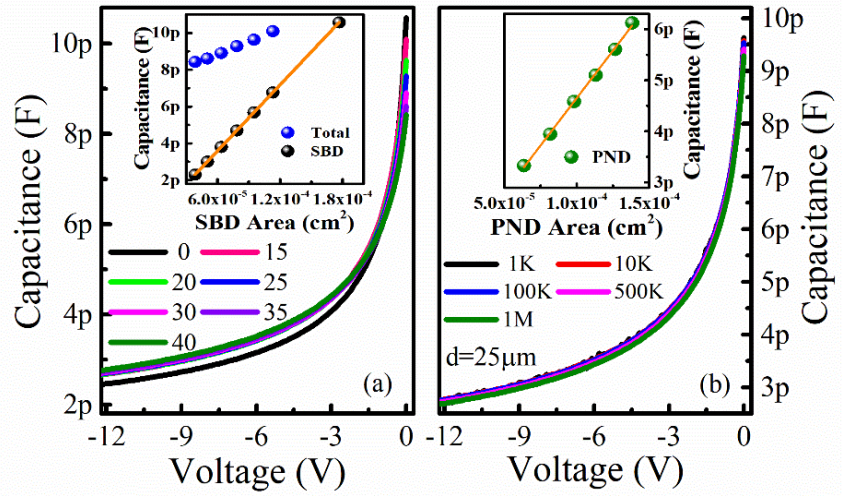

Figure 5-10. The C–V curves (a) of the circular diodes with different guard ring length and the frequency-dependent C–V measurements for diode with 25μm guard ring.

Figure 5-11 shows the effect of the p-NiO guard ring length on the off-state breakdown characteristics of the vertical didoes. Under relatively low reverse bias (<50 V), the leakage currents for SBDs with different guard ring length are comparable. The breakdown voltage of the SBDs without any termination is approximately 100 V. The introduction of NiO guard ring is effective to enhance the breakdown voltage although the leakage current is comparable. It was found that the breakdown voltage decreases with the increasing guard ring length. A maximum breakdown voltage of approximately 250 V was obtained for the diode with 15μm guard ring, while it decreases to approximately 150 V when the length is larger than 25μm (inset of Figure 5-11). It worth noting that these values are still lower than the theoretical one with a 14μm drift layer. The possible reason is ascribed the planar structure of thin p-NiO guard ring (100 nm). In the conventional vertical SBD with p-GaN termination structure, the p-type region formed by Mg^+ ion implantation or

trench-filling-regrowth was buried in the n-GaN drift layer with a depth of approximately 500 nm [20]. Compared with the planar structure, the buried p-type region enhances the lateral depletion region which helps to shield the peak electric field at the surface. Secondly, we recently fabricated quasi-vertical GaN heterojunction diodes on sapphire substrate with 200 nm p-NiO anodes. A breakdown voltage of approximately 700 V was realized after optimized the annealing conditions [31]. Therefore, we need to introduce a trench-filling process with thick p-NiO to further improve the reverse breakdown voltage.

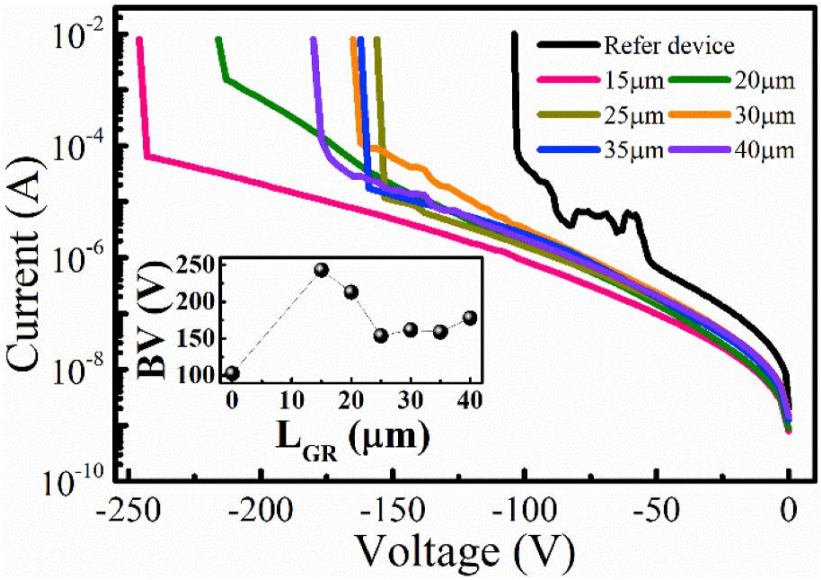

Figure 5-11 The off-state breakdown characteristics of the vertical didoes with different p-NiO guard ring length.

Finally, we simulated the effect of the guard ring on the forward conduction and reverse breakdown characteristics by using Silvaco TCAD. Figure 5-12 shows the current density distribution of the diode without and with a 25μm guard ring under a forward voltage of 1 V. It demonstrates that the current conduction path covers all the anode area in the conventional SBD (Figure 5-12a). While for the diode with a guard ring, the existence of depletion region under the p-NiO region will reduce the conduction path. The current conduction mainly occurs below the Schottky contact part as shown in Figure 5-12b.

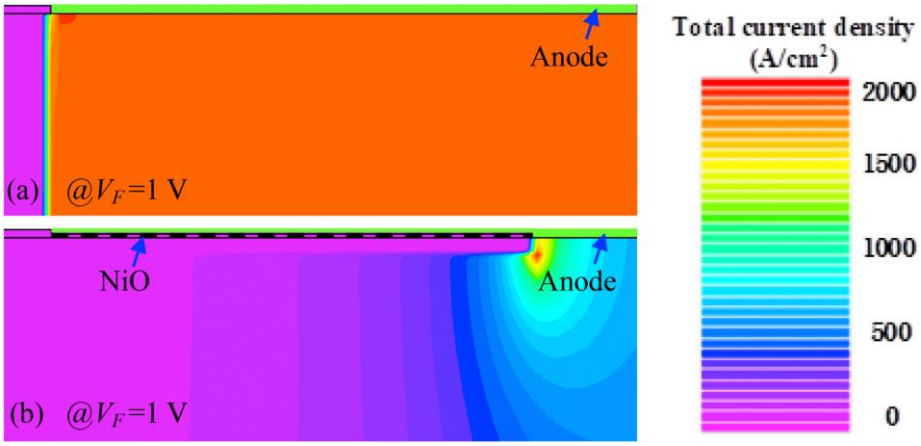

Figure 5-12 The current density distribution of the diode without and with a 25 μ m guard ring under a forward voltage of 1 V

Therefore, the on-resistance increases with the increasing guard ring length. When the SBD without termination is set to reverse bias, the electric field concentrates at the anode/GaN interface along with an obvious crowding at the edge of the anode electrode (Figure 5-13a). The introduction of guard ring can suppress the electric field at the anode/GaN interface effectively, which helps to enhance the breakdown voltage (Figure 5-13b). Besides, the simulation results demonstrate that the electric field intensity and distribution under reverse bias are comparable for diodes with different guard ring length. This is not consistent with the variation of breakdown voltage versus guard ring length, as shown in inset of Figure 5-11. The mechanism is still not clear now and a possible reason may be ascribed to the imperfect NiO/GaN interface. Under high reverse voltage, the electron tunneling will be enhanced with the assistance of the GaN/NiO interface states. Therefore, the risk of tunneling leakage current increases along with the increasing guard ring length, resulting in the decrease of breakdown voltage.

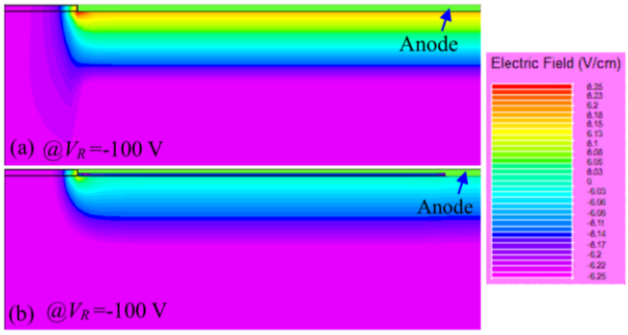

Figure 5-13 The electric field distribution of the diode without and with a 25 μ m guard ring under a reverse voltage of 100 V.

§5.5. Conclusions

In conclusion, the AlGaN/GaN Schottky barrier diode temperature sensor was

fabricated by using the recessed anode structure. Compared with the conventional planar diode, the recessed anode SBD show a relatively lower turn-on voltage and better Schottky contact characteristics. The I-V curves at all temperature show typical rectification characteristics along with a ZTC bias point. Above ZTC point (fully-turn-on region), the relatively large series resistance would degrade the temperature error and linearity along with a larger loss, which is not suitable for temperature sensor application. Below ZTC point (sub-threshold region), the I-V characteristics are linear and shift negatively with the increasing temperature, following the TE model. The temperature dependent forward voltage at a fixed current shows good linearity, resulting in a sensitivity of approximately 1.0 mV/K. The sensitivity shows a decreasing trend with the increasing current level, which is in agreement with the thermionic emission model. Those results indicate that the recessed anode AlGaN/GaN SBD is suitable to integrate with GaN-based power device for temperature sensor application.

A kind of vertical GaN SBD temperature sensor was fabricated on GaN substrate. The temperature-dependent I-V characteristics from 25 °C to 200 °C present a ZTC bias point of approximately 0.6 V. The forward-current decreases with increasing temperature due to large Rs (caused by mobility degradation). Below the ZTC bias point (sub-threshold range), the current increased gradually with the increasing temperature due to the decrease of the turn-on voltage. In the sub-threshold range, the forward-voltage at a fixed current decreased linearly with the increasing temperature, resulting in a sensitivity of approximately 1.3 mV/K. The sensitivity shows a linear relationship with the current density after take account of the diode area.

Furthermore, p-NiO was selective area deposition by reactive sputtering to serve as the guard ring structure of vertical GaN Schottky barrier diode. The forward-biased I-V characteristics of diodes with different guard ring length is dominated by the SBD region. The deduced n and φ_b values through TE model are comparable for all diodes, while the series resistance increased by nearly two times due to the depletion region at the p-NiO/GaN interface will reduce the conduction path. The increasing depletion region can also be confirmed form the C-V curves, indicating the total capacitance is the shunt of SBD and PND capacitance.

Therefore, GaN based diode as a temperature sensor could be integrated into AlGaN/GaN pH sensor. According to the structure of the pH sensor, different structure of temperature sensor should be chosen to obtain suitable turn-on voltage,

reverse voltage and sensitivity.

§5.6. References

[1] L. He, F. Yang, L. Li, Z. Chen, Z. Shen, Y. Zheng, Y. Yao, Y. Ni, D. Zhou, X. Zhang, L. He, Z. Wu, B. Zhang, Y. Liu, High threshold voltage uniformity and low hysteresis recessed-gate Al_2O_3/AlN/GaN MISFET by selective area growth, IEEE Trans. Electron. Dev. 64 (2017) 1554–1560.

[2] K. J. Chen, O. Häberlen, A. Lidow, C. Tsai, T. Ueda, Y. Uemoto, Y. Wu, GaN-on-Si power technology: devices and applications, IEEE Trans. Electron. Dev. 64 (2017) 779–795.

[3] A. Kwan, Y. Guan, X. Liu, K. J. Chen, A highly linear integrated temperature sensor on a GaN smart power IC platform, IEEE Trans. Electron. Dev. 61 (2014) 2970–2976.

[4] V. A. Krasnov, S. V. Shutov, S. Y. Yerochin, A. N. Demenskiy, High temperature diode sensors based on InGaN/AlGaN structures, J. Vac. Sci. Technol. B 36 (2018) 022905 1-5.

[5] S. Madhusoodhanan, S. Sandoval, Y. Zhao, M.E. Ware, Z. Chen, A highly linear temperature sensor using GaN-on-SiC heterojunction diode for high power applications, IEEE Electron. Device Lett. 38 (2017) 1105–1108.

[6] D. Li, X. Sun, H. Song, Z. Li, H. Jiang, Y. Chen, G. Miao, B. Shen, Effect of asymmetric Schottky barrier on GaN-based metal-semiconductor-metal ultraviolet detector, Appl. Phys. Lett. 99 (2011) 261102.

[7] W. Mtangi, P. J. Janse van Rensburg, M. Diale, F. D. Auret, C. Nyamhere, J. M. Nel, A. Chawanda, Analysis of current–voltage measurements on Au/Ni/n-GaN Schottky contacts in a wide temperature range, Mater. Sci. Eng. B 171 (2010) 1–4.

[8] S. Yamamoto, Y. Kihara, K. Shiojima, Mapping of inhomogeneity and thermal degradation of Au/Ni/n-GaN Schottky diodes using scanning internal photo-emission microscopy, Phys. Status Solidi B 252 (2015) 1017–1023.

[9] J. -P. Ao, A. Suzuki, K. Sawada, S. Shinkai, Y. Naoi, Y. Ohno, Schottky contacts of refractory metal nitrides on gallium nitride using reactive sputtering, Vacuum 84 (2010) 1439–1443.

[10] L. Li, A. Kishi, T. Shiraishi, Y. Jiang, Q. Wang, J. -P. Ao, Y. Ohno, Evaluation of a gate-first process for AlGaN/GaN heterostructure field-effect transistors, Jpn. J.

Appl. Phys. 52 (2013) 11NH01.

[11] L. Li, A. Kishi, Q. Liu, Y. Itai, R. Fujihara, Y. Ohno, J. -P. Ao, GaN Schottky barrier diode with TiN electrode for microwave rectification, IEEE J. Electron Devices Soc. 2 (2014) 168.

[12] S. Fujita, Wide-bandgap semiconductor materials: for their full bloom, Jpn. J. Appl. Phys. 54 (2015), 030101.

[13] B. J. Baliga, Gallium nitride devices for power electronic applications, Semicond. Sci. Technol. 28 (2013) 074011.

[14] K. J. Chen, O. Häberlen, A. Lidow, C. Tsai, T. Ueda, Y. Uemoto, Y. Wu, GaN-on-Si power Technology: devices and applications, IEEE Trans. Electron. Dev. 64 (2017) 779–795.

[15] J. Hu, Y. Zhang, M. Sun, D. Piedra, N. Chowdhury, T. Palacios, Materials and processing issues in vertical GaN power electronics, Mater. Sci. Semicond. Process. 78 (2018) 75–84.

[16] T. Oka, Recent development of vertical GaN power devices, Jpn. J. Appl. Phys. 58 (2019) SB0805.

[17] Y. Sun, X. Kang, Y. Zheng, J. Lu, X. Tian, K. Wei, H. Wu, W. Wang, X. Liu, G. Zhang, Review of the recent progress on GaN-based vertical power Schottky barrier diodes (SBDs), Electronics 8 (2019) 575.

[18] K. Mochizuki, T. Mishima, A. Terano, N. Kaneda, T. Ishigaki, T. Tsuchiya, Numerical analysis of forward-current/voltage characteristics of vertical GaN Schottky-barrier diodes and p-n diodes on free-standing GaN substrates, IEEE Trans. Electron. Dev. 58 (2011) 1979–1985.

[19] H. Hasegawa, S. Oyama, Mechanism of anomalous current transport in n-type GaN Schottky contacts, J. Vac. Sci. Technol. B 20 (2002) 1647–1655.

[20] Y. Zhang, Z. Liu, M. Tadjer, M. Sun, D. Piedra, C. Hatem, T. Anderson, L. Luna, A. Nath, A. Koehler, H. Okumura, J. Hu, X. Zhang, X. Gao, B. Feigelson, K. Hobart, T. Palacios, Vertical GaN junction barrier Schottky rectifiers by selective ion implantation, IEEE Electron. Device Lett. 38 (2017) 1097–1100.

[21] J. R Laroche, F. Ren, K.W. Baik, S. J. Pearton, B.S. Shelton, B. Peres, Design of edge termination for GaN power Schottky diodes, J. Electron. Mater. 34 (2005) 370–374.

[22] T. Hayashida, T. Nanjo, A. Furukawa, M. Yamamuka, Vertical GaN merged PiN Schottky diode with a breakdown voltage of 2 kV, APEX 10 (2017), 061003.

[23] H. Sakurai, M. Omori, S. Yamada, Y. Furukawa, H. Suzuki, T. Narita, K. Kataoka, M. Horita, M. Bockowski, J. Suda, T. Kachi, Highly effective activation of Mg-implanted p-type GaN by ultra-high-pressure annealing, Appl. Phys. Lett. 115 (2019) 142104.

[24] T. Pu, Y. Chen, X. Li, T. Peng, X. Wang, J. Li, W. He, J. Ben, Y. Lu, X. Liu, J. -P. Ao, Gate structure dependent normally-off AlGaN/GaN heterostructure field-effect transistors with p-GaN cap layer, J. Phys. D Appl. Phys. 53 (2020) 415104.

[25] X. Li, T. Pu, T. Zhang, X. Li, L. Li, J.-P. Ao, p-NiO/n-GaN heterostructure diode for temperature sensor application, IEEE Sensor. J. 20 (2020) 62–66.

[26] L. Li, J. Chen, Z. Liu, T. Que, X. Gu, L. He, Y. Liu, Fast and slow interface traps in transparent NiO gated AlGaN/GaN heterostructure field-effect transistors, Appl. Surf. Sci. 475 (2019) 1043–1047.

[27] L. Li, X. Li, T. Pu, S. Cheng, H. Li, J.-P. Ao, Vertical GaN-based temperature sensor by using TiN anode Schottky barrier diode, IEEE Sensor. J. 21 (2021) 1273–1278.

[28] N. Yildirim, K. Ejderha, A. Turut, On temperature-dependent experimental I-V and C-V data of Ni/n-GaN Schottky contacts, J. Appl. Phys. 108 (2010) 114506.

[29] R. Vetury, N. Zhang, S. Keller, U. Mishra, The impact of surface states on the DC and RF characteristics of AlGaN/GaN HFETs, IEEE Trans. Electron. Dev. 48 (2001) 560–566.

[30] L. He, L. Li, T. Que, J. Zhang, C. Feng, Z. Liu, Q. Wu, J. Chen, Q. Qiu, Y. Wang, C. Li, Q. Zhang, Y. Liu, Impact of dislocation pits on device performances and interface quality degradation for E-mode recessed-gate Al_2O_3/GaN MOSFETs, J. Alloys Compd. 854 (2021) 157144.

[31] Y. Ren, L. Li, N. Liu, K. Zhang, C. Li, Z. Chen, B. Zhang, Quasi-vertical GaN heterojunction diodes with p-NiO anodes deposited by sputtering and post-annealing, Vacuum 182 (2020) 109784.

Chapter 6: Conclusions and Future works

§6.1. Conclusions

The pH sensor based on AlGaN/GaN heterostructure with high Al content (35%) in the barrier layer with a 16 nm transition layer of 25% Al content shows better surface sensitivity (S_V) of 56.01mV/pH, which is higher than that (53.94 mA/pH) of the sensor with 25% Al content, but worse current sensitivity S_A (-0.09544 mA/pH Vs -0.10166 mA/pH). A NEW 'sensitivity' (current sensitivity) S is defined to describe the characteristic of pH sensor, which shows the relationship between the drain current and the pH value, which is very important in application while the reference electrode can be omitted.

However, threshold voltage increases from approximately -1.6 V to approximately -0.8 V when measured in alkaline solution for 5 times, along with a decreasing output current. The high-resolution SEM photos show that there are high density hexagonal pits with the size of approximately 100 nm on the device surface, presenting the etching effect of the dislocations during alkaline sensing. The XPS demonstrated that the intensity of the Ga3d and Al2p spectra decreases after pH sensing measurement, implying the variation of chemical component occurs in the upper AlGaN thin layer. Furthermore, many voids with a size of approximately 100 nm were observed from the TEM pictures, which is comparable with that of the SEM. Combining with the EDX, the degradation in electrical performance can be attributed to the transformation of AlGaN into oxide as well as the followed alkaline solution dissolve.

The top layer of GaN effectively prevents the reaction of aluminum on the surface with the solution. Compared with the device without recessed-gate, the threshold voltage of the device with recessed-gate has a significant positive shift from -3.33 to -0.31 V, and the maximum transconductance is greatly improved about 150%, from 0.8 to 2 mS. The current sensitivity of AlGaN/GaN-based ISFET pH sensors has been improved by 61%, from 52.25 to 84.39 μA/pH by recessed-gate structure and ammoniate water treatment. The key factors to improve the current sensitivity of AlGaN/GaN-based sensors are potential sensitivity and transconductance. The dry etching recess process can be used to improve the transconductance. But the surface defects introduced during the dry etching decreases potential sensitivity slightly. Then, ammonium hydroxide treatment can be used to improve surface condition, that is, to

increase potential sensitivity.

According to the test results of pH meters made of AlGaN/GaN sensors, GaN-based ISFETs can measure the pH value of solution with similar circuit, whether working in the linear region or saturation region. The measurement is stable and repeatable. The small current in the linear region can make the measurement stable and fast, but the resolution is very low. High resolution can be obtained in the saturated region, but the measurement is unstable due to excessive current.

The AlGaN/GaN Schottky barrier diode temperature sensor was fabricated by using the recessed anode structure. Compared with the conventional planar diode, the recessed anode SBD show a relatively lower turn-on voltage and better Schottky contact characteristics. The I-V curves at all temperature show typical rectification characteristics along with a ZTC bias point. Above ZTC point (fully-turn-on region), the relatively large series resistance would degrade the temperature error and linearity along with a larger loss, which is not suitable for temperature sensor application. Below ZTC point (sub-threshold region), the I-V characteristics are linear and shift negatively with the increasing temperature, following the TE model. The temperature dependent forward voltage at a fixed current shows good linearity, resulting in a sensitivity of approximately 1.0 mV/K. The sensitivity shows a decreasing trend with the increasing current level, which is in agreement with the thermionic emission model. Those results indicate that the recessed anode AlGaN/GaN SBD is suitable to integrate with GaN-based power device for temperature sensor application.

A kind of vertical GaN SBD temperature sensor was fabricated on GaN substrate. The temperature-dependent I-V characteristics from 25 °C to 200 °C present a ZTC bias point of approximately 0.6 V. The forward-current decreases with increasing temperature due to large Rs (caused by mobility degradation). Below the ZTC bias point (sub-threshold range), the current increased gradually with the increasing temperature due to the decrease of the turn-on voltage. In the sub-threshold range, the forward-voltage at a fixed current decreased linearly with the increasing temperature, resulting in a sensitivity of approximately 1.3 mV/K. The sensitivity shows a linear relationship with the current density after take account of the diode area.

Furthermore, p-NiO was selective area deposition by reactive sputtering to serve as the guard ring structure of vertical GaN Schottky barrier diode. The forward-biased I-V characteristics of diodes with different guard ring length is dominated by the SBD region. The deduced n and φ_b values through TE model are comparable for all diodes,

while the series resistance increased by nearly two times due to the depletion region at the p-NiO/GaN interface will reduce the conduction path. The increasing depletion region can also be confirmed form the C-V curves, indicating the total capacitance is the shunt of SBD and PND capacitance.

Therefore, GaN based vertical Schottky barrier diode as a temperature sensor could be integrated into AlGaN/GaN pH sensor. According to different structure of pH sensors, different structure of temperature sensors could be chosen to obtain suitable turn-on voltage, reverse voltage and sensitivity.

Finally, a few simple sentences highlight the above conclusions.

(1) The pH sensor based on AlGaN/GaN heterostructure with higher Al content in the barrier layer shows better surface sensitivity.

(2) There is the etching effect of the dislocations during alkaline sensing.

(3) The top layer of GaN effectively prevents the reaction of aluminum on the surface with the solution.

(4) pH sensor with recessed-gate shows higher threshold voltage and higher maximum transconductance.

(5) Ammonium hydroxide treatment can be used to increase potential sensitivity.

(6) pH meters made of AlGaN/GdN sensors can measure the pH value of solution stably and repeatedly but slowly due to junction temperature.

(7) Both the recessed anode AlGaN/GaN SBD and vertical SBD with guard ring are suitable to integrate with GaN-based pH sensor to make the measurement fast. They are suitable for different sensor structures.

§6.2. Future works

From the previous works, we still have a lot of works to do to obtain a fast, stable and accurate pH meter based on GaN.

First of all, as for the device structure, we need to grasp several aspects: the first is to ensure the Al composition to obtain larger current and improve the resolution. Secondly, there should be a cap layer to prevent Al from being corroded. Then we need to add a recess to improve the threshold voltage and transconductance. Finally, we need to integrate a real-time temperature sensor to measure the device temperature (whether the junction temperature or external environment temperature). The choice

of planar or vertical temperature sensor depends on the structure of pH sensor.

In the circuit design, there are still many issues to be optimized. The IC with higher accuracy can be selected for the measurement circuit, and a comparison circuit should be used to make the measurement more accurate. LCD needs to select more digits.

In terms of software, in addition to the existing functions, it can be considered to record the results of each measurement in real time, including the source and drain current and the real-time temperature of the device. And it can be read out through USB interface. In this way, we can see the relationship among pH value, current and temperature intuitively, which would be very important whether for research work or for actual application so that the calibrated measurement can be stable, fast and accurate.

Acknowledgements

This paper is carried out during my study in University of Tokushima, from April 2018 to September 2021. On the completion of my thesis, I would like to thank all those who have helped and supported me in the past three and half years.

First and foremost, I would like to give my sincere gratitude to my supervisors, Associate Professor Jin-Ping Ao. Professor Ao has devoted a lot of energy to guide and help me, both in research and specific life. His knowledge, his way of life and his working attitude and feelings all make me feel great positive energy. I can't believe that if it wasn't for him, I would still have made such achievements under such circumstances.

I would like to gratefully acknowledge the Department of Electrical and Electronic Engineering for providing the resources and needs during the thesis. I would like to extend my appreciation to Professor Shiro Sakai, Professor Masao Nagase, Professor Yoshiki Naoi, Professor Masanobu Haraguchi, for their unconditional help during this research.

I would also especially like to thank Dr. Liuan Li in School of Electronics and Information Technology of Sun Yat-Sen University for the support of my research.

I would like to thank Dr. Xiao Wang, Dr. Yuyu Bu, Ms. Yue He and Mr. Guoqiang Chen et. al in Microelectronics School of Xidian University for their support of my research.

Many thanks extend to the members Xiaobo Li, Taofei Pu, Tian Xie, Ruiling Wang, et al in Ao group, for their help and patience in my research and life.

I would also especially like to thank Professor Xichuan Cao and his team in the School of materials and physics, China University of Mining and Technology for the support of my research.

I would also especially like to thank Mr. Lingu Nie for his great support in circuit making and software writing.

I would also like to thank all my colleagues in my company for their hard work, so that my research can go on smoothly.

Last and certainly not the least, thanks to my wife and my daughter, they always gave me the courage to accept this challenge at this age and overcome all kinds of difficulties in the past four years.

Publication list

Scientific Papers

[1] ***Jiyu Zhou***, Xiaobo Li, Taofei Pu, Liuan Li, Jin-PingAo, "Vertical GaN Schottky barrier diodes with area-selectively deposited p-NiO guard ring termination structure", Superlattices and Microstructures, Vol. 151, March 2021, pp. 106820 (1-6).

[2] ***Jiyu Zhou***, Xiaobo Li, Taofei Pu, Yue He, Xiao Wang, Yuyu Bu, Liuan Li, Jin-Ping Ao, "Surface sensibility and stability of AlGaN/GaN ion-sensitive field-effect transistors with high Al-content AlGaN barrier layer", Applied Surface Science，2021, under review.

[3] Ji-Yao Du, ***Ji-Yu Zhou***, Xiao-Bo Li,Tao-Fei Pu,Liu-An Li, Xin-Zhi Liu, Jin-Ping Ao, "Band alignment between NiOx and nonpolar/semipolar GaN planes for selective-area-doped termination structure", Chin. Phys. B Vol. 30, No. 6 (2021) 067701.

[4] Yue He, Xiao Wang, ***Ji-Yu Zhou***, Ting-Ting Wang, Meng-Ke Ren, Guo-Qiang Chen, Tao-Fei Pu, Xiao-Bo Li, Mao Jia, Yu-Yu Bu, Jing-Pin Ao, "Enhanced pH Sensitivity of AlGaN/GaN Ion-Sensitive Field-Effect Transistor by Recess Process and Ammonium Hydroxide Treatment", IEEE Transactions on Electron Devices, Vol. 68, No. 3, pp. 1250-1254, March 2021.

International Conference Presentations

[1] ***Jiyu Zhou***, Tian Xie, Taofei Pu, Xiaobo Li, and Jin-Ping Ao, "AlGaN/GaN heterostructure pH sensors with high Al composition in the barrier layer", ***16th China International Forum on Solid State Lighting (SSLCHINA 2019) & 2019 International Forum of Wide band Gap Semiconductor (IFWS 2019)***, 25-27 November, 2019, Shenzhen, China.